Chemically modified graphene as nano-adsorbent for environmental applications

Rabita Mohd Firdaus

Université de Lorraine, Collegium Sciences et Technologies, Institut Jean Lamour
Ecole Doctorale C2MP « Chimie – Mécanique – Matériaux – Physique »

THÈSE

Pour l'obtention du titre de :

Docteur de l'Université de Lorraine

Spécialité : chimie des matériaux

Présentée par :

Rabita M. FIRDAUS

Graphène chimiquement modifié et auto-assemblé comme adsorbant pour des applications en environnement

---

Thèse soutenue publiquement le 13 Décembre 2022 (Thèse en cotutelle avec Universiti Sains Malaysia) à devant le jury composé de :

Mme. Catherine JOURNET	Professeur des Universités	Rapportrice	Laboratoire des Multimatériaux et Interfaces – Université Claude Bernard Lyon 1, France
M. Siang-Piao CHAI	Professeur des Universités	Rapporteur & Président	School of Engineering Monash University, Malaisie
M. Abdul Rahman MOHAMED	Professeur des Universités	Directeur de thèse	School of Chemical Engineering, Universiti Sains Malaysia, Malaisie
Mme. Brigitte VIGOLO	Chargée de Recherche, HDR	Directeur de thèse	Institut Jean Lamour – Université de Lorraine, France
M. Alexandre DESFORGES	Maître de Conférences	Invité	Institut Jean Lamour – Université de Lorraine, France
M. Keat Teong LEE	Professeur des Universités	Invité	School of Chemical Engineering, Universiti Sains Malaysia, Malaisie
Mme. Noorashrina A. HAMID	Maître de Conférences	Invitée	School of Chemical Engineering, Universiti Sains Malaysia, Malaisie

CHEMICALLY MODIFIED GRAPHENE AS NANO-ADSORBENT FOR ENVIRONMENTAL APPLICATION

RABITA BT. MOHD FIRDAUS ACHUTAN

UNIVERSITI SAINS MALAYSIA

2023

CHEMICALLY MODIFIED GRAPHENE AS NANO-ADSORBENT FOR ENVIRONMENTAL APPLICATION

by

RABITA BT. MOHD FIRDAUS ACHUTAN

Thesis submitted in fulfillment of the requirements

for the degree of

Doctor of Philosophy

January 2023

ACKNOWLEDGEMENT

I would like to thank and praise the Almighty, for granting me countless blessings, knowledge, and opportunities that allowed me to successfully complete this thesis. Apart from the efforts of me, this thesis would not have been successful without the encouragement and guidance provided by many other individuals. I would like to take this opportunity to thank them.

My deepest gratitude goes out to both my university, Universiti Sains Malaysia (USM), and the University of Lorraine (UL) for giving me the opportunity to complete this study. Besides, I'd like to thank both my supervisors, Professor Ir. Dr. Abdul Rahman Mohamed and Dr Brigitte Vigolo for their guidance and support, especially for their confidence in me. Having both of you as mentors has helped me become a better person in my academic career. Your extraordinary support made it possible for me to complete this thesis.

Moreover, I would like to thank everyone who has contributed to the positive atmosphere at USM and Institut Jean Lamour (IJL) laboratory. I would like to thank all my friends, technicians, and office staffs especially Dr Izzati, Prof Jean-François Pierson, Dr Alexandre Desforges, Dr Osama, Qlao, Killian, and Mauricio who have always supported me in difficult times. I'd like to express my gratitude to Dr. Hazwan for his administrative assistance on behalf of the Cotutelle Program. Special thanks to all my close friends in USM and IJL, for their kindness, friendliness, and open arms to share the knowledge during my study.

In recognition of the financial support, I received throughout my PhD studies, I am grateful to the Ministry of Europe and Foreign Affairs (MEAE) through the Hubert Curien- Hibiscus (PHC) Collaboration Grant (203/PJKIMIA/6782004), the Ministry of Higher Education Malaysia and the French Ministry of National

Education. Besides, this work has also received financial support from the French Embassy in Malaysia, Campus France, and the Institute of Postgraduate Studies (IPS), USM through the Universiti Sains Malaysia Fellowship.

As a final note, this work has been specially dedicated to my parents, Mr. Mohd Firdaus Achutan b Abdullah and Mrs. Norazmah Yusoff. I would like to express my deepest gratitude and appreciation to all of you for your unflagging loves and supports throughout my life. Ramona, Asri, Ratika Alia, Rihana, Afiqah, Clemira, Harith, you guys have been my support system since day one and always been my pillar of strength. There are no words to express how grateful I am to all of you. A lot of love and many thanks go out to each of you. I really hope I made all of you proud!

Rabita, 2022

TABLE OF CONTENTS

LIST OF TABLES

LIST OF FIGURES

LIST OF SYMBOLS

		Unit
C	Concentration at time t	mg mL^{-1}
C_0	Initial concentration	mg mL^{-1}

LIST OF ABBREVIATIONS

2D	Two-dimensional
3D	Three-dimensional
ALD	Atomic layer deposition
Al	Aluminium
Al_2O_3	Alumina
BOD	Biochemical oxygen demand
BET	Brunauer–Emmett–Teller
CDIC	Carbon Dioxide Information Analysis Center
Cu	Copper
CO_2	Carbon dioxide
COD	Chemical oxygen demand
CVD	Chemical Vapour Deposition
CNTs	Carbon nanotubes
CR	Congo red
EELS	Electron energy loss spectroscopy
FLG	Few layer graphene
FTIR	Fourier transform infrared spectroscopy
GA	Graphene aerogel
GBMs	Graphene-based macrostructures
GHGs	Greenhouse gases
GNFs	Graphene nanofibers
GNPs	Graphene nanoplatelet
GO	Graphene oxide

HFCs	Hydrofluorocarbons
MLG	Multi-layer graphene
NGA	Nitrogen doped graphene aerogel
NOAA	National Oceanic and Atmospheric Administration
NiOOH	Nickel oxide hydroxide
N_2O	Nitrous oxide
PFC	Perfluorocarbons
PECVD	Plasma-enhanced CVD
PAN	Polyacrylonitrile
PEI	Polyethylenimine
PMMA	Polymethylmethacrylate
rGO	Reduced Graphene Oxide
SEM	Scanning electron microscopy
SLG	Single layer graphene
SSA	Specific surface area
SiO_2	Silicon dioxide
SF_6	Sulfur hexafluoride
TEM	Transmission electron microscopy
XPS	X-ray photoelectron spectrometry

LIST OF APPENDIX

CHEMICALLY MODIFIED GRAPHENE AS NANO-ADSORBENT FOR ENVIRONMENTAL APPLICATION

ABSTRACT

Carbon dioxide (CO_2) emissions and pollution by dyes have a significant environmental impact, and it is imperative that cost-effective and recyclable adsorbents are developed to reduce their effect on the ecosystem and human health. Research was conducted to develop porous graphene-based macrostructures for two different environmental applications including adsorption of CO2 gas and Congo red dye respectively. The first part of this research is focused on developing 2D graphene oxide (GO) and further modifications on GO were carried out with two different approaches: physical and chemical activation. The structural and the chemical properties of the prepared activated graphene were deeply characterized by means of scanning electron microscopy (SEM), transmission electron microscopy (TEM), Raman spectroscopy, Fourier transform infrared spectroscopy (FTIR), X-ray photoelectron spectrometry (XPS) and Brunauer–Emmett–Teller (BET) nitrogen adsorption. The temperature used for the activation process was found to be the key parameter leading to enhance CO_2 adsorption capacity of the GO-based materials. The specific surface area was increased from 219.3 $m^2\ g^{-1}$ for starting GO to 762.5 $m^2\ g^{-1}$ and 1060.5 $m^2\ g^{-1}$ after physical and chemical activation, respectively. The performance of CO_2 adsorption was gradually enhanced with the activation temperature for both approaches. For the best performances, a factor of enhancement of 6.5 and 9 after physical and chemical activation, respectively was reached. The CO_2 adsorption capacities for physically and chemically activated graphene were 27.2 mg g^{-1} and 38.9 mg g^{-1}, respectively,

at 25 °C and 1 bar. In addition, the impact of the used temperature for the activation treatment on the CO_2 adsorption capacity has been investigated and discussed leading to a comprehensible mechanism. The second phase of this study was to construct 3D graphene based monoliths (GBMs) by self-assembling of GO in which GO was reduced by hydrothermal method using ascorbic acid, as the reductant agent. Different concentrations of GO (1-6 mg mL^{-1}) in the starting stable aqueous dispersion obtained at pH 10 were investigated to optimize the self-assembly process. The structural properties including surface area, pore volume, pore size and surface chemistry were measured and discussed considering their performance for CO_2 capture. The results showed that the optimized adsorbents (2 mg mL^{-1}) exhibited the highest surface area and total pore volume of 331 m^2 g^{-1} and 0.80 cm^3 g^{-1} respectively. In the developed 3D GBMs, the best CO_2 adsorption capacity (74.0 mg g^{-1}) was measured at a GO concentration of 2 mg mL^{-1}, nearly twice than that measured for activated 2D graphene. In the second part, a thin layer of alumina was deposited on the optimized 3D GBMs to prepare a 3D Al_2O_3 / GBM hybrids. In order to deposit alumina homogeneously on the inner walls of the porous structures, atomic layer deposition (ALD) technique was selected since its principle involves the use of gaseous precursors that facilitate their diffusion. Furthermore, alumina is shown to be deposited at the core of 3D GBMs using advanced and powerful characterisation techniques such as focused ion beam technology (FIB), transmission electron microscopy (TEM), scanning transmission electron microscope (STEM) and electron energy loss spectroscopy (EELS) mapping. This is an unprecedently detailed study of 3D Al2O3 / GBM hybrids, which has not previously been reported. The growth mechanism of alumina on the graphene surface was as well investigated. In contrast to the most approaches which require

additives (surfactants or polymers) to enhance graphene reactivity for ALD deposition, reduced GO forming porous aerogel that offers sufficient seeding sites for alumina formation. The proposed growth mechanism comprises a nucleation stage that results in the formation of primarily islands and leading for the highest ALD duration to a continuous covering layer for high ALD cycles. The 3D Al_2O_3 / GBM hybrids were initially used for CO_2 adsorption studies, however, the adsorption capacity gained was reduced from 74.0 mg g^{-1} to 25.95 mg g^{-1} compared to the 3D GBMs. Thus, in this section, the prepared 3D Al_2O_3 / GBM was used for another environment application which is dye adsorption study. The adsorption capacity of Congo red (CR) of the 3D Al_2O_3 / GBM is much higher than that of pristine / uncovered 3D GBMs. The dominant mechanism in the adsorption process of CR dye by the designed 3D Al_2O_3 / GBM is based on favourable electrostatic interactions between alumina surface and CR. This work is therefore proof-of-concept research in which the 3D Al_2O_3 / GBM hybrids was employed as a superior key component in the construction novel materials for adsorption system with promising adsorption performance toward dye pollutants.

GRAPHENE CHIMIQUEMENT MODIFIE ET AUTO-ASSEMBLE COMME ADSORBANT POUR DES APPLICATIONS EN ENVIRONNEMENT

RESUME DETAILLE EN FRANÇAIS

Nous faisons actuellement face à des problèmes environnementaux majeurs à cause de l'impact de l'activité humaine sur la nature, ce qui compromet l'équilibre des écosystèmes et des hommes eux-mêmes. L'environnement est défini comme la somme totale de tous les éléments vivants et non vivants y compris les processus qui influencent la vie humaine. La pollution, quant à elle, fait référence à la dégradation des ces composants de l'environnement, tels que l'atmosphère, l'eau et les sols. Les activités humaines tels que l'urbanisation, l'industrialisation, l'exploitation minière et le tourisme sont les principaux contributeurs à la pollution mondiale. Historiquement, les industries ont contaminé notre environnement, surtout depuis le début de la révolution industrielle, et notamment, en raison de l'utilisation croissante des énergies fossiles. Au XIX^{e} siècle et pendant une grande partie du XX^{e} siècle, le charbon a été utilisé pour faire fonctionner les machines plus rapidement en remplacement du travail humain. S'ajoute à la pollution décriée de l'air par le dioxyde de carbone (CO_2) par exemple, les sols et l'eau peuvent également être contaminés par l'industrie. Par exemple, les colorants et les métaux lourds sont largement utilisés dans les textiles, l'impression, les cosmétiques, le cuir, les produits pharmaceutiques, les revêtements et de nombreux autres procédés industriels. Par conséquent, une grande quantité d'eau des rivières et d'eau souterraine est polluée par des colorants, des ions de métaux lourds et des composés organiques tels que des polymères et des détergents, qui ont également un impact négatif sur les sols et les écosystèmes. Dans les pays en développement, la

croissance de l’activité humaine présente certains avantages, mais elle doit être prise en considération à un stade précoce, car il est bien établi que de fortes concentrations de pollution affectent négativement la santé et l'économie. Grâce aux principes et pratiques de développement durable, couplés à la recherche locale et internationale, la pollution atmosphérique (en particulier sur l'adsorption de CO_2) et la pollution de l'eau (en particulier l'élimination des colorants) peuvent être limitées ou éliminées, réduisant ainsi les risques pour la santé. En tant que scientifique, notre responsabilité est de trouver des solutions, soit en nous adaptant à ces problèmes et en atténuant leurs effets. Ceci est le plus approprié pour le système naturel, mais il faut parfois plusieurs décennies pour rectifier les problèmes qui existent depuis longtemps en raison de conditions environnementales fortement dégradées. Par conséquent, développer des traitements efficaces pour lutter contre la présence de ces polluants dans la nature représente un aspect majeur à considérer avec urgence.

L'ingénierie environnementale utilise l'adsorption comme l'une des méthodes de traitement les plus efficaces pour réduire la concentration des contaminants en raison de sa robustesse, sa flexibilité et sa facilité d'utilisation. L'une des méthodes les plus rentables, les plus simples et les plus sûres pour éliminer les contaminants de l'environnement est en effet l'adsorption, qui fait l'objet de recherches approfondies pour lutter contre la pollution de l'air et aussi de l'eau. Un des objectifs de ces recherches est de développer des matériaux avec une haute capacité d’adsorption et d’augmenter l’affinité adsorbant-adsorbat. L'adsorption sur des adsorbants solides, en particulier des adsorbants à base de nanomatériaux carbonés, est l'un des moyens les plus efficaces pour capturer le CO_2 ainsi que pour éliminer les colorants. En outre, l'adsorption est également

considérée comme une méthode efficace car elle peut éliminer complètement différents types de colorants. Le procédé d'adsorption peut être physique ou chimique. L'adsorption physique se produit lorsque les molécules d'adsorbat (contaminants) sont liées à la surface de l'adsorbant par une force de liaison physique, forces de van der Waals, par exemple, tandis que l'adsorption chimique implique des liaisons chimiques entre l'adsorbat et l'adsorbant. L'adsorption présente des avantages par rapport aux autres méthodes pour une application pratique en raison de sa conception simple et un faible investissement en termes de coût initial et de terrain requis. Le procédé d'adsorption est largement utilisé pour le traitement des polluants organiques et inorganiques et rencontre une grande attention dan la communauté des chercheurs. Généralement, les taux d'adsorption sont influencés par diverses propriétés chimiques et physiques des adsorbants et des adsorbats ; par exemple, la surface, la porosité, la taille des pores, la dispersion de la taille des pores, la stabilité, la multifonctionnalité (propriétés magnétiques et mécaniques), la charge de surface et la chimie de surface de l'adsorbat. En outre, l'affinité de l'adsorbat, en fonction des propriétés chimiques de la surface de l'adsorbant, est également cruciale. En chimie, un matériau adsorbant est une substance, généralement de nature poreuse avec une grande surface, capable d'adsorber un matériau à sa surface par l'action de forces intermoléculaires. En outre, les adsorbants sont généralement utilisés sous forme de pastilles sphériques, de tiges, d'objets moulés ou de structures monolithiques comprises entre 0,5 et 10 mm. À l'heure actuelle, les adsorbants commerciaux à base de carbone sont les matériaux les plus largement utilisés dans les applications environnementales et énergétiques car ils sont non toxiques, peu coûteux, renouvelables, facilement récupérables des altérations, facilement disponibles et ne produisent pas de boues

résiduelles. Dans l'industrie, le graphène, le gel de silice, le charbon actif, l'alumine activée (oxyde d'alumine) et la zéolite sont parmi les adsorbants les plus fréquemment utilisés. Le choix des adsorbants dépend de certains facteurs, notamment la taille des particules, la nature chimique, la taille et la distribution des pores, la surface et la polarité de surface.

Le graphène, un adsorbant à base de carbone, semble être un adsorbant potentiel pour éliminer une large gamme de polluants (tels que le CO_2, les NO_x, les métaux lourds, les colorants, etc.). K. Novoselov a fait une découverte qui a changé le monde à bien des égards. Cette étonnante substance carbonée 2D découverte est le graphène, d'une épaisse atomique où les atomes de carbone hybridés sp^2 forment un réseau hexagonal dit en nid d'abeille. En raison de ses propriétés particulièrement remarquables (mécaniques, électriques, thermiques, optiques), le graphène est devenu depuis plusieurs années une grande attraction des scientifiques. Le graphène est le plus fin, le plus léger (1 m^2 = 0,77 mg) et le composé la plus dure (entre 100 et 300 fois plus résistant que l'acier) ainsi que le meilleur conducteur thermique et électrique avec une conductivité thermique de 5 $kW.m^{-1}.K^{-1}$ et une mobilité électronique de 15 000 $cm^2.V^{-1}.s^{-1}$. De plus, le graphène présente différents dérivés avec des propriétés différentes mais tout aussi intéressants. Différentes formes de graphène, notamment l'oxyde de graphène (GO) et l'oxyde de graphène réduit (rGO), sont récemment apparues comme des nanomatériaux prometteurs comme matériaux alternatifs pour limiter la pollution de l'environnement et d'autres applications telles que le stockage et la conversion d'énergie, entre autres, en raison de leur structure nano-dimensionnelle fonctionnelle et exceptionnelle. Le GO est un matériau unique qui peut être considéré comme une feuille d'épaisseur nanométrique possédant diverses

fonctionnalités oxygénés telles que les groupes époxyde, carbonyle, carboxyle et hydroxyle. Afin de transformer le graphite en GO, des groupes fonctionnels contenant de l'oxygène sont attachés à la surface par un processus d'oxydation qui accompagne le phénomène d'exfoliation. De plus, les caractéristiques du GO peuvent être modifiées par fonctionnalisation en fonction de l'application.

Le GO a donc l'avantage d'être facilement produit à partir de graphite (un matériau bon marché) en utilisant différentes méthodes chimiques, ce qui se traduit par un taux de production élevé et exceptionnellement rentable. Une deuxième caractéristique du GO est sa capacité à former des colloïdes aqueux stables qui peuvent être utilisés pour assembler des structures macroscopiques avec des processus en solution simple et faible coût. Le premier objectif de ce projet de thèse a été atteint en synthétisant et en caractérisant du GO à utiliser comme matériau de départ pour la préparation d'adsorbants à base de graphène 2D et 3D. Le GO a été synthétisé par la méthode de Hummers qui permet une production de graphène en quantité élevée (grammes) avec une rentabilité exceptionnelle. Dans cette étude, la modification chimique de la surface de GO est réalisée par deux approches très différentes (réduction chimique et dépôt d'un oxide métallique par Atomic Layer Deposition (ALD)). La caractérisation des matériaux préparés est réalisée de façon poussée en utilisant un ensemble de techniques complémentaires.

La première partie du travail de thèse a porté sur l'activation du GO par voie chimique et physique et leurs performances pour l'application de capture de CO_2 a été étudiés. Quatre caractéristiques différents ont été analysées, notamment (i) la surface ; (ii) le volume des pores ; (iii) la taille des pores et (iv) le taux de réduction chimique des groupes oxygénés de surface. Selon les résultats, premièrement, le GO activé chimiquement à 800 °C (GO-CA 800), possède une surface spécifique

(SSA) plus élevée que le GO activé physiquement à 900 °C (GO-PA 900) qui est de 1060,5 $m^2 g^{-1}$ et 762,5 $m^2 g^{-1}$, respectivement. Deuxièmement, GO-PA 900 (2,31 $cm^3 g^{-1}$) présente un volume de pores plus élevé que GO-CA 800 (0,99 $cm^3 g^{-1}$). Troisièmement, GO-CA 800 a des pores plus petits que GO-PA 900, à 3,65 nm et 12,14 nm respectivement. Enfin, le GO-CA 800 présente une surface avec moins de groupes oxygénés par rapport à GO-PA 900, ce qui en réduit l'acidité de surface et rend l'adsorbant GO-CA 800 potentiellement plus propice à la capture du CO_2. Les résultats d'adsorption montrent, tout d'abord, une augmentation significative de la capacité d'adsorption après activation qu'elle soit chimique ou physique par rapport au GO de départ (Figure 1). Par ailleurs, la capacité d'adsorption après activation chimique est supérieure à celle mesurée après activation physique dans les meilleures conditions. Cela peut s'expliquer par une surface, des pores plus petits et une surface moins acide pour GO-CA 800 que pour GO-PA 900.

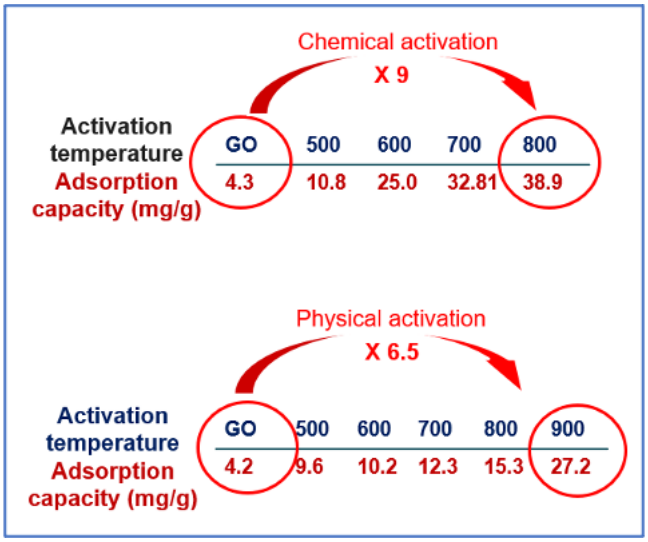

Figure 1 Capacité d'adsorption du CO_2 en fonction de la température d'activation par voir chimique (en haut) et par voie physique (en bas).

Le deuxième volet de la thèse concerne l'assemblage du GO en réseau interconnecté de feuilles de graphène dont l'intérêt réside sans conteste dans l'exploitation de sa surface d'adsorption dans un matériau macroscopique, ce qui permet d'éviter les problèmes de toxicité d'un matériau divisé et de pouvoir envisager la recyclabilité de l'adsorbant développé. Le GO peut être transformé en rGO par un processus de réduction. Il existe de nombreuses techniques pour la conversion de GO en rGO et chaque méthode développée a ses propres avantages et inconvénients. En outre, en fonction des paramètres de synthèse de réduction, une large gamme de tailles de nanopores, dans les matériaux rGO, peut être obtenue, ce qui permet à rGO d'être potentiellement applicable comme matériau de départ pour un processus de modification ultérieure. Dans le cadre de l'exploitation des propriétés des nanofeuillets de graphène 2D à l'échelle du nanomètre, leur assemblage dans des structures macroscopiques hiérarchisées ou macrostructures à base de graphène (GBM) a suscité l'intérêt des chercheurs ces dernières années. Le réseau carboné sp^2 pouvant être fonctionnalisé de plusieurs manières, la polyvalence de ces GBM en termes d'affinité chimique est un outil remarquable pour contrôler les interactions d'interface. Pour toutes ces raisons, de tels substrats à surface intelligente font l'objet de nombreuses études dans la communauté scientifique.

Parmi les articles de revue déjà publiés et liés au sujet des GBM 3D ces 4 dernières années, la plupart d'entre eux se concentrent sur des domaines d'application particuliers centrés néanmoins sur des problématiques environnementales et énergétiques. Au fil des années depuis la découverte du "matériau miracle" en tant que premier cristal 2D d'épaisseur atomique isolé, le nombre de publications liées aux macrostructures 2D et 3D à base de graphène n'a cessé d'augmenter (Figure 2).

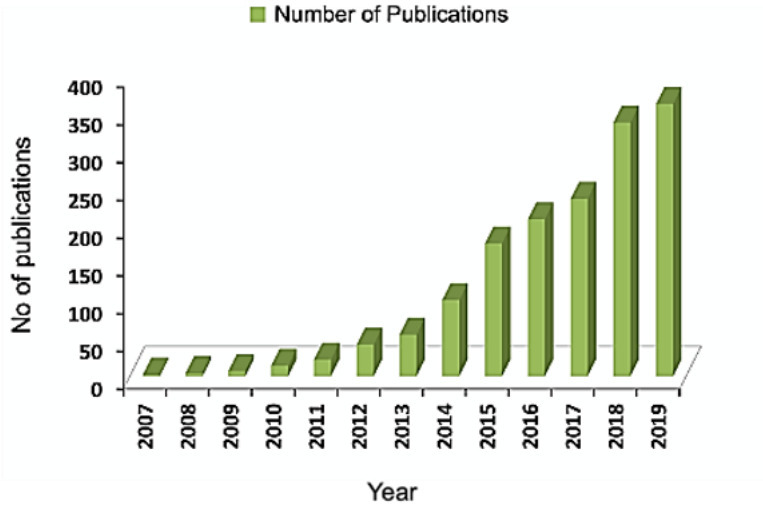

Figure 2 Nombre de publications de 2007 à 2019 sur le thème du graphène 2D et 3D (source Web of Science).

Pour ce travail de thèse, les travaux ont porté sur la modification du graphène 2D en réseaux poreux macroscopiques 3D de graphènes auto-assemblés (GBM). Le processus hydrothermal utilisé permet à partir d'une dispersion homogène de GO (à pH 10) d'induire l'auto-assemblage des nanofeuillets de GO réduits en raison de la modification chimiquement des groupes fonctionnels de surface par une réaction de réduction.

La combinaison de la surface carbonée des GBM avec des composés inorganique est un sujet relativement nouveau. Les chercheurs utilisent la plupart du temps des méthodes d'imprégnation en phase liquide où un précurseur du composé inorganique est solubilisé dans l'eau et la formation du composé à base de métal avec des GBM 3D est ensuite initiée pour qu'il se dépose sur les surfaces du graphène. De nouvelle techniques de dépôt en phase gaz comme l'ALD, que nous avons utilisée, permet un meilleur contrôle de la pureté du dépôt et permet une meilleure diffusion des précurseurs inorganiques au cœur du matériaux poreux.

Nous avons ainsi modifié chimiquement les parois de graphène du GBM 3D en utilisant la technique ALD pour l'élimination du colorant rouge Congo (RC) pour une application de traitement de l'eau. Des images par microscopie électronique à balayage (MEB) des GBM préparées après le dépôt de l'alumine sont montrés sur la figure 3.

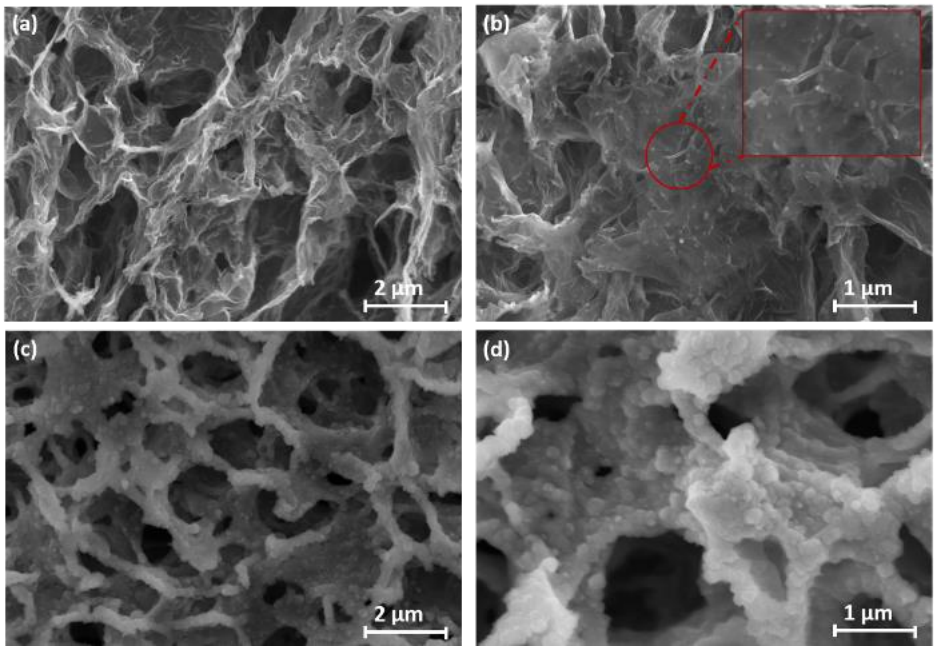

Figure 3 Images typiques de MEB des GBM après dépôt d'alumine par ALD a) et b) 50 cycles et c) et d) 300 cycles.

D'après les observations par MEB de la figure 3 réalisées sur une fracture au cœur des matériaux hybrides poreux préparés, l'alumine semble présente sur toutes les surfaces graphéniques internes. Ce résultat a été confirmé par des méthodes de pointe comme des observations par microscopie électronique en transmission (MET) sur des lames minces découpées au cœur du matériau par focused ion beam (FIB) ; approche non encore trouvé dans la bibliographie pour ce type de matériau. La capacité d'adsorption du RC de ces hybrides s'est révélée très intéressante avec capacité d'adsorption (89 %) très supérieure à celle du GBM 3D

(20 %) au premier cycle et une adsorption d'élimination du RC de 98 % au deuxième cycle. Nous avons ainsi développé un hybride alumine/graphène poreux non encore rapporté pour la dépollution de l'eau.

CHAPTER 1

INTRODUCTION

1.1 Environmental pollution

Generally, environment is defined as the sum total of all the living and non-living elements as well as the processes that influence human life. Pollution, on the other hand, refers to the degradation of environmental components, such as the atmospheric, water, and soil. Human activities such as urbanization, industrialization, mining, and tourism are among the main contributors to global environmental pollution (Ajibade et al., 2021; Zhou et al., 2021). Historically, industries have contaminated our environment, especially since the start of the industrial revolution, and in particular, due to the increasing use of fossil fuels. Coal was used in the 19th century and for much of the 20th century to make machines work faster, replacing human labour. Added to the decried pollution in air by carbon dioxide (CO_2) for example, soils and water can also be contaminated by industry. For example, dyes and metals have widely been used in textiles, printing, cosmetics, leather, pharmaceuticals, metal plating, and many other industrial processes (Elgarahy et al., 2021; Kamil Kadhim Lawi et al., 2021). Consequently, this results in a large amount of river water and groundwater being polluted with dyes, heavy metal ions and organic compounds such as polymers and detergents, which also have negatively impact soils and ecosystems. In developing countries, the increasing number of human activities has certain benefits, but it should be taken into consideration at an early stage because high concentrations of pollution have been well established to negatively affect health and economics (Ghorani-Azam et al., 2016; Manisalidis et al., 2020). With the help of sustainable development

principles and practices, coupled with local and international research, atmospheric and water pollution can be contained or eliminated, reducing health risks. Thus, in the following sections, these issues are discussed in more detail.

1.1.1 Atmospheric pollution

Over the past few decades, greenhouse gases (GHGs) emissions and atmospheric pollutants have been increasing rapidly worldwide due to the rapid growth of the global economy based on fossil fuels. Besides, the combustion of non-renewable fossil fuels accounts for approximately 80 % of global energy consumption, resulting in massive CO_2 emissions and leading to global warming. The term global warming refers to the increase in average temperature of Earth's atmosphere and oceans observed over the past few decades (Al-Ghussain, 2019). In general, global warming occurs when our atmosphere traps the heat radiating from the Earth toward space. As the sunlight reaches the Earth, clouds, atmospheric particles, the reflective ground surface, and the surface of the oceans naturally reflect about 30 % of the sunlight back to space, while the remaining heat is absorbed by the oceans, the air, and the land (Purba et al., 2022). In spite of this, some of the solar energy is absorbed by gases in the atmosphere known as GHGs which are responsible of Earth's atmosphere warming. Several GHGs present in the atmosphere create a barrier layer that trap the heat to escape. These gases include CO_2, methane (CH_4), nitrous oxide (N_2O), and industrial gases hydrofluorocarbons (HFCs), perfluorocarbons (PFCs), sulfur hexafluoride (SF_6), etc. Among these gases, CO_2 is the primary GHG emitted through human activities (deforestation, fossil fuel burning, transportation, electricity, industries, etc..). In comparison to other GHGs, CO_2 gas alone accounts for approximately three-fourths of the global warming effect (Walker et al., 2022). Approximately 76% of total GHGs are

produced by burning fossil fuels in industrial processes (including oil refineries, power plants, ammonia/ethylene oxide production, cement production, and iron/steel production), forestry, and agriculture. This global issue has become a big challenge nowadays due to its detrimental effect to the Earth and its entire ecosystem. In order to address this issue, the Paris Climate Agreement 2015 replaced the Kyoto Protocol 1997, which was ratified by 200 countries. It aims to reduce greenhouse gas emissions worldwide while maintaining the Earth's temperature rise to below 2 °C above the pre-industrial levels, which are defined as the average temperature between 1850 and 1900. In order to achieve the target, negative emissions must be controlled (Wigley, 2018). Besides, it also has been decided to limit the atmospheric CO_2 emission to 550 ppm within the next 100 years. Many industrial companies around the world have implemented a variety of measures to limit their CO_2 emission through numerous measures such as the Kyoto Protocol, the Copenhagen Accords and the Cancun Agreements. In order to reach this target, renewable energy sources must be considered in conjunction with a low carbon economic approaches. There have been several CO_2 capture technologies proposed and developed so far (Dindi et al., 2019; Yoro and Daramola, 2020). Among them, adsorption has been suggested as a possible method due to its low energy consumption, simplicity of design, and less corrosive nature (Adegoke et al., 2022; Aghel et al., 2022; Akeeb et al., 2022).

1.1.2 Water pollution

Today, water pollution is one of the most significant threats to the environment due to the amount of toxic chemicals introduced into water bodies, such as groundwaters, lakes, rivers, oceans, etc., where they are dissolved or suspended or settle on the surface (Saravanan et al., 2021). In this way, the quality

of the available water and ecological systems is degraded. Moreover, pollutants indeed seep through to groundwater, which could contaminate the water use in daily activities, including drinking. In spite of the fact that water pollution can occur in various ways, one of the primary sources should be attributed to the large amount of presence of non-biodegradable organic compounds, especially those from textile dyes, cosmetic, pharmaceutical, photography, plastics and paper industry (Berradi et al., 2019). As a result of the presence of sulphur, naphtha, acetic acid, dyes, nitrates, soaps, and heavy metals such as copper, lead, arsenic, cadmium, nickel, mercury and cobalt, as well as certain auxiliary chemicals, the effluents are highly toxic.

Presence of sulphur, naphthol, vat dyes, nitrates, acetic acid, soaps, chromium compounds and heavy metals like copper, arsenic, lead, cadmium, mercury, nickel, and cobalt and certain auxiliary chemicals all collectively make the effluents highly toxic (Manzoor and Sharma, 2020; Velusamy et al., 2021). Other harmful chemicals present in the water may be formaldehyde based dye fixing agents, hydro carbon based softeners and non-bio degradable dyeing chemicals. Additionally, the most significant environmental damage caused by the textile industry is the remaining discharge of partly or nontreated effluents into water bodies, which comprises about 80 % of the total emissions produced by this industry (Laxmi and Kaushik, 2020; Liu et al., 2017). It has been reported in the past that a many effluents have been contaminated by dyes; in fact, it is stated that nearly 8×10^5 tonnes of dye stuffs are discharged each year along with more than 1×10^5 tonnes of commercial dyes (Slama et al., 2021a). These pollutants pose a toxic, mutagenic, and carcinogenic risk to living organisms due to their resistance to biodegradation and decomposition in nature, as well as their incompatibility and

accumulation within the food chain. Thus, a reliable and sustainable solution should be developed. There are many ways to remove dyes from the wastewater such as adsorption, ion exchange, coagulation-flocculation, membrane etc. However, adsorption remains the most effective method for removing pollutants in wastewater since it is a cost-effective, simplicity of design, ease of operation and non-toxic materials and development of ideal adsorbent has been a growing concern for most environmental researchers (Rathi and Kumar, 2021).

1.2 Adsorption

Adsorption on solid adsorbents, particularly carbon-based adsorbents, is one of the most efficient means of capturing CO_2 as well as removing dyes. Besides, adsorption is also considered as an effective method. In principle, the adsorption process can be both a physical and chemical process. A physical as well as a chemical process can be employed in the process of adsorption. Physical adsorption occurs when adsorbate molecules (contaminates) are bound to the adsorbent surface by a physical bonding force called van der Waals forces while chemical adsorption involves chemical bonds between the adsorbate and adsorbent (Barquilha and Braga, 2021). Adsorption has advantages over other methods due to its simple design and the fact that it requires a low initial investment in terms of both cost and land required (Saxena et al., 2020). The adsorption process is widely used for treatment of organic and inorganic pollutants and meet the great attention from the researchers. In general, adsorption happens by adhering substrate to solid or liquid, called sorbent or adsorbent, by adhesion of gaseous, liquid, or solid materials. There are two types of adsorption systems, liquid-gas and liquid-liquid. When a liquid material is used as an adsorbent, its interfacial layer is referred to as a film, micelle, or emulsion. In the case of solid-liquid or solid-gas systems, the adsorbent is solid,

so the interfacial layer model is approved for the adsorption process. Interfacial layers describe the equilibrium between the bulk and adsorbent phases. In the first region, the substrate binds to the sorbent surface, while in the second region, the sorbent surface layer is present. In order to understand the mechanism of interfacial layers, two principals must be considered: physical adsorption and chemical adsorption (Deng *et al*., 2019).

Generally, adsorption rates are influenced by various chemical and physical properties of adsorbents and adsorbates; for example, surface area, porosity, pore size, pore size dispersion, stability, multifunctionality (magnetic and mechanical properties) surface charge, and surface chemistry of the adsorbent (Busetty, 2019; Sahoo and Prelot, 2020; Yang et al., 2021). Besides, the affinity of the adsorbate, depending on the chemical properties of the adsorbent surface is also crucial. In chemistry, adsorbent material, usually porous in nature with a high surface area, that is capable of adsorbing material on its surface through the action of intermolecular forces. Besides, adsorbents are usually used as spherical pellets, rods, moulded objects, or monolithic structures ranging between 0.5 and 10 mm. At present, commercial carbon-based adsorbents are the most widely used materials in environmental and energy applications as they are non-toxic, low-cost, renewable, easily recoverable from alters, readily available, and produce no waste sludge (Rout and Jena, 2021; Saravanan et al., 2022; Soffian et al., 2022). In industry, graphene, silica gel, activated carbon, activated alumina (alumina oxide), and zeolite are among the most frequently used adsorbents. The selection of adsorbents depends on some factors including the particle size, chemical nature, pore size and distribution, surface area and surface polarity.

1.3 Graphene based materials

1.3.1 Pristine or ideal graphene

In 2004, two scientists from Manchester University, A. Geim and K. Novoselov, made a serendipitous breakthrough, a discovery that will change the world in many ways (Geim and Novoselov, 2010). This amazing 2D-carbon material, known as graphene, exhibits a hexagonal structure and sp^2-bonded carbon atoms. To date, few methods have been used to synthesize completely two-dimensional (2D) atomic crystals. The extraordinary characteristics of graphene originate from the 2p orbitals, which form the π state bands that delocalize over the sheet of carbons that constitute graphene. Besides, due to its special and superior properties (mechanical, electrical, thermal, optical), graphene has become the main attraction among scientists for a number of years. Graphene is the thinnest, lightest ($1\ m^2 = 0.77\ mg\ m^{-2}$) and hardest substance (between 100-300 times stronger than steel) as well as it possesses remarkable thermal and electrical conductors with a thermal conductivity of $5\ kW\ m^{-1}\ K^{-1}$ and an electron mobility of $15{,}000\ cm^2\ V^{-1}\ s^{-1}$. Moreover, graphene's zero band gap and its engineered analogue, which has a small overlap between valence and conduction bands, have provided tremendous opportunities for applied and fundamental research. A single layer of graphene can withstand up to $42\ N\ m^{-1}$ of stresses, with Young's modulus of 1.0 TPa (Abooalizadeh et al., 2021; Mortazavi, 2017). The phonon pathways in single layer graphene are different. Indeed, graphene, even at this lower conductivity, performs better than copper (Cu) (Tiwari et al., 2018).

1.3.2 Graphene derivatives

A monolayer of carbon atoms is commonly present as an ultrathin film, particularly when it is pasted with templates (Tiwari et al., 2018). Further, this monolayer graphene can be skimmed off and redeposited onto a substrate for further use. Additionally, graphene can also be seen in other forms as derivatives. Figure 1.1 show the structural of ideal graphene, GO and rGO and 3D graphene based macrostructure (GBMs)

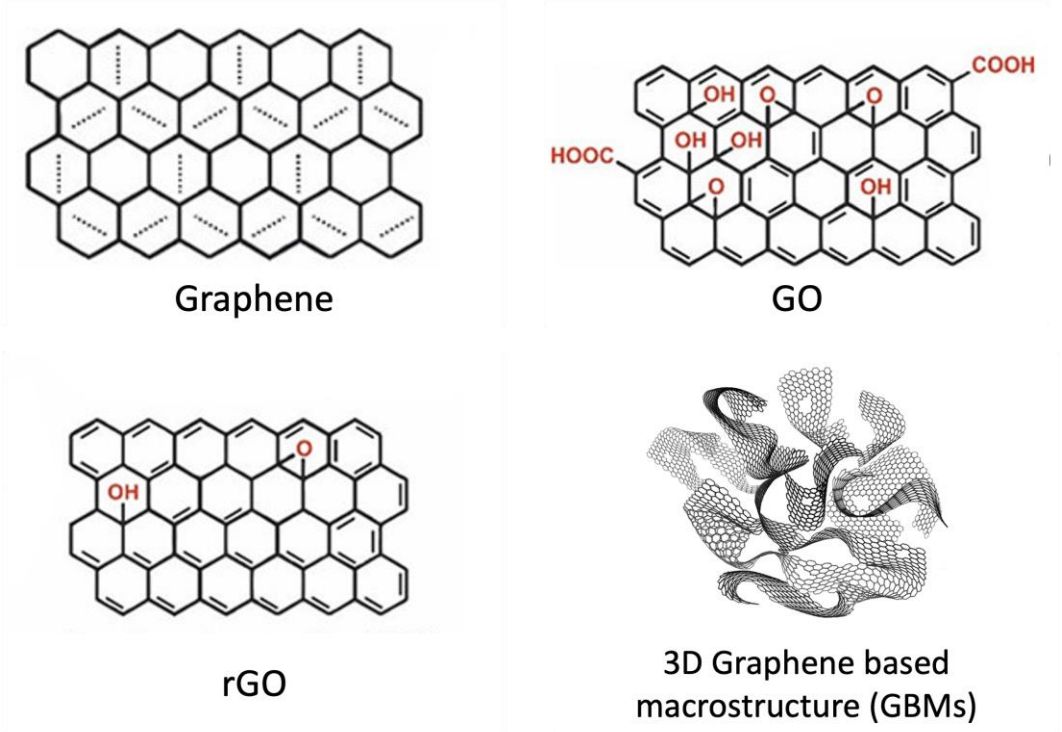

Figure 1.1 Illustration of ideal graphene, GO and rGO and 3D graphene based macrostructure (GBMs) (Anwar *et al*., 2020).

Different forms of graphene include GO and reduced graphene oxide (rGO) have recently emerged as a promising nanomaterials for alternative environmental remediation materials and other applications such as energy storage and conversion among others due to their functional nano-dimensional structure and outstanding

properties. GO is a unique material that has various oxygen-containing functionalities such as epoxide, carbonyl, carboxyl, hydroxyl groups (Lin et al., 2016; Tiwari et al., 2016). Furthermore, the characteristics of GO can be altered by different functionalization techniques. In addition to its electron-rich oxygen species, GO also has an electron-rich graphene backbone, making it an excellent material for a variety of applications, particularly in material chemistry.

GO has the advantage of being easily produced using graphite (a material that is cheap) using different chemical methods, resulting in a high production rate that is exceptionally cost-effective. A second characteristic of GO is its ability to form stable aqueous colloids that can be used to assemble macroscopic structures with less expensive solution processes. Although GO sheets contain some defects on the surface, the overall size of the unit cells is similar to graphene. Thus, GO is an oxidized version of graphene containing oxygen. GO can also be transformed into rGO through a reduction process (Papageorgiou et al., 2015). There are numerous techniques for the conversion of GO to rGO and each developed method has its own advantages and disadvantages (Tiwari et al., 2016; Yang et al., 2015). Besides, depending on the reduction synthesis parameters, a wide range of nanopore sizes, in rGO materials can be achieved, which allows rGO to be potentially applicable be used as starting material for further modification process. It is also important to understand that different reduction processes will result in different quality rGOs with highly altered properties. The reduction process, along with affecting the dispersibility of rGO, also has an impact on the colloidal behaviour of rGO due to a decrease in the critical concentration of coagulation. Even though the graphene structure is not fully recovered by the reduction of GO, rGO still holds useful properties such as controllable functionality, high electric and thermal

conductivity, readily available initial materials, and a simple and cheap way to prepare the material.

The utilization of graphene sheets into macroscopic structures is one of the important issues due to the fact that 2D graphene sheets are likely to restack together in bulk materials due to strong interactions and van der Waals forces. As a result of aggregation of graphene sheets and crumbling, the surface area, and mechanical strength of graphene decrease significantly, negatively impacting its practical application. Nowadays, the study of three dimension (3D) graphene materials has recently attracted much attention due to their ability to preserve the intrinsic properties of 2D graphene sheets as well as provide advanced functions with improved performance in a variety of applications, notably environmental applications, by inhibiting the agglomeration behaviour of 2D graphene sheets (Shen et al., 2015). According to recent studies, the assembly of graphene into 3D hierarchical architectures has been recognized as one of the most promising strategy for either "top down" or "bottom up" nanotechnology and has become one of the most active research fields in the past four years. The bottom-up methods comprise the synthesis of 3D graphene-based macrostructures (GBMs) from alternative carbon sources either by CVD or epitaxial growth while the top-down methods involve the separation of stacked layers within graphite to yield graphene nanosheets, also called exfoliation. In the top-down methods, the intention is to induce an increase of the inter-layer spacing and exfoliate the graphene layers by means of mechanical and/or chemical forces. These two techniques ultimately contribute to the framework of different types of graphenes (Mohd Firdaus et al., 2020). The structure, morphology, and properties of the resulting graphene, such as

type of graphene, surface chemical properties, structural quality and also its physical properties are usually dependent on the fabrication process.

The 3D macrostructures have become increasingly popular, resulting in new collective physiochemical properties that are remarkably different from the properties of the individual building blocks and bulk materials (Shen et al., 2015). Today, the potential application of 3D macrostructures has been greatly enhanced. In relation to 3D GBMs, it is important to mention that most of the research has arisen since 2013, making 3D GBMs at a very early stage with interesting prospects. In 3D GBMs, micropores, mesopores, and macropores are combined together such that micropores and mesopores provide high surfaces, while macropores ensure that all surfaces are accessible. Surface properties of 3D GBMs are highly dependent on the experimental conditions and graphene characteristics, which are critical to the self-assembly process. Despite that limitation, 3D monoliths based of graphene have some advantages in terms of their integrated morphology, which reduces toxicity as it is not a nanoparticle powder, facilitate easy manipulation, and prevent the release of nanosheets into the environment.

1.4 Problem Statement

Environmental engineering employs adsorption as one of the most effective methods of treatment for contaminants due to its robustness in handling a wide range of pollutants, as well as its ease of use. One of the most cost-effective, simplest, and safest methods of removing contaminants from the environment is adsorption, which is being researched extensively both for air and water pollution, with the goal of evaluating the relation between the adsorption capacity and the adsorbent characteristics of various adsorbent-adsorbate systems. Graphene, a

carbon-based adsorbent, appears to be a potential adsorbent for removing a wide range of pollutants (such as CO_2, NOx, heavy metals, dyes, etc.). The release of 2D graphene into the environment, however, poses a potential health risk due to rapid increase in production and applications.

One of the key objectives of this domain study is to monitor the graphene intersheet interactions that are the driving force for the self-assembly process and possibly prevent or restrict the 2D graphene restacking to maximize the accessible surface area and porosity of the prepared 3D GBMs. The self-assembly technique is sensitive to the experimental conditions used (concentration of temperature graphene, drying phase) and to the graphene characteristics (size and shape, thickness, surface chemistry) which both have a major impact on the resulting properties of 3D GBMs. At the current stage of 3D GBMs development, it is not clear which of the approach strategies lead to the best material in term of surface and structural properties. Further fundamental investigations are needed in order to better control the assembly process and the structural properties including surface area, pore volume and pore size. Besides, the chemistry and interaction forces involved in the process of self-assembly are also not yet fully understood.

In this work, the fabrication of 3D GBMs with a two-step approach including an environment-friendly hydrothermal assembly process incorporating with ascorbic acid (AA) as a reductant are described. Due to the sensitivity of the self-assembly technique, the effect of the GO concentration of the starting GO dispersion (at pH 10) was particularly investigated in order to determine how it impacts the fragility and porosity of GBMs. Next, the chemical modifications by functionalization or combination with different compounds, such as nitrogen containing group, surfactants, organic polymer and metal or metal oxide, are of

great interest for GBMs since they have been shown to enhance the affinity for the target molecules (pollutants) on the surface of 3D GBMs. However, it appears that most of the modification methods are complex, and the chemistry of the modified 3D GBMs surfaces with other compounds is a relatively new subject. In previous studies, researchers have used the impregnation method to combined metal-based compounds with 3D GBMs in order to modify their chemical properties, and this method is quite common. The accessibility to the internal walls of the 3D GBMs and the diffusion issue, however, make it difficult to control graphene interactions even after assembling the 3D GBMs. Thus, a novel and revitalised technique involving gas phase metal deposition, by atomic layer deposition (ALD) on the 3D GBMs surface is proposed. Since it operates under a gas phase, it offers advantages in terms of precursor diffusion; no contamination; phase control of deposited inorganic compounds; and the ability to deposit nano-films or nanoparticles.

The chemical modification of 3D GBMs surfaces by ALD is a relatively new field, so it is vital to fully understand the surface chemistry and the structural properties of the material. As a result of their shape and morphology, this 3D GBMs hybrids have been found to be quite challenging to characterize. Thus, proper characterization techniques need to be selected in order to fully understand the characteristic of the developed materials. In order to better understand the fabricated material, some standard and advanced characterization techniques have been applied to study the surface chemistry and structural properties of the chemically modified 3D Al_2O_3 / GBM hybrids. SEM and advanced methods (TEM/STEM/EELS on thin lamellas prepared by FIB) are among the techniques used.

1.5 Research Objectives

The objective of this research is to investigate and optimize the chemical modification of graphene-based materials to make their practical use reliable for environmental applications. The aim of the research is achieved via the following objectives to:

1. To synthesis and characterize GO to be used as starting materials for the preparation of 2D and 3D graphene-based adsorbents and to study the related mechanisms.

2. To study the structural and the chemical properties of activated GO by chemical and physical activation and analyse their performance for CO_2 capture in term of material properties.
3. To modify 2D graphene into 3D macroscopic self-assemblies of graphene (GBMs) for CO_2 capture.

4. To chemically modify the 3D GBMs by ALD to achieve the successful hybrid materials for removal of Congo red dye.

1.6 Scope of Study

The scope of this work covers the synthesis of GO, assembly of 3D GBMs and the modification of 3D GBMs by using suitable chemical approaches. The as-synthesised adsorbents were characterized using elemental analysis (EDX), scanning electron microscopy (SEM), transmission electron microscopy (TEM) and scanning TEM (STEM), surface area and pore size distribution with N_2 adsorption-desorption isotherms by Brunauer–Emmett–Teller (BET), Fourier Transform infrared spectroscopy (FTIR), Thermogravimetric Analysis (TGA),

Raman spectroscopy and X-ray photoelectron spectroscopy (XPS). The adsorption study for CO_2 using pristine GO and activated graphene by physical and chemical activation were investigated to determine the optimum adsorption conditions. Then, pristine 3D and modified 3D GBMs by ALD were investigated on Congo Red (CR) dye removal application.

1.7 Thesis Organization

There are five chapters covered in this thesis and each chapter describes the detail of the research study. Chapter 1 (Introduction) provides a general overview of the thesis. This chapter starts with a brief introduction on environmental pollution. Then, the adsorption process and GBMs materials including graphene and graphene derivative are also described in detail. The chapter also encloses problem statement, research objectives and scope of study. Finally, it is followed by the organization of thesis.

Chapter 2 (Literature review) consists of survey of published literature that has been done on the research topic. The section begins with the background of environmental pollution, particularly air and water pollution. The following section briefly discussed the concept of adsorption and the mechanism. Besides, further discussion was well discussed regarding family of graphene, the properties and synthesis method of 2D and 3D graphene. Later, the surface modification of graphene in term of physical and chemical modification and modification by combining metal-based particles or thin films with graphene and further by ALD of aerogel are being discussed in this section.

Chapter 3 (Materials and Methods) describes the detail of material and chemicals used throughout this study. Description of experimental set up, the 2D

and 3D GBMs preparation, structural, surface, and chemical characterization, process variable studies and adsorption study are presented in this chapter.

Chapter 4 (Result and Discussion) comprises the important research findings gained from this work. This chapter is the main components, and it consists of four sections which includes preparation of GO as starting material and its characterization to verify the success of the synthesis. Next, the modification of GO by physical and chemical activation were studied and further characterization for both approaches were performed and the performance towards CO_2 capture by these two approaches was studied and discussed. Furthermore, the self-assembling process of 2D GO by chemical reduction using AA into 3D interconnected hierarchical porous networks and the optimization study of the outcome 3D GBM. In addition, the mechanism of AA reduction and crosslinking has also been discussed. Lastly, the chemically modified 3D GBMs by ALD by alumina covering is presented in section. All the morphological and structural characterizations as well as performance towards removal of Congo Red have been described accordingly.

Chapter 5 (Conclusions and Recommendations) summarizes all the important findings obtained from this research work. The future recommendations are presented as well.

CHAPTER 2

LITERATURE REVIEW

The present chapter reviews the literature on nanomaterials having a potential to be used as nano-adsorbents for environmental applications, especially graphene-based materials. Section 2.1 gives a brief overview on various types of environmental pollution, both air and water pollution. The following section discusses briefly the concept of adsorption and its mechanism. Section 2.3 focuses on carbon based materials as adsorbent, specifically graphene and further discussion of graphene, graphene derivatives, their properties and synthesis of 2D and 3D graphene-based materials. Besides, in section 2.4, the surface modification of graphene in term of physical and chemical modification, modification by combining metal-based particles or thin films with graphene and further by ALD on 3D porous graphene-based aerogel surface are discussed in this section. Lastly, for section 2.5, the effects of surface area, pore size, and surface chemistry on environmental performance are discussed and a summary about the obtained results are included in section 2.6.

2.1 Environmental pollution

2.1.1 Air pollution by CO_2

CO_2 is a chemical compound comprised of one carbon and two oxygen atoms. It is also known as a colourless and non-flammable gas at normal temperature and pressure. As a primary contributor to greenhouse gases, it is typically ranked higher than other pollutants such as methane, water vapor, nitrous

oxide, and ozone, which accounts for nearly three-quarters of the total pollution. In response to rising global energy demand, CO_2 concentrations in the atmosphere are rising significantly as a result of high combustion of organic materials and fossil fuel. According to the Carbon Dioxide Information Analysis Center (CDIAC), the global emissions rose from 2 billion tons of CO_2 in 1900 to over 35 billion tons in 2015 while the data from Global Carbon Project showed an additional annual increase of 2.7 % and 0.6 %, respectively in 2018 and 2019 (Le Quéré *et al*., 2015). In fact, increasing in CO_2 emission and other greenhouse gasses leads to an increase in the average global temperature.

The independent analyses by NASA's and the National Oceanic and Atmospheric Administration (NOAA) reported that the average global surface temperature of the earth has risen more than 1 ^{o}C since 1880 and they believe the emission of this century will also contribute to detrimental climate change in the short and long term (Smith *et al*., 2008). In order to combat global warming, Kyoto Protocol encourages 37 developed nations and the European Union to diminish the greenhouse gas emissions by an average of 5.2 % below those of 1990 between 2008 and 2012 (Lau *et al*., 2009). Besides, the Paris climate agreement also intends for the global temperature increase to be restricted to 1.5 ℃ or 2 °C above pre-industrial level by 2100. Concerns regarding the sharp rise in CO_2 concentration in the atmosphere and its effect on climate change have sparked a global research initiative to capture and store CO_2 gas from point source emissions. In fact, emission of CO_2 to the atmosphere can be reduced by few ways, for instance by reducing energy intensity, reducing carbon intensity, and improving the carbon capture and storage (CCS). Nonetheless, it is reported that, at sustainable costs, the

CCS strategy was able to reduce more than 50 % of current CO_2 emissions from the point sources (Hasan *et al*., 2015).

The main principle of the CCS is illustrated in Figure 2.1(a) where the CO_2 emission is first captured, then the compressed CO_2 is transported through the pipelines for storage in geological formations including in ocean, mineral carbonates, or used as feedstock for industrial processes (Firdaus *et al*., 2021). In addition, the CO_2 capture is more probably to be implemented to large point sources like power plants compared to small and mobile sources like transportation, as it is more cost-effective. Basically, there are three forms of carbon capture approaches depending on the source of fuel, CO_2 partial pressure and gas flow pressure which are: (1) direct air capture (DAC) (2) oxyfuel combustion, (3) pre-combustion and (4) post-combustion (Madejski *et al*., 2022). The summary of the CO_2 capture approaches is presented in Figure 2.1(b). Post combustion has been found to be more favourable according to research. In post-combustion, CO_2 is absorbed after fossil fuels are burned with air, thus allowing the CO_2 to be separated from the NO_x and SO_2 flue gases. Additionally, it offers process simplicity, extremely low energy consumption, simplicity of regeneration, affordable prices, lack of harmful substances and can be applied to a broad range of temperatures.

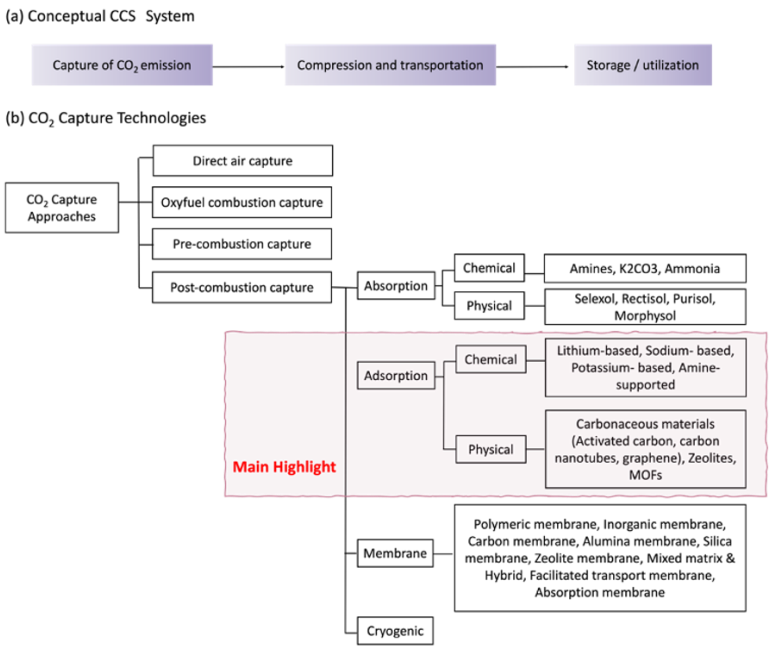

Figure 2.1 (a) The main principle of the CCS (b) type of CO_2 capture technologies.

2.1.2 Water pollution

Water is a critical resource for both global life and human development. The major industries that are causing the release of dyes in the environment are shown in Figure 2.2. The major effluents seen in the global environment are generated by the textile, dyeing, paper and pulp, tannery, and paint industries, as well as the dye manufacturing industry. In terms of water consumption and pollution, the textile industry accounts for approximately 54 % of all dyes released into the environment. Globally, the textile industry generates approximately one trillion dollars annually, contributes 7 % of world exports, and employs approximately 35 million people.

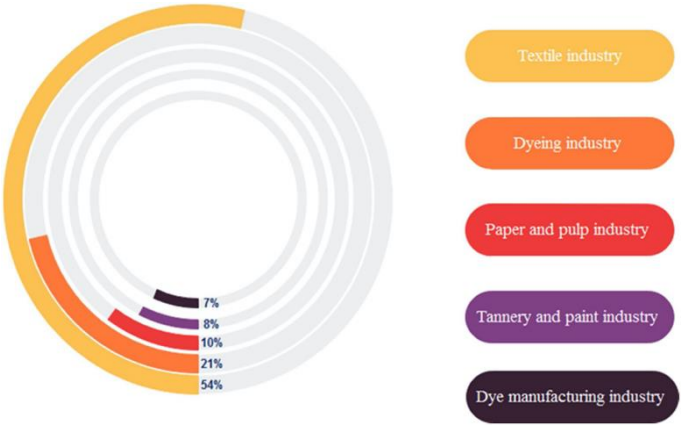

Figure 2.2 Several major industries release dyes into the environment (Samsami *et al*., 2020).

Textile industry is however responsible of primarily damages to the environment caused by the discharge of untreated effluents into water bodies, which typically account for 80 % of the total emissions produced by the textile industry. In most residual waters from the textile industry, there are relatively high levels of chemical oxygen demand (COD) and biochemical oxygen demand (BOD) and a greater emphasis should be placed on non-biodegradable organic compounds, particularly textile dyes (Orts *et al*., 2018). Further, textile dyes not only degrade the aesthetic quality of water bodies, but also inhibit plant growth, impair photosynthesis (Hassan and Carr, 2018), enter the food supply chain, and cause recalcitrance and bioaccumulation, as well as promote mutagenesis, toxicity, and cancer (Sharma *et al*., 2018).

According to Slama *et al.*, the textile industry uses dyes and pigments to colour their products, and there are more than 100,000 dyes available commercially with over 8 $x10^5$ tonnes of dyes produced per year (Slama et al., 2021b). Additionally, these dyes are considered as one of the significant pollutants and they

are referred to as 'visible pollutants'. A range of classes of dyes is used in textile industry including disperse, reactive, acid, basic, direct, azoic, sulfur, and direct dyes. Table 2.1 presents a detailed description of dyes according to their application. In particular, vat, azoic, sulfur, and disperse dyes are insoluble in water and therefore easy to separate from effluent. In contrast, dyes can also be soluble organic compounds, including reactive, direct, basic, and acid dyes and due to their high solubility in water, some conventional methods are not effective in removing them.

At the end of the 1990s, dye removal methods consisted only of preliminary water purification processes such as equalization and sedimentation since there was no limitation on dye effluent discharge (Robinson *et al.*, 2001). However, after permissible dye effluent release, standards were established and improvements were made by introducing more effective dye removal methods including physical, chemical and biological treatments (as shown in Figure 2.3).

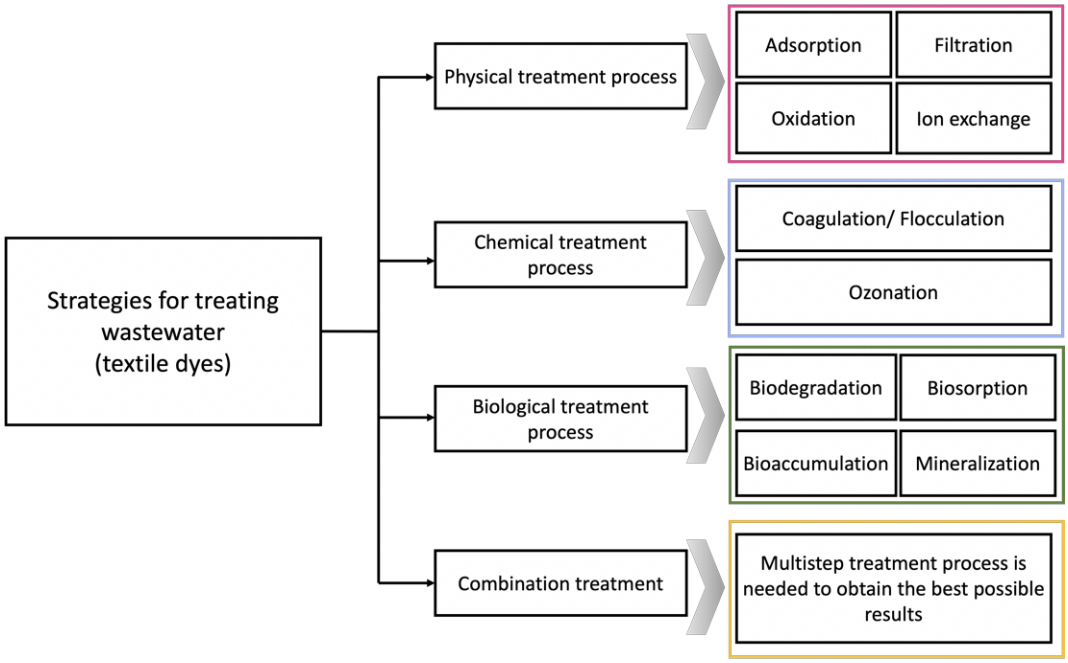

Figure 2.3 Treatment strategies for textile dyes discharges.

Table 2.1 Usage classification of dyes(Gregory, 1990)

Class of dye	Substrates	Chemistry	Example of dye	Loss as effluent (%)
Anionic / Acid	Nylon, silk, wool, inks, paper and leather	Azo (including premetallised), antraquinone, triphenylmethane, azine, xanthene, nitro and nitroso	Indian ink, Congo red, Nigrosoine	5-20
Cationic or basic	Paper, modified nylon, polyacrylonitrile inks and polyester	cyanine, hemicyanine, diazahemicyanine, diphenylmethane, triarylmethane, azo, azine, xanthene, acridine, oxanine and anthraquinone	Methylene blue, Toluidine blue, Thionine, and Crystal violet	0-5
Direct	Paper, Cotton, rayon, nylon and leather	Azo, phthalocyanine, stilbene and oxanine	Diamine scarlet; Congo red; Direct brown; Chlorazol dyes	5-30

Table 2.1 Continue

Class of dye	Substrates	Chemistry	Example of dye	Loss as effluent (%)
Disperse	Polyamide, polyester, acrylic, acetateand plastics	Azo, anthraquinone, styryl, nitro and benzodifuranone	Disperse Orange 1; Disperse Red 9; Disperse Red 11; Disperse Red 60; Disperse Yellow 26; Disperse Yellow 42	0-10
Reactive	Cotton, nylon, wool and silk	Azo, anthraquinone, phthalocyanine, formazan, oxanine and basic	Reactive blue; Cibacron brilliant yellow; Reactive blue 19; Reactive red 15; reactive brown; Reactive yellow 8	10-50
Sulphur	Cotton and rayon	Indeterminate structures	Indophenol and Sulfur black	10-40
Vat	Cotton, rayon and wool	Anthraquinone (including polycyclic quinines) and indigoids	Synthetic alizarin and Alizarin yellow	5-20

Physical dye removal methods are generally straightforward methods accomplished through mass transfer mechanisms. There are many conventional physical methods for dye removal, including adsorption, membrane filtration, nanofiltration or ultrafiltration, ion exchange, etc. For chemical treatment methods, it is essential to use chemical agents and incorporate all aspects of chemistry so that the desired outcome can be achieved. The most commonly used chemical dye removal methods consist of coagulation / flocculation, advanced oxidation, ozonation, ultraviolet irradiation, and electrochemical destruction. Despite the fact that chemical treatments appear to be effective, chemical dye removal is generally more costly than physical and biological methods.

In most countries, textile wastewater is treated with a biological method in order to remove dye. In this method, dye effluents are treated with both aerobic and anaerobic processes before they are discharged into the environment. A major factor that led to the selection of this dye removal method was its affordability and ease of implementation. Despite this, coloured water remains in the environment as a result of this treatment alone not being sufficient to eliminate all hazardous particles from textile dye wastewater. Over the past 30 years, there were numerous dye removal methods developed, but only a few are actually used by the concerned industries todays due to the limitations associated with most of them. In general, branches of physical dye removal, particularly adsorption, are the most commonly utilized methods. It is often the simplicity and efficiency of these methods that lead to their selection. Comparatively to biological or chemical dye removal, this method is the least chemically intensive. Besides, considering that this method does not involve living organisms, it is considered to be more predictable.

2.2 Concepts of adsorption for environmental application

In theory, adsorption is described as an equilibrium-diffusion reaction of a molecule from a liquid or gas to a solid surface, which passes through both the gas and liquid channels simultaneously or counterfactually through a packed column (Julbe *et al*., 2019). In practical terms, adsorption capacity is influenced primarily by the mass transfer between the adsorbate and adsorbent surface as well as the adsorption reaction rate.

Adsorption can also lead to an increase in surface energy as the surface molecules experience bond deficiency, making them energetically favourable to adsorption of molecules. In contrast, desorption refers to the physical process of releasing an previously adsorbent substance from a surface. In this case, the molecule gains enough energy to overcome the binding energy activation barrier to enter the surface. Mechanism of physical and chemical adsorption are depicted in Figure 2.4, and these are described in detail further below.

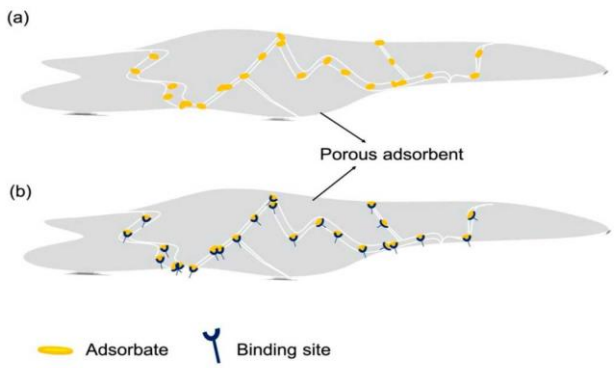

Figure 2.4 Mechanisms of (a) physisorption and (b) chemisorption processes.

Adsorption for either gas or liquid can be classified into two categories based on the adsorption force: physical adsorption and chemical adsorption. In

Table 2.2, physical and chemical adsorption are compared in relation to gas or liquid adsorption. Physisorption takes place due to van der Waals interactions: weak electrostatic forces that occur between molecules. When the molecules of the adsorbate hit the surface with low energy, vibrations of the lattice of the solid can dissipate the heat, allowing the molecules to be trapped on the surface. However, when they hit the surface with excessive energy, the molecules cannot be dissipated by the adsorbent and bounce off. In addition, physisorption is only significant at low temperatures due to the ease of reversal of physical binding, even with vibrational motion present (Deng *et al*., 2019).

Table 2.2 Comparison of physical and chemical adsorption (Tran *et al*., 2016; Y. Wang *et al*., 2019).

	Adsorption categories	
	Physical adsorption	**Chemical adsorption**
Electron transfer	No electron transfers (Maybe polarization might occur)	Electron transfer leading to formation of the bond
Adsorption force	Van der Waals force between molecule	Strong chemical bond; (e.g.: hydrogen bonding, covalent and ionic bond)
Selectivity	Non-selective adsorption	Selective adsorption
Adsorption layer	Monolayer or multilayer adsorption	Monolayer adsorption
Adsorption heat	Low adsorption heat (10–40 J / mol)	High adsorption heat (20–400 kJ / mol)
Adsorption rate	Fast	Slow
Stability	Instable	Stable
Activation energy	Low activation energy	High activation energy
Binding energy	High binding energy (10–100 meV)	Low binding energy (1–10 meV)

Chemisorption, in contrast to physisorption, requires stronger forces: indeed, in this case the adsorbate forms a real chemical bond (usually covalent) with the adsorbent's surface (B. Liu et al., 2017). The change in enthalpy is much greater (from 40 to 400 kJ mol^{-1}, always negative as adsorption is a spontaneous process). In some cases, chemisorption is an activated process, which means that the adsorbate must have a minimum amount of energy in order to be adsorbable. This process is dependent upon an energetic barrier separating the physisorbed and chemisorbed states. If the free molecules have a lower energy than the barrier, then, the adsorbate will chemically attach to the adsorbent; or else, it will be desorbed (Lyu *et al*., 2020). Nevertheless, if the barrier is lower than the energy of free molecules, all molecules physisorbed will quickly form a chemical / covalent bond with the adsorbent surface and will undergo rapid chemisorption. It is therefore necessary to provide energy to the system in order to break the covalent bond between the chemisorbed molecules and the adsorbent surface in order to be detached from the surface.

A monolayer of adsorbate molecules can be chemisorbed to an adsorbent surface: once the surface has been filled with adsorbate molecules, no more bonds are available, so adsorption ends, or it is in dynamic equilibrium with desorption. Additionally, the surface of the adsorbent plays an important role in the adsorption process, and adsorbents with larger surfaces will adsorb substances more efficiently. This is why porous compounds or, more generally, those with the greatest surface area per unit volume, such as porous-based nanomaterials, are the best adsorbents.

2.3 Carbon-based materials for environmental application

Activated carbon (AC) was historically among the first carbon-based adsorbents used for CO_2 capture and dye removal due to its abundant feedstock, low-cost materials, high available surface, and high adsorptive characteristics (Singh *et al*., 2019, 2018). Based on the adsorption process, traditional method has great limitations in CO_2 retention ability as well as for wastewater technology. In recent years, carbon based materials including graphene, carbon nanotubes (CNTs) etc. have been considered as promising adsorbents for environmental due to their high adsorption capacity, low cost and wide availability. The development of advanced adsorbent materials with better properties and absorbability is therefore vital. In order for them to be an ideal material for environmental applications, a variety of factors must be taken into account including the structure, properties, nature of the materials, etc and according to the recent research, graphene, in particular, could be an ideal material to be used in environmental applications because of its unique physical and chemical properties (Chowdhury and Balasubramanian, 2016a; Sui *et al*., 2013).

2.3.1 Graphene and graphene derivative

In recent years, graphene, a carbon allotrope, has triggered a new "gold rush," attracting widespread attention as the first 2D atomic crystal. Figure 2.5 shows the structure of defect-free or low-defected graphene. The ideal graphene is composed of sp^2 assembled carbon atoms packed densely in a two-dimensional hexagonal lattice at an average interlayer distance of 0.142 nm. In terms of conductivity, graphene is an extremely good conductor of electricity and heat. The

stability of graphene can be attributed to its tightly packed carbon atoms as well as the hybridization of its sp^2 orbitals (Farjadian *et al*., 2020).

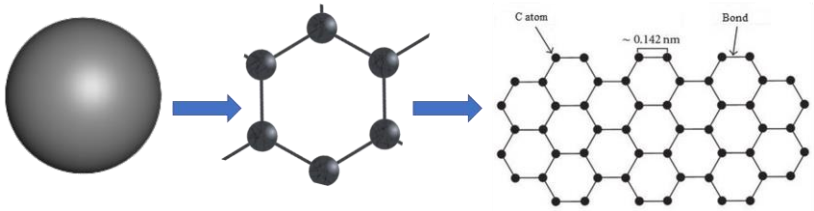

Figure 2.5 Ideal graphene structure.

Currently, graphene is the thinnest and strongest material with a large specific surface area (SSA), and it has been extensively utilized as a possible adsorbent material due to its unique physicochemical features. Low-defected graphene exhibits nonlinear elastic behaviour, making it the strongest and stiffest nanomaterial ever discovered. Furthermore, at room temperature, the optimal 2D crystal quality results in a thermal conductivity of approximately 5300 W m^{-1} K^{-1}, which is nearly 50 % greater than CNTs and five times higher than aluminum (Al) or Cu (Karthik *et al*., 2021).. In fact, increase in conductivity can be attributed to the presence of highly mobile electrons within graphene layer. They are known as π orbitals which overlap one another and help to enhance the carbon to carbon bonds in graphene. Besides, the performance of graphene as an electrical conductor has been found to be 100 times higher than silicon used in computer conductors and 5000 times faster than graphite. Graphene also has remarkable optical and optoelectronic capabilities. A defect-free graphene nanosheets possesses an inherent strength of 130 GPa at 0.25 strain and a Young's modulus of 1.0 TPa, which is 200 times stronger than steel strength (Karthik *et al*., 2021). Graphene, in addition to having excellent mechanical characteristics to CNTs, has rapid carrier

dynamics due to carrier-carrier and carrier-phonon scattering. Aside from its robustness, flexibility, thermally stable, and environmentally stable, it also exhibits excellent resistance to gas permeation. All of these unique features of graphene and its derivatives make them appropriate for a wide range of advanced applications, particularly in environmental remediation (Karthik *et al*., 2021; Yousefi *et al*., 2019).

Graphene is a critical building component for allotropes of carbonaceous materials like fullerenes, CNTs, and graphite, all of which may be synthesized and manipulated at a minimal cost. In recent years, several techniques have been developed in order to isolate inexpensive graphene from low-cost graphite without metallic impurities. In addition to the ideal graphene, GO, rGO, graphene nanofibers (GNFs), graphene nanoplatelets (GNPs) and chemically modified graphene are widely used graphene materials. In Figure 2.6, graphene and its basic derivative are shown. GO, in contrast, has many oxygen-containing functional groups and exhibits different chemical and physical properties.

rGO is a form of GO that has been reduced by chemical, thermal and other methods. In terms of oxygen content, purity, surface chemistry, number of layers, lateral dimensions, defect density, and composition, the graphene family differs significantly (Magne *et al*., 2022). Graphene is also accessible in the form of GNPs, which are made of several (5-20 usually) graphene layer stacked. Furthermore, due to van der Waals interactions, pristine GNPs may easily agglomerate. Doping of graphene by heteroatoms, an effective method for improving graphene properties and performance has attracted a lot of interest, particularly in relation to nitrogen (N - graphene) (Hu *et al*., 2018; Li *et al*., 2021). Generally, doping graphene sheets

with N atoms results in three types of common bonding arrangements inside the lattice: pyridinic N, graphitic N, and pyrrolic N. Besides, N - Graphene hybridised with inorganic composites can display better characteristics and improved performances, making it useful in the fields of energy, biomedical, biotechnology, and pollutants removal.

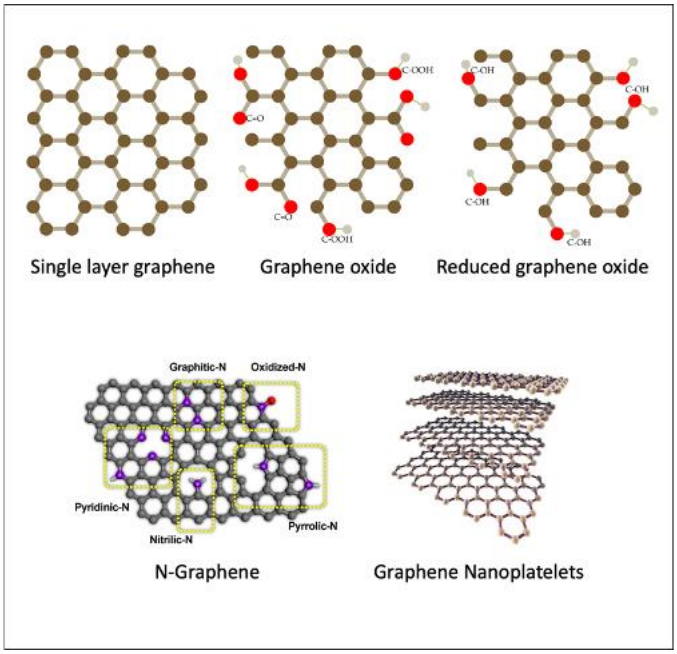

Figure 2.6 Illustration of graphene and its basic derivatives (Anwar *et al*., 2020).

2.3.2 Graphene synthesis

Graphene was discovered in 2004 by Andre Geim and Konstantin Novoselov, who received in 2010 the Nobel Prize in Physics for their "groundbreaking experiments" (Geim and Novoselov, 2010). Graphene and its derivatives have now become an emerging subject, with multiple different synthesis methods being investigated, including physical, chemical and

mechanical processes. As illustrated in Figure 2.7, researchers classified synthesis approaches in two major categories: bottom-up and top-down.

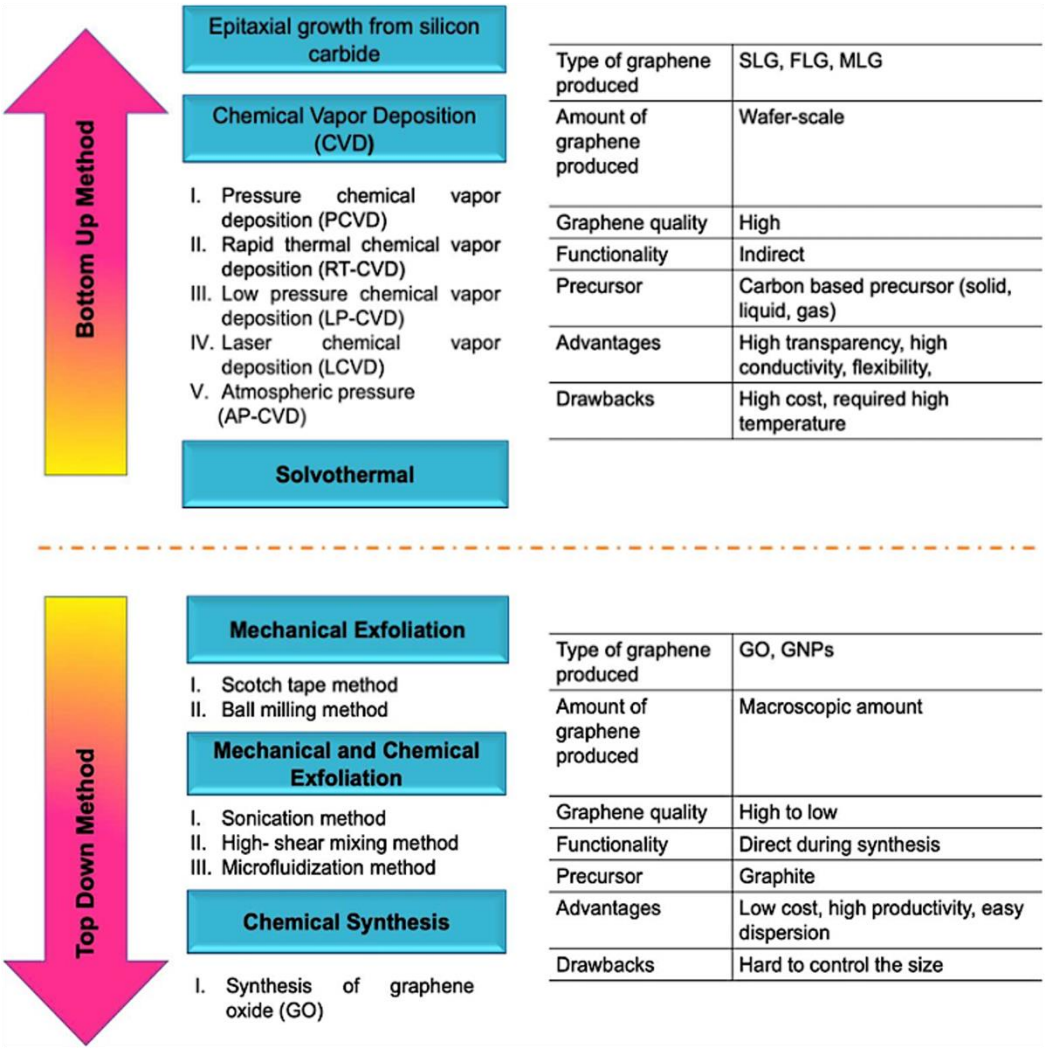

Figure 2.7 Schematic of top-down and bottom-up approaches for graphene synthesis.

There are several processes that are utilized to fabricate graphene. These include graphite intercalation and exfoliation, Chemical Vapour Deposition (CVD), arc discharge of graphite in hydrogen and helium atmospheres, graphene reduction, and graphene epitaxial growth. In principle, the bottom-up methods comprise the synthesis of graphene from alternative carbon sources either by CVD or epitaxial growth while the top-down methods involve the separation of stacked layers within

graphite to yield graphene also called exfoliation. In the top-down methods, the intention is to induce an increase of the inter-layer spacing and exfoliate the graphene layers by means of mechanical and / or chemical forces (Kumar *et al*., 2019; Mohd Firdaus *et al*., 2020).

These two techniques ultimately contribute to the framework of different types of graphene. The structure, morphology, and properties of the resulting graphene, such as type of graphene, surface chemical properties, structural quality and also its physical properties are usually entirely dependent on the fabrication process. Bulk synthesis of graphene by CVD under specific conditions is becoming possible even if standard bottom-up methods are not often compatible with production of large quantities of graphene. The top-down methods can be used in the large-scale synthesis. Some challenges including surface defects that arise during sheet separation and sheet re-agglomeration have to be considered for such approach. Despite all the modifications, the most important aspect of the produced graphene nanomaterials is its structural quality and the ability to control the surface chemistry. It is important to note that graphenic materials can possess significantly different chemical properties based on the nature of their functional groups as well as the presence of defects. The bottom line is that each application has its own preferred method of synthesis, and each method produces interesting nanomaterials because of their nanoscale dimensions and the desired properties they possess (Hao *et al*., 2015).

Typically, GO is a few layer graphene with numerous O-containing groups bonded to its carbon atoms, including hydroxyl, epoxy, carboxy and carbonyl at its basal plane or edges. The presence of these oxygen-containing functional groups

distinguishes GO from other graphenes or graphene derivatives, as they might also affect electrical, electrochemical and mechanical properties. GO is classified as hydrophilic and negatively charged materials, as a result of its sufficient hydrophilic surface groups, allowing stable dispersion in water (Smith *et al*., 2019). Besides, GO also shows higher chemical performances with higher reactivity compared to pristine graphene whose inertness impedes some applications to be considered.

2.3.3 2D graphene to 3D graphene-based macrostructures

As part from exploiting the properties of 2D graphene at the nanometer scale in electronics in particular, their assembly in hierarchized macroscopic structures or graphene based macrostructures (GBMs) has grown of interest among the scholars in recent years, especially for environmental applications (Figure 2.8).

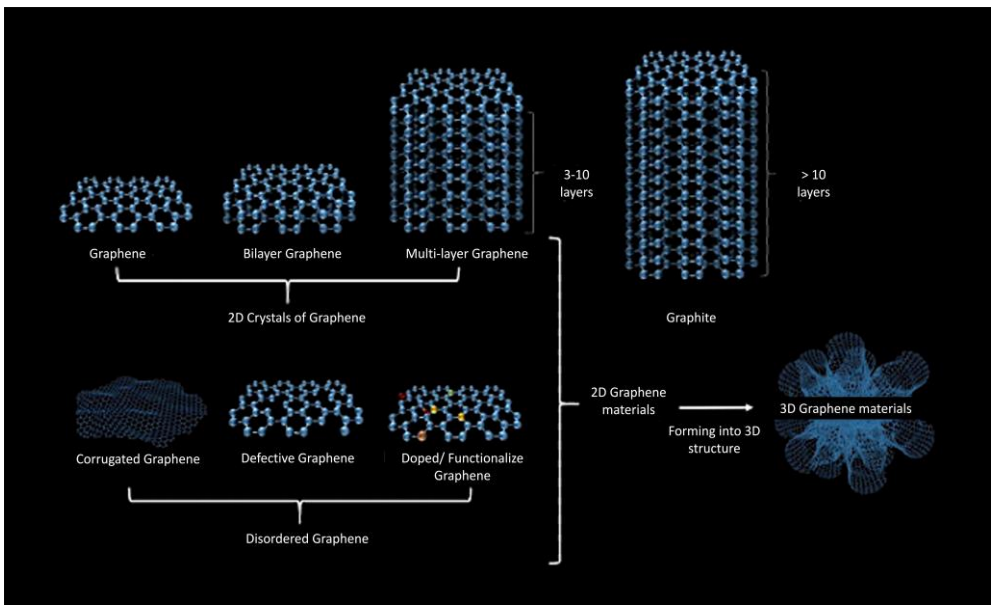

Figure 2.8 Illustration of the relationships among graphene, 2D graphene materials, 3D graphene materials, and graphite (Sun *et al*., 2020).

Since the sp^2 carbon network can be functionalized in many manners, versatility of these GBMs in term of chemical affinity is a remarkable tool to control the interface interactions. For all these reasons, such substrates with high and tunable surfaces are the focus of numerous studies in the scientific community. Different strategies have been developed to create 3D GBMs as shown in Figure 2.9.

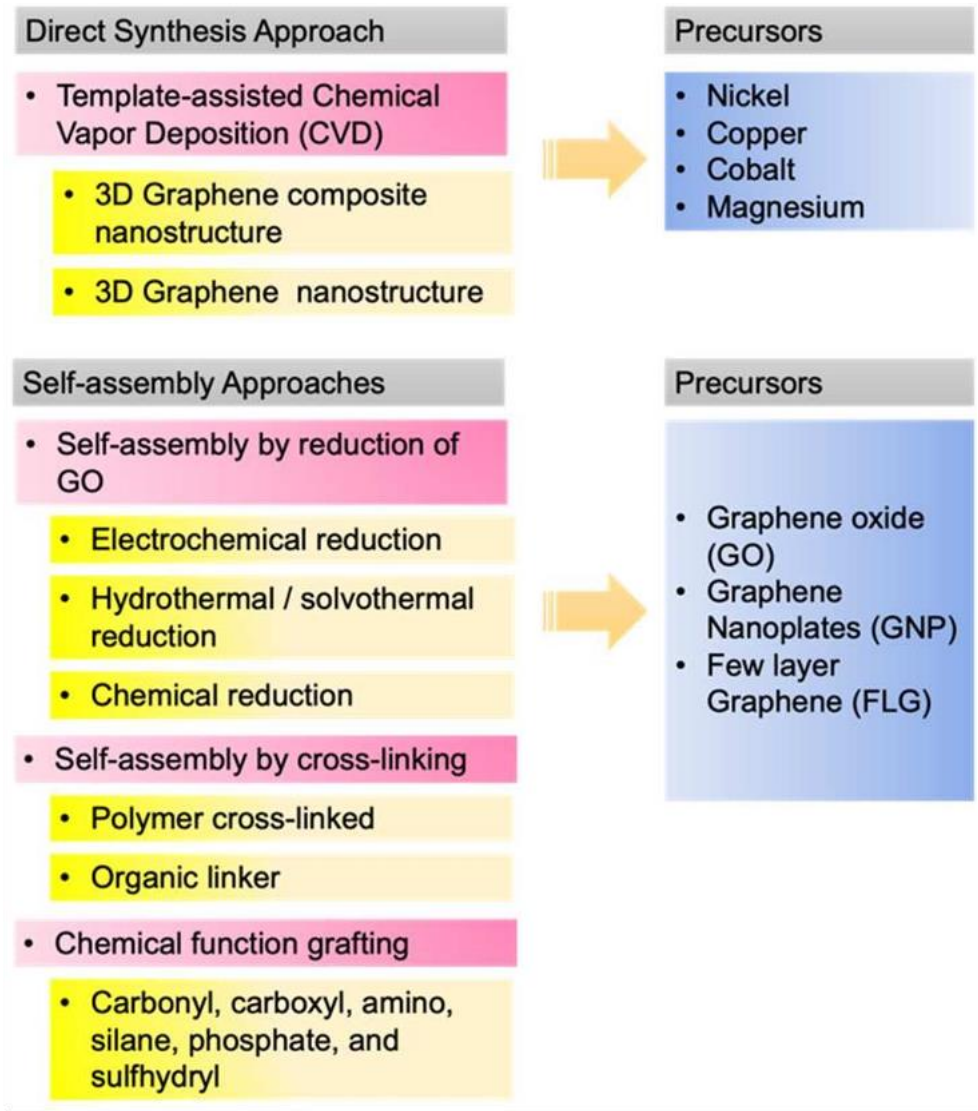

Figure 2.9 List of the methods with their corresponding material precursors used to construct 3D GBM.

In fact, graphene can be seen as a bridge between the nanoscale and the bulk materials. Compared to a finely divided powder of graphene, such hierarchical structured materials such as hydrogels, aerogels, foams or sponges are of great interest for a large number of applications. Surface and interfacial phenomena plays a crucial role in CO_2 capture and dye removal application because they provide both a large and accessible surface as well as a high level of regeneration. Extensive research has been centred around the preparation of 3D structures of graphene, such as 3D GBM, graphene sponges or graphene aerogel (GA). For that purpose, two main routes are usually investigated.

For direct synthesis of 3D GBMs, the used graphene is most commonly grown by CVD from a template that contains the catalyst. For the second approach family, the as-synthesized graphene nanosheets are assembled by a non-direct procedure to form 3D GBMs (Zhang *et al*., 2019). In that later case, GO is widely used as a graphene precursor due to its high dispersion ability in aqueous media, functionality and stability. Additionally, the use of GO as a starting material for synthesis of GBMs is very effective because oxygen atoms are present on both the basal plane and edge, making them capable of reacting covalently with different compounds and thus generating new materials with properties adaptable to specific applications. If superior physical properties are required, non-GO-graphene such as SLG, FLG, MLG, and GNPs are preferentially used as the starting material for 3D assembly of graphene. These graphene types are highly hydrophobic, with a significant tendency to restack via van der Waals forces, resulting in reduced surface area, electrical and mechanical capabilities that limit the use of graphene in various applications.

One approach to address this constraint is to introduce functional groups with more attached active sites. As a result of this function being introduced to the surface of graphene, the materials will become more favourable prior to assembly. Self-assembly phenomenon due to induced attractive forces can occur due to hydrophobic interactions and π–π stacking between the reduced nanosheets of GO for example. However, the subsequent 3D graphene-based material suffers of low mechanical resistance (Yin *et al*., 2012). Thus, procedures inducing strong covalent bonds between the graphene within the 3D structure allowing to improve mechanical reinforcement of the materials have been proposed. The method to prepare GBMs by both direct and non-direct approaches are discussed in detail in the following sections.

2.3.3 (a) Direct synthesis approaches to prepare 3D graphene-based macrostructures

The CVD method has been reported as a useful method for developing 3D graphene nanostructures which can enable mass production of high-quality graphene materials within complex 3D architectures with controllable crystallinity and layer numbers, thereby significantly improving the efficiency of graphene-based energy devices (Liu *et al*., 2014; Y. Zhang *et al*., 2019). Generally, in CVD technique, there are two routes often used in the production of 3D GBM which are: (i) synthesis of 3D graphene composite materials and (ii) synthesis of 3D pure graphene after metal catalyst and oxide removal.

2.3.3 (a)(i) Pure graphene 3D GBM prepared by CVD

Metal-catalysed CVD techniques for 3D GBM preparation are now scalable, facile, and potentially appropriate for industrial production. However, the

main disadvantages of these techniques include relatively high metal consumption, a limited selection of metal microstructures, and metal residues remaining in the products, which leads to an increase of the manufacturing costs. For example, there is interest in using ultrathin metal films as catalysts that can be removed by etching at the end. Ma and co-workers reported such method using copper as catalyst at low temperature by a plasma-enhanced CVD (PECVD) process enhancing that way the growth of vertical graphene (VG) (Ma *et al*., 2015). They proposed, at the early stage of VG growth, a thin layer of amorphous carbon was formed on the substrate and later graphene started to grow while the amorphous carbon remained. This condition led to simultaneous growth of graphene and carbon islands. Then, the graphene continued growing in vertical orientation due to sheath effect and ion bombardment between bulk plasma and the substrate. They also found that the growth of the VG was improved as copper was used as catalyst.

Zeng *et al.* reported that with few steps, they had successfully developed a novel 3D graphene fiber (Zeng *et al*., 2018). They started with the electrospinning of polyacrylonitrile (PAN) nanofibers with air stabilization and carbonization in ammonia (NH_3), and further with the growth of graphene sheets in a vertical orientation of the fibers (Figure 2.10). As a result, they found that the 3D graphene fibers were densely structured and connected with the edges completely exposed on the surface, resulting in superior performance in various property including electrical conductivity, electromagnetic shielding and hydrophobicity.

2.3.3 (a)(ii) 3D interconnected graphene-based composite materials

The first group who used CVD to synthesize 3D structures based on graphene was Chen's group. They particularly developed a method to form 3D-

graphene foams with a Ni foam template. On the same principle as CVD used for 2D graphene growth, the procedure was based on decomposition of CH_4 at 1000 °C.

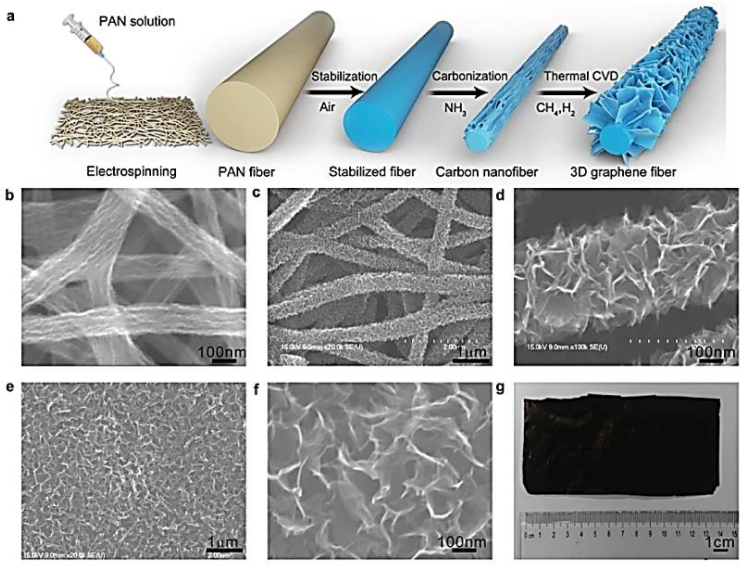

Figure 2.10 Preparation process and structure of the 3D graphene fibers. a) A schematic illustration of the preparation process. b) A SEM image of the carbon fibers carbonized in NH_3. c,d) SEM images of the 3D graphene fibers grown for 4 h at CH_4 concentration of 11.1 % and 1100 °C. e,f) SEM images of the 3D graphene fibers grown for 10 h at CH_4 concentration of 11.1 % and 1100 °C. g) An optical image of the 3D graphene fibers membrane (Zeng *et al*., 2018)

Then, the grown graphene films precipitated onto the porous surface of the nickel foam and it was then etched off. During this step, the graphene network could collapse; thus, a thin poly (methyl methacrylate) (PMMA) coating was deposited on the surface of the graphene sheets. A solution of heated acetone was then needed to remove PMMA and finally graphene foam / polydimethylsiloxane (PDMS) composites were formed by PDMS prepolymer infiltration into the free-standing

graphene foams. In addition, few years later, other kinds of template were used such as Cu, cobalt (Co) and magnesium (Mg) to grow the 3D GBM.

Dong *et al.* reported a procedure using two facile steps to synthesize 3D GBM involving cobalt oxide (Co_3O_4) nanowires as catalyst. They found that the 3D graphene / Co_3O_4 composite exhibited excellent electrochemical and electrocatalytic properties. Besides, the open pore system of the composite and large accessible active area made it a promising candidate for ion diffusion and transport kinetics.

Aside from CVD, the combination of a few techniques for the development of 3D GBMs with composite materials has recently gained more attention. For example, Hu *et al.* have investigated the effect of rGO aerogels on Ni_3Fe / Co_9S_8 composites by a calcination-hydrothermal approach for oxygen reversible electrocatalysis. They found that the SSA increased up to 137.5 $m^2 g^{-1}$ with a large pore-size range from 20 to 300 nm after adding rGO aerogels as support. The addition of composites to GBMs led to more attached active sites, faster electron / ion transport, and improved structural stability. The synergistic effects of the conductive and 3D porous graphene network could potentially deliver high capacity and exhibit superior cycle life with good energy conservation.

Typically, 3D GBMs have been used as a support for the composite materials in some applications like energy storage, as it is incredibly useful for the rapid transportation of electrolytes through their porous conductive structures, thereby facilitating extra charge-storage reactions. Wang *et al.* developed a novel 3D macroscopic nickel oxide hydroxide (NiOOH) / solvothermal-induced pure graphene hydrogels and found that their modified composite material revealed large

SSA up to 887 m^2 g^{-1} and they demonstrated high specific capacities, speed capacities and longer cycle life in performance terms. Using a similar approach, this composite material has a high SSA of 850 m^2 g^{-1} and a well-developed 3D porous network of continuous pores ranging in size from sub micrometres to a few micrometres (Wang *et al.*, 2016a).

2.3.3 (b) Self-assembly approaches to prepare 3D graphene-based macrostructures

In most works, self-assembly of graphene into hierarchized macrostructures (*i.e.* GBMs) are synthesized from GO which is reduced by different methods, such as electrochemical reduction, hydrothermal, solvothermal reduction or chemical noble metal and metal oxide in GO aqueous dispersions. As the starting based material, GO or rGO can be also used together with surfactants or polymers in order to limit agglomeration. Additionally, rGO may be an alternative form of GO that has been modified by various methods, including chemical and thermal, to minimize the amount of oxygen in the GO, as oxygen may cause the GO to be less stable in some applications (Shahdeo *et al*., 2020). Most of the researchers used this approach to fabricate self-assembled GBMs with more advanced and complex building blocks. To date, 3D-GBM have been considered as promising materials thanks to their properties including porous network, ultralight weight, high surface area, stability, electrical conductivity, or mechanical strength.

2.3.3 (b)(i) Self-assembly of GO by hydrothermal or solvothermal reduction

Hydrothermal or solvothermal reduction is effective to synthesize 3D graphene-based hybrid materials. The hydrothermal method can be defined as a technique that induces chemical reactions in aqueous solution above the boiling

point of water. The solvothermal method usually involves organic solvents (instead of water) and the chemical reaction occurs at a temperature higher than the solvent boiling point under high pressure (Xu *et al*., 2015). Essentially, in both processes, first, GO is homogeneously dispersed in the chosen solvent and the GO's oxygenated functional groups are reduced during the chemical reaction leading to attractive hydrophobic interactions occurring between the produced rGO nanosheets. GO is widely used as a precursor of graphene composites because it is economical to fabricate on a large scale and easy to process (Yan *et al*., 2020). Besides, GO has an abundant aromatic nucleus along with oxygen-containing groups. The oxygen-containing groups decorate the basal plane and edges of the compound, resulting in hydrophilic properties and uniform dispersion in water. As the reduction process proceeds, local phase separation will occur, caused by the removal of hydrophilic groups, resulting in further modification of the intersheet interactions to prepare the self-assembly phenomenon. As a result of hydrogen bonding between residual hydrophilic regions of the reduced GO and water, water molecules adsorb on the surface of the reduced GO and act, that way, as a spacer to prevent parallel aggregation of nanosheets (Jing *et al*., 2022). Depending on the used experimental conditions, the strength of the integrated stacking system increases as well as the number of cross-links often under addition of heat and energy. These approaches can be applied to some other materials to have the 3D heterostructures as the combination of other components may alter the structures as well as the functions to support certain forms of application.

It is well known that the pH has a significant impact on 3D graphene characteristics prepared by the hydrothermal process. Thus, Garcia-Bordejé *et al.* conducted an experiment on the effect of pH and time towards the microstructure

and surface chemistry of gas. Figure 2.11 illustrates the mechanism of the hydrothermal reduction process at different pH levels. From the results, they found that, in alkaline conditions, the morphology of the 3D macrostructures was twisted and potentially bent at the border resulting in higher porosity while in the acidic medium, the aerogel architecture was less porous and denser (García-Bordejé *et al*., 2018). The hydrothermal reduction process mechanism was commonly started with GO synthesizing using the modified Hummers' method and continued with dispersion in water eventually with addition of surfactants as it could easily disperse graphene (Xu *et al*., 2010a).

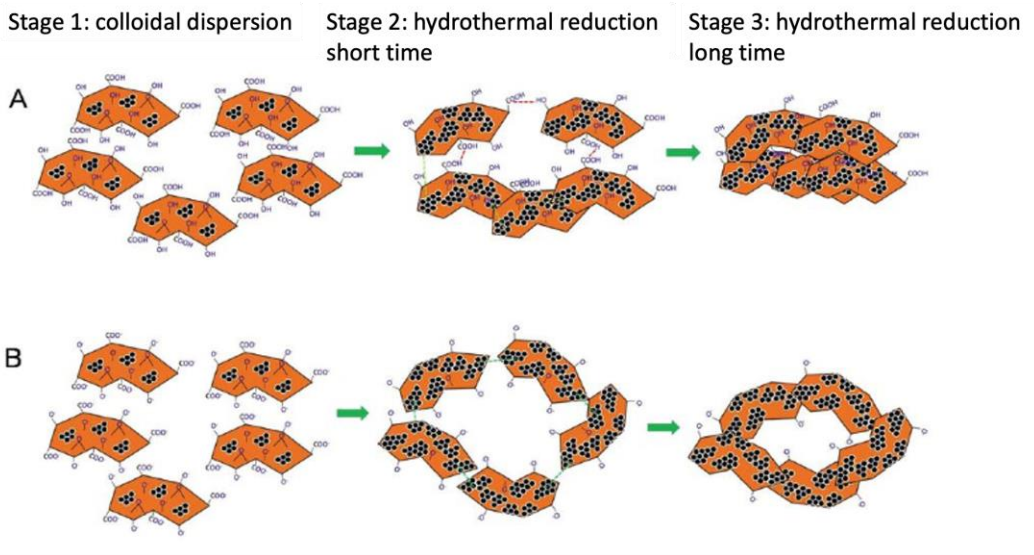

Figure 2.11 Scheme of the possible mechanisms of the hydrothermal reduction process of graphene under pH 3 (A) and under pH 11 (B) at different stages. The red dashed lines indicate H-bond interactions while the green dashed lines indicate van der Waals hydrophobic interactions (García-Bordejé *et al*., 2018)

Generally, the oxygenated functionalities decreased significantly after the hydrothermal or solvothermal reduction process, and a large amount of π-conjugation was restored to make it possible to convert to rGO. In this condition,

interfaces via all the bonds were capable to organize complex architectures such as 3D building blocks (Xu *et al*., 2015). Interestingly, doping of graphene within the GBMs could be efficiently prepared using simple one-step hydrothermal or solvothermal route. Yang *et al.* have reported a facile hydrothermal approach to produce N doped GBMs. Initially, GO was reduced by a hydrothermal treatment in the presence of ammonium hydroxide in Teflon-lined reactor which was sealed in a steel autoclave. After freeze-drying, the N doped GBMs possessed hierarchical porous structure with SSA around 200 $m^2 g^{-1}$. According to the findings, N doped GBMs exhibits a large diffraction peak, revealing the typical characteristic peak of graphene aerogel structure. This was also supported by the SEM analysis, showing 3D porous structure interconnected. The N doped GBMs enabled efficient diffusion of both bacterial cells and electron mediators in the interior space of a 3D electrode (Yang *et al*., 2016). Long *et al.* reported a large scale chemical reduction and nitrogen doping of GO they achieved simultaneously using N_2H_4 and ammonia under hydrothermal environment. They found that the structure and surface chemistry of the modified graphene sheets were strongly dependent on the hydrothermal temperature as different temperatures could play a dominate role in the N doped GBMs and multiple reactions may occur simultaneously (Long *et al*., 2010).

Freeze drying or freeze casting is one of the step used in developing 3D GBMs as it eliminates the solvent without damaging the 3D graphene framework by utilizing the anisotropic solidification behaviour of the used solvent, e.g. water or organic solvent (Y. Lin et al., 2016). Besides, as mentioned earlier, freeze- drying is normally used in conjunction with hydrothermal or solvothermal reduction process. After the gelation by reduction of GO in a dispersion state, the solvent is

gently removed by freeze drying to preserve the hierarchical porous structure of the material. Rodríguez-Mata *et al.* conducted a study to evaluate and compare the degree of reduction or gelation effects on the formation of microchannels. In this study, GO was first reduced to rGO by hydrothermal reduction, and later the hydrogel obtained was frozen using two separate methods, bulk freezing (BF) and unidirectional freezing (UF). They found that UF offered substantially lower densities and higher specific pore volumes than BF for the two shortest periods (45 and 75 min), and that UL also resulted in more ideal cylinders than BF. In addition, in terms of efficiency, the UF approach of aerogels contributed to the creation of GBMs with aligned and continuous microchannels, allowing an intermediate cross-linking degree of rGO nanosheets, thus providing a higher absorption ability of non-polar solvent and aromatic compounds (Rodríguez-Mata *et al*., 2019).

2.3.3 (b)(ii) Self-assembly of graphene oxide by chemical reduction

Chemical reduction is one of the most frequently used approaches to prepare 3D GBMs. Usually in this method, either organic or inorganic reducing agent is simply added to GO dispersed in water to induce its reduction and it gives rise to rGO material. Advantageously, such chemical reaction occurs at low temperatures (below 100 °C and often at room temperature) compared to hydrothermal and solvent thermal methods (Lin *et al*., 2017). In this method, several common reducing agents are used: hydrazine, vitamin C, sodium ascorbate, sodium borohydride ($NaBH_4$) etc. In the work from Chen and Yan, four separate reducing agents were used, including sodium bisulfite ($NaHSO_3$), hydrogen iodide (HI), vitamin C and hydroquinone under a temperature of 95 °C, which was ideal for preserving highly ordered macropores in the prepared 3D graphene architecture.

The GBMs by using HI have shown to lead to the highest value for electrical conductivity and as well a high value in density and degree of reduction. The authors believed the density and degree of reduction could be the important factors for electrical conductivity as well (Chen and Yan, 2011). The self-assembly could evolve, triggered by the hydrophobic and π–π stacking interactions of the GO structures, resulting in high thermal stability, mechanical strength, and electrical conductivity of 3D graphene framework. Through simultaneous self-assembly of GO reduction, Zhang and his co-workers produced 3D graphene hydrogels for dye adsorption and catalysis applications. As an environmentally friendly substance with multiple functional groups, L-cysteine (L-Cys) is easily produced under mild conditions. L-Cys is known as an environmentally friendly substance. It has been shown that L-Cys molecules can form polymeric networks in solution that serve as templates for self-assembly of GO molecules in 3D frameworks when combined with one another. As a result of gasifying L-Cys (NH_3 and hydrogen sulfide (H_2S)), the emitted H_2S reduced graphene material, enabling the preparation of graphene in one step (Zhang *et al*., 2015).

2.3.3 (b)(iii) Self-assembly by organic linker

Organic self-assembly provides an easy way to synthesize functional nanomaterials with the aid of some organic linkers like glucose, b-cyclodextrin, chitosan, and deoxyribonucleic acid (DNA) molecules. These latter can be linked to graphene or GO into a 3D network by covalent bonds. Xu *et al.* reported a strategy way to form 3D multifunctional GO / DNA composite self-assembled hydrogel (GO / DNA SH) (Xu *et al*., 2010b). Double-stranded DNA (dsDNA) was added to an aqueous solution of GO under heating condition at 90 °C for 5 min.

They found that the dsDNA was unwound during the heating process to single-stranded DNA (ssDNA) chains that bridged adjacent GO sheets via strong noncovalent interactions. Besides, their GO / DNA SH showed a good stability, possibly due to the strong binding of DNA chains by several noncovalent interactions, including π- π stacking and hydrophobic interactions between DNA bases and GO structure, as well as electrostatic and hydrogen bonding interactions. Additionally, there were parameters that needed to be addressed during the creation of 3D GO / DNA SH. For example, the concentration of GO and dsDNA, as with an ideal condition, it could increase the mechanical strength of the resulting self-assembled hydrogel. Indeed, the authors believed that the reliability of the 3D network was critical in designing and manufacturing a hierarchical graphene-based material, and this could be achieved by increasing the cross-linking sites between GO sheets and DNA chains. In a recent study, Guo and colleagues modified chitosan / GO composites to act as an effective dye remover. It was found that the $-NH_2$ groups belonging to the chitosan chains reacted with the COOH groups on GO as the C-O stretching vibration (by FTIR) of NHCO and the N-H bending of $-NH_2$ were shifted to a lower value and the amount of acetylated amino group NHCO was increased. Besides, various types of non-covalent interactions have been observed in this case, resulting in the observed strong binding of chitosan to GO or rGO surfaces. In addition, they discovered that adding GO or rGO slightly changed the structure of chitosan. It may be due to interactions involving electrostatic interactions and hydrogen bonds between the amine base and the oxygen-containing GO groups. In subsequent tests, the modified chitosan / GO composite was evaluated as adsorbent in textile wastewater for the removal of reactive dyes and showed a significant adsorption capacity of 32.16 mg g^{-1}(Guo *et al*., 2016).

2.3.3 (b)(iv) Self-assembly by cross-linking by polymer

In general, the formation of 3D GBMs with the help of polymers has been proven to improve the physical characteristics of the materials. Polymers can interact with graphene thanks to either π–π or hydrogen interactions. In 2016, Fang *et al.* synthesized a highly ordered 3D GBMs with the aid of poly(vinyl alcohol) (PVA) polymers for molecular transfer (Fang *et al*., 2016). Their preparation method comprised three steps which are pre-reduction of GO by $NaBH_4$, sulfonation using sulfanilic acid ($C_6H_7NO_3S$) and sodium nitrite ($NaNO_2$) and lastly the post-reduction by hydrazinium hydroxide (N_2H_5OH). During the sulfonation process, a simple acid base reaction took place where after the addition of hydrochloric acid, nitroso ions were formed by the reaction of sodium nitrite in the acidic medium to form diazonium salt (Mukhopadhyay and Batra, 2019). The sulphonic acid groups were successfully grafted to the surface of rGO as it could be evidently seen in the FTIR spectrum. Later, the preparation of modified graphene / PVA was performed by hydrothermal reaction at 180 °C for 6 h. During this process, the PVA chains acted as bridges to link two adjacent sheets of the modified graphene and finally formed a 3D bulk composite with uniform spacing of the interlayer. Wang *et al.* synthesized 3D self-assembly polyethyleneimine-modified GO hydrogel (PEI-GHs) and they investigated the adsorption performance of uranium using these hybrid materials. In this study, PEI was chosen because it could be easily grafted to the matrix since it has both secondary amines in the linear chain and primary secondary and tertiary amino groups in the branched amines. A possible mechanism involving PEI being either directly adsorbed on the GO surface or covalently functionalized by amide cross-linking reaction between –COOH groups of GO and $–NH_2$ groups of PEI. Then, after the freeze-drying, the

assembled structure retained its structural quality, resulting in the 3D porous hierarchical structure. The development of strong amide bonds in the PEI-GHs resulted in a high adsorption capacity and removal efficiency in high concentration uranium (VI) when compared to graphene hydrogel (Wang *et al*., 2017).

Self-assembly by process reduction and cross-linking are promising methods to integrate various nanostructured materials into macroscopic substances. Another route that can be used to initiate the 3D GBM by attaching functional groups such as carbonyl, carboxyl, amino, silane, phosphate, and sulfhydryl on the surface or edges of the graphene. In that case, other than GO which bears a lot of structural defects, high structural quality graphene materials, e.g. GNPs or graphene flakes, can be also used. One of the principal advantages of using high-quality graphene is that its physical properties can be optimized. Besides, since the graphene are covalently linked, they could exhibit higher mechanical properties than for 3D GBM where only H-bonding, π-π or van der Waals interactions are responsible for the mechanical strength. However, for such less common approaches to prepare 3D GBMs, many challenges and unresolved issues remain. Samadaei *et al.* synthesized functionalized GO with EDA and poly (amidoamine) (PAMAM) simultaneously with the reduction process to form the 3D GBMs (Samadaei *et al*., 2015). EDA was used to reduce the GO and to convert epoxides into amino alcohol. After N, N'-dicyclohexylcarbodiimide and 4-dimethylaminopyridine were introduced, the occurred cross-linking with rGO resulted in the final product of rGO-NH_2, which could be used in further modification processes such as amination. Other than reducing and functionalizing GO, EDA also played a role to link the GO nanosheets within the hierarchical structure. The bonds could occur based on the two amine functionalities on both

sides of the ethylene moiety that could attack the epoxy carbon carboxylic moiety of two GO layers, helping to link the structure and developing that way a 3D porous graphene network.

2.3.4 3D graphene combined with metal-based nanoparticles

The 3D structure of graphene combined with metal based compound can be employed with efficiency for environmental depollution. Furthermore, it introduces a novel approach for fabricating nanostructured materials into macroscopic devices, paving the way for the successful use of nanomaterials to environmental issues. When 3D GBMs are combined with metal oxide NPs such as TiO_2, SnO_2, MoS_2 and Cu_2O, it showed high photoelectrochemical activity with enhanced light absorption, improved photocurrent, and highly efficient charge separation properties, resulting in higher photocatalytic performance via metal oxide NP incorporation (Qiao *et al*., 2019). Moreover, the 3D GBMs with integrated metal oxide NPs such as FeOx and MnOx is likely to be used in the future as a catalyst for pollutant transformation. Wu *et al.* reported 3D N doped GBM supported Iron(II,III) oxide (Fe_3O_4) NPs made by hydrothermal self-assembly. This was followed by freeze drying and thermal treatment using polypyrrole as the nitrogen precursor. The SEM images revealed graphene with homogeneous dispersion of Fe_3O_4 nanoparticles, and BET analysis indicated that the composites exhibited a high SSA (Wu *et al*., 2012). An efficient and green method was developed by Xiao and colleagues to synthesize Iron(III) oxide (Fe_2O_3) particles decorated GBMs by hydrothermal method. Through hydrothermal treatment, Fe_2O_3 NPs were dispersed uniformly on graphene sheets, and the composites formed a 3D network. A large-scale Fe_2O_3 / GA synthesis method using this strategy is feasible and

environmentally friendly. Besides, a synergistic interaction between uniformly dispersed Fe_2O_3 NPs and GA results in excellent electrochemical properties. With a robust 3D framework of graphene, highly conductive networks were created, characterized by a large surface area and short diffusion paths (Xiao *et al.*, 2013). Other studies have also been reported in the literature where metal oxides such as alumina (Al_2O_3) , silicon dioxide (SiO_2), TiO_2, and zinc oxide (ZnO) have been used through the different approaches to synthesize 3D graphene. All in all, effective synthesis, easy regeneration, variable morphology, and low cost make metal oxides an excellent candidate for usage as a template for environmental applications.

2.3.5 Key factors to control 2D graphene self-assembly to 3D graphene-based macrostructures

Recently, significant efforts have been made to develop interesting graphene materials or to gain a deeper understanding of graphene materials' formation and properties. Due to its high hydrophobic properties, lack of functional groups, and difficulty in manipulation, pristine graphene is difficult to apply on a large scale. GO has been combined with a variety of organic or inorganic compound for flexible applications to produce graphene materials with enhanced properties. Furthermore, because the surface of GO can modify different functional groups, it is beneficial to the specific adsorption of various targets. As a result of covalent bonds or / and multiple non-covalent intermolecular forces, such as stacking interactions, electrostatic interactions, and hydrogen bonds, building blocks derived from organic or inorganic molecules can self-assemble into functional nanostructures with a variety of morphologies and enhanced mechanical properties.

Recently, researchers have designed and constructed a series of 3D GBM with various frameworks (e.g., hydrogels, aerogels, sponges, and foams) (Liu and Qiu, 2020; Wang *et al*., 2020). The relationships among graphene, 2D graphene materials, 3D graphene materials and graphite are demonstrated in Figure 2.11. These 3D GBMs not only retain the intrinsic properties of graphene, but also possess new collective physiochemical properties, including high porosity, low density, large SSA and unique electrochemical performance. Meanwhile, 3D GBM get multi-level pores structures (micropore, mesopore and macropore) and internal connection framework, endowing them with improved surface accessibility and better mass transport. Although 3D GBMs are gaining increasing attention in a variety of fields, there are still several challenges to overcome before their commercialization.

2.4 Surface modification of graphene

The potential of graphene has been briefly discussed in the previous section. Consequently, the rapid development of this material has led to major advances in the synthesis and application of nanomaterials. In comparison to CNTs, graphene-based composites have been shown to be stronger, stiffer, and less prone to failure than composites infused with CNTs, making GBM an excellent material for environmental remediation. In general, surface modification refers to the process of changing a material's physical, chemical, and morphological characteristics for the purpose of remediating specific environmental issues. In preparation of adsorbents, the surface chemistry may be modified through a variety of methods including mechanical, thermal, chemical, or even combinations of these methods known as mechanochemical and thermochemical processes. Additionally, it can be improved

by the incorporation, elimination, and freezing approaches. As a result of these techniques, a wide range of surface properties, including surface energy, surface charges, roughness, surface area, hydrophobicity, reactivity, and functional group, can be altered.

2.4.1 Physical modification

Basically, for gaseous adsorption, it requires physical activation of the adsorbent in order to improve the performance. Physical activation, in theory, involves carbonizing porous materials at high temperatures with activation agents, often steam or CO_2 (Benítez *et al*., 2019). Basically, the mechanism begins with a thermal decomposition of the carbon source material, which is followed by the addition of an activating agent. This is a slow oxidation process in which oxygen interacts with carbon atoms, resulting in the formation of pores. The oxygen in the system is also slightly chemisorbed to the surface, creating oxygen-based complexes. Activation of CO_2 is a method of extracting any carbon from solid and then converting it to CO at a temperature higher than 800 ^oC one of the approaches to develop highly porous materials with an expected maximized adsorption due to the large surface area produced. In particular, electron transfer can activate the CO_2 molecules to promote a shift of its electron character, making it nucleophilic and much reactive with C–C (or C–H) bonds. The development of such materials could be due to the production of new pores by opening closed pores or enlarging existing pores caused by devolatilization and carbon- CO_2 reaction. Graphene-based nanostructures have been investigated as precursor by various groups (Santhiran *et al.*, 2021). Xia *et al.* synthesized hierarchically macroporous graphene-based carbons (HPGCs) through CO_2 activation. Interestingly, they observed that the

optimal temperature for CO_2 activation is 850 ^oC. In the experiment, the GO was heated under N_2 atmosphere before being blown with CO_2, which theoretically leads to the formation of mesopores (3.80 nm) and macropores (>50 nm) as a result of the reaction. During the activation process, the oxidizing agent, CO_2, reacts with GO, resulting in micropores (2 nm) being formed. In addition, during activation, closed pores are opened and those that already exist are widened. As a result of BET analysis, the SSA of the GO and the total pore volume gradually increased from 51 to 459 $m^2\ g^{-1}$ and 0.05 to 1.17 $cm^3\ g^{-1}$, respectively, after activation. Besides, high-resolution TEM shows the presence of abundant micropores (2 nm), as well as small mesopores (2-5 nm). However, when the oxidation temperature is raised up to 950 °C, some holey defects are observed within the curved layer (Xia, 2014).Similarly, Liu *et al.*, used GO as the starting material for the physical activation in order to obtain highly porous and metal-free carbonaceous materials. They proved that by this method, the surface of activated GO has improved by the factor of 3 from 206 $m^2\ g^{-1}$ to 611 $m^2\ g^{-1}$. They believe that through CO_2 activation, GO will undergo effective gasification, resulting in greater porosity and less reduction in oxygen groups. Additionally, physical activation can vary or adjust the surface chemical nature of activated graphene with certain unique characteristics (Liu *et al*., 2013).

2.4.2 Chemical activation and functionalization

Essentially, the surface chemistry of graphene is driven by the presence of functional groups, doping of heteroatoms, metal or metal oxide, and coating of organic polymer on the surface. The addition of nitrogen function could also modify the surface chemistry as it promotes an increase in the functional basicity that

increases the capacity for adsorption. Different methods have been reported to prepare nitrogen-doped graphene materials, such as post-synthetic ammonia treatment and the most popular is direct synthesis with usage of nitrogen-containing precursors. For example, Rodríguez-García *et al.* explore the replacement of graphene by GO in order to avoiding the reduction stages with hydrazine and chemical activation treatments in nanocomposites prepared with polyaniline or Fe_3O_4 nanoparticles. They found that, the highest micropore volume is reached when GO are coated with the polymer polyaniline (PANI) and the composite substantially enhances the porosity of the material. The presence of O groups in GO allows one to modulate the chemical composition in the surface by joining different types of materials resulting in new nanocomposites (Rodríguez-García *et al*., 2019). Besides, it has been demonstrated by Mahmoodi *et al.*, that a top-down approach can be used to synthesize rGO nanosheets from graphite, and further improvements to the material's structural properties have been achieved by chemically modifying the rGO surface with cetyltrimethylammonium bromide (CTAB) (Mahmoodi *et al*., 2017).

Recently, Wimalika Thalgaspitiya *et al.* prepared a highly efficient adsorbent from molybdate-intercalated hydrotalcite (HT-MoO_4). A hydrothermal approach was used to fabricate TiO_2-rGO nanocomposites doped with transition metals (Mn, Mo, Ni, Co, and W). According to the BET results, the synthesized composite materials exhibits large surface area of 165 to 245 mg g^{-1} with the pore size distributions is in the range of 3–5 nm. Based on the EDX mapping data, Mo-TiO_2 / rGO composite materials showed a homogeneous distribution of transition metal dopants throughout the material. Among the transition metal dopants, Mo-TiO_2 / rGO demonstrated good structural properties for the optimum performance

condition. In conclusion, in order to develop new and high-quality nanomaterials for certain applications, it is necessary to understand what structural characteristics and what chemical modifications have a greater impact on their properties (Thalgaspitiya *et al*., 2020)

Using various types of synthetic methods, Ye *et al.* modify GBM with various chemical modifications, including doping with nitrogen, activating with potassium hydroxide (KOH), and mixing with fibers. According to this study, successive modifications have improved the micropore volume, decreased the crystallite size, and, therefore, improved the performance of the materials (Ye *et al*., 2022). For chemical activation, the process usually has several steps, including one thermal step combined with several chemical approaches. In the literature, various activating agents, including zinc chloride ($ZnCl_2$), sodium hydroxide (NaOH), phosphoric acid (H_3PO_4), and potassium hydroxide (KOH), have typically been studied. Among these, NaOH and KOH seem to be most preferred. The purpose of activation is to improve the SSA or pore volume of activated graphene through opening new pores and developing the existing pores.

2.4.2 (a) Metal impregnation on the surface of graphene

Another chemical surface modification that can be done on the surface of graphene is by introducing metal or metal oxide. Generally this metal or metal oxide impregnation is commonly produced via wet impregnation or sol–gel chemistry, in which a novel technique for producing solid materials from small molecules. This technique is usually used for the fabrication of metal oxides (Van Langenhove and Paul, 2015). In general, these designing and making were regarded as low-cost and low-temperature approaches. However, proper control of the chemical composition

during the impregnation process to generate desirable structural properties might be challenging at times.

For example, Gaspar et al impregnated activated carbons with transition metal oxides (CoO, Co_3O_4, and CrO_3) in order to prepare them for the complete catalytic oxidation of benzene, and they discovered that when impregnation was performed after activation, the impregnated species were deposited on the internal surface, blocking part of the initial porous texture (Alvim-Ferraz and Gaspar, 2005). Besides, Zhang et al, investigated over a series of activated carbon (AC) supported Co as a function of Co loading. From the BET analysis, SSA of the Co impregnated activated carbon reduce about 30 % after the impregnation process together with the pore volume. Furthermore, they also found that, excess Co (>25 wt.%) had a detrimental impact not only on catalyst performance, but also on support surface properties.

Liquid / wet approach for introducing metal composites on carbon based materials provides unique opportunities, however the diffusivity of colloidal nanoparticles is generally slow and it might take a long time for all particles to migrate into the pores of the support (Munnik et al., 2015). Thus, various novel or revitalised techniques involving gas phase metal deposition on the carbon surface are discussed in the next section.

2.4.3 Modification by combining metal-based particles or thin films with graphene

Along with the morphology structure, the structural, mechanical property and surface chemistry of 3D GBMs are also crucial parameters for adsorption performance. Although pure 3D graphene shows some promise for adsorption, it is

important to make the necessary surface functionalization according to the properties of certain contaminants. The main effects of chemically modification the surface are improving the structural properties, mechanical properties and tuning the surface chemistry with providing extra functional groups. Besides, by coating after supercritical drying, this property can be modulated. The high aspect ratio of the internal pores makes surface modification more complex, preventing line-of-sight techniques such as sputtering and evaporation from being used. Moreover, liquid-phase surface modification is complicated by pore collapse due to capillary forces in aerogel pores and slow diffusion. To address these limitations, ALD is a powerful vapor-phase deposition technique that is suitable for conformally coating ultra-high-aspect- ratio structures, due to its self-limiting surface reactions and sub-nanometer control of material (Gayle *et al*., 2021).

2.4.4 Modification by atomic layer deposition

ALD is a gas phase thin film deposition technique which has been discovered and developed independently in the 1960s in the Soviet Union and in 1974 in Finland (Ahvenniemi *et al*., 2017; Malygin *et al*., 2015). This technique is characterized by exposing the substrate to an alternating sequence of vapor phase reactants. Due to the self-saturating nature of the surface reactions, the film thickness can be controlled at the atomic scale. ALD has been used to deposit conformal thin films or NPs islands onto the surfaces of a wide range of high-aspect-ratio structures, such as graphene, anodic alumina (AAO), silicon trenches, track-etched polycarbonate membranes, nanowires, CNTs, lateral high-aspect-ratio (LHAR) structures, and others (Gayle *et al*., 2021). In ALD, precursors play a critical role since their chemistry determines the growth and properties of the films

deposited. Furthermore, the growth temperature can also affect the roughness, crystallinity, and composition of the films.

ALD can deposit a broad variety of materials, including oxides, nitrides, sulphides, and elemental metals, which provides a great degree of material diversity. The advantages of ALD, including precise thickness and compositional control as well as conformal coating of complex geometries, make it attractive for surface and interfacial engineering of these devices. Early studies of ALD on aerogels focused on Al_2O_3 and ZnO coatings on silica aerogels thickness and composition coated aerogels have since been utilised for a range of applications such as battery electrodes (Yu *et al*., 2014), dye-sensitized solar cells (Zhou *et al*., 2022), water purification and environmental remediation (Yang *et al*., 2018).

Zhu and co-workers reported a method for the synthesis of graphene and CNT carpet hybrids by firstly forming the graphene onto the surface of Cu foil through CVD, and then depositing Fe and Al_2O_3 on the graphene-covered Cu foil through e-beam evaporation, followed by growing CNT carpet directly on the graphene surface. In general, high-resolution microscopy and surface area measurements were used to characterise ALD coatings on aerogels. In this work, they used STEM to examine the atomic structure of graphene–CNT junctions, and from the images, they confirmed that there is a covalent bond between the graphene and CNTs in junction areas of the hybrid materials. Besides, BET analyses indicated that they have an exceptional surface area (Zhu *et al*., 2012). Wang *et al.* have successfully fabricated ZnO nanomembranes / graphene aerogel composites through ALD. This work describes a novel electrode structure based on 3D GBMs coated with ZnO nanomembranes. 3D GBMs were fabricated using a template-free,

freeze-drying technique, followed by ALD coating with ZnO nanomembranes. According to their findings, changes in the number of ALD cycles can be used to control the composition of 3D GBMs / zinc composites (D. Wang *et al*., 2019).

In principle, a typical ALD process consists of several ALD cycles with each ALD cycle comprising four characteristic steps, which are shown in Figure 2.12 for the prototypic trimethylaluminum (TMA) / H_2O process: first, the TMA precursor reacts with the hydroxyl groups (-OH) on the porous GBM surface (Saleem *et al*., 2014). These hydroxyl groups are replaced with aluminum methyl groups (Al-CH_3). The by-product methane and excess TMA are then purged from the chamber. After purging, water was introduced to consume unstable methyl groups on the surface of porous graphene and form stable aluminum hydroxyl groups (Al-OH). A flow-through geometry along with long pulse and purge times was used to form a homogeneous coating both on the surface and inside of the aerogel. These characteristics, combined to the low synthesis temperature and the versatility in term of materials that can be deposited, make ALD a highly suitable technique for the synthesis of Al_2O_3 / porous graphene.

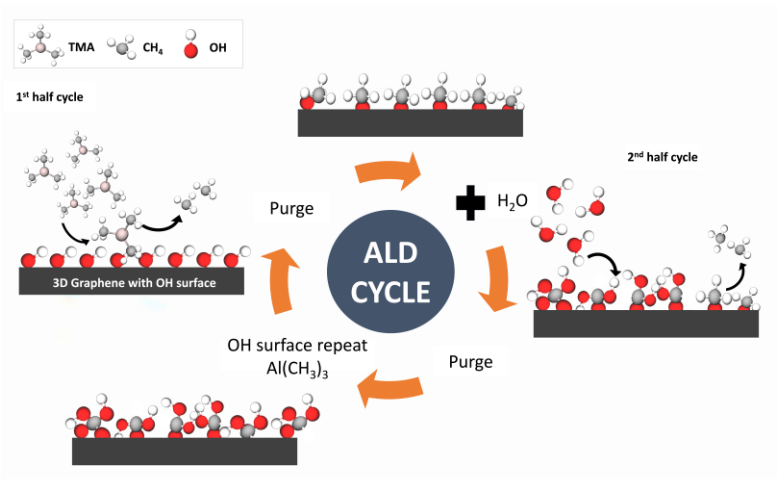

Figure 2.12 Reaction mechanism ALD process.

2.5 Properties vs. performance

Formation of 3D GBM is especially desired to exploit their surface area to develop innovative materials for their application in energy and environment. High SSA and highly interlinked pores make these 3D GBM the ideal material for the next generation of nanostructured materials. The surface area of 3D GBM is one of the main characteristics usually reported in literature because it strongly impacts their performances. The porosity (pore size distribution or pore volume) of GBM is the second key parameter studied. Generally, the GBM pore size can be categorized into three main scales, (1) in-plane pores for carbon porous materials; (2) interlayered pores for 2D graphene (3) in-plane pores and interlayered pores for 3D graphene (Firdaus *et al*., 2021). In addition, if the pore size is too small, the guest molecules or reactant compounds, diffusion within the material and access to the reactive surface is limited. Moreover, too large pore diameter or two weak interconnectivities within the GBM will lead to fragile materials which consequently lose their interest for any application.

Table 2.3 reviews the progress of the works regarding the surface area, the porosity and density. The main reason is that most often, FLG (including GO and rGO) or MLG are used as graphenic material to build the macroscopic structure. This is difficult to give the value in surface these GBM could reach, however, several hundreds of $m^2\ g^{-1}$ could be a minimum for a reasonable surface expected for these GBMs considering the high surface of the building block used. Even if most of the works report surface area below 1000 $m^2\ g^{-1}$, GBMs with exceptional high surface areas (> 1000 $m^2\ g^{-1}$) have been reported (Chowdhury and Balasubramanian, 2016b). These 3D GBMs could be prepared by either the direct

method or by the self-assembly approach. Except for these works, yet there is still limitation and most of the reported works seems to have moderate (500-1000 $m^2 g^{-1}$) (Sun et al., 2018; Singh et al., 2017) and low surface (50-500 $m^2 g^{-1}$) (Sui *et al*., 2013; Jiang et al., 2017). In some cases, the obtained 3D GBM displayed a hierarchical porous network structure containing mesopores with low surface of less than 100 $m^2 g^{-1}$. Within the macrostructure, the 2D graphene suffers from aggregation during the growth or the self-assembly process due to attractive forces, such as π- π or van der Waals.

Many 2D graphene systems can be used for 3D GBMs designing and the relevant parameters impacting the self-assembly mechanisms are difficult to be tested and evaluated separately. In recent works, some of them such as pH or 2D graphene size have been reported to strongly affect the assembly of GO. The porosity structure is also difficult to control and depends on highly sensitive nanoscale phenomena. Most often, the authors claim the high performance of their materials also well supported by the shown results in term of adsorption capacity, specific capacitance etc. The reported results are rarely compared with less expensive materials such as typical activated carbons. Many of these GBMs are, however, much more costly than activated carbons and therefore the new investigation strategies are required to develop new approaches that enable the surface area and pore interconnectivity to be maximized together without reducing the mechanical properties.

The characteristics of each graphene type depend on the synthesis method (and the related characteristics) and the methods further used for the 3D macrostructure preparation are also closely linked to the graphene type produced.

This is the reason why it is important to know the principle and the respective properties of the graphene produced by each synthesis method. Another important aspect is that a large amount 2D graphene material is required to prepare GBM. For example, Chowdhury and Balasubramanian fabricated a highly ordered GBM with large SSA and interconnected hierarchical pore networks (Chowdhury and Balasubramanian, 2016a). More significantly, through various stacking techniques, the gas flow channel and pores can be controlled, resulting in excellent CO_2/N_2 stability and fast adsorption kinetics as well as stable CO_2 adsorption/desorption cycling process. Besides, the addition of functional compounds such as oxygen-containing groups has also been shown to be useful for the design of a good porous material for CO_2 absorption. Sui *et al.* synthesized 3D hydrothermal holey reduced graphene oxide (HRGO) with high pore capacity and large surface area (Sui and Han, 2015). Their graphene-based adsorbent displayed an enhanced CO_2 capture efficiency due to textural properties and various molecular interactions, *e.g.* acid-base interactions, polar interactions, and hydrogen bonding between CO_2 and HRGO. Similarly, the incorporation of functional groups of doping heteroatoms, such as nitrogen, sulfur, oxygen, and phosphorus, has also been shown to be promising dopants for CNTs and graphene-based adsorbents to improve their capacity to adsorb CO_2 (Bandosz *et al*., 2016; Li *et al*., 2016). The N doped GBMs adsorbent was synthesized by a simple hydrothermal method using ammonia as a dopant (Sui *et al*., 2015). The N doped GBMs possessed a hierarchical structure with high porosity significantly conducive to the mass diffusion process and the exposure of adsorption sites for adsorbates. Besides, high charge density at nitrogen sites of N doped GBMs could maximize the contact with polarizable CO_2

molecules through interactions between dipole and quadrupole which can greatly impact the efficiency of CO_2 capture.

Some authors have attempted to remove dyes from wastewater using graphene-based adsorbents. A study by Tiwari *et al.* described the use of rGO hydrogel for the uptake of rhodamine B and methylene blue in water with 97 % removal capacity within two hours, and the sorption was due to cation-anion and π-π interactions (Tiwari *et al*., 2013). In three consecutive cycles, they reported removal capacities of 80 and 100 % for methylene blue and rhodamine B, respectively. Accordingly, they suggested that the method could be utilized in both environmental and industrial applications. In a study on the removal of CR dyes from synthetic wastewater, Noha Almoisheer *et al.* prepared GO / silica / single-wall CNTs (GO / SiO_2/ SWCNTs) composites by a hydrothermal method (Almoisheer *et al*., 2019). A maximum capacity of 456.15 mg g^{-1} for CR adsorption was obtained at optimum conditions (20 °C, 330 min) using GO / SiO_2/ SWCNTs composites at pH 3.0 as compared to pristine SiO_2 and SWCNT. Adamantia Zourou *et al.* used GBM to synthesize GO / copper ferrite nanohybrids, and found that the prepared adsorbents exhibited good adsorption capacity rates, as well as, good recyclability, even after five cycles of reutilization (Zourou *et al*., 2022).

Sui *et al.* synthesized 3D amine-graphene porous materials with two different methods: (1) by hydrothermal reduction of graphene (HTG) using Teflon-lined stainless-steel autoclave at 180 °C for 12 h and (2) by cross-linking approach under mild conditions (Sui *et al*., 2013). Based on SEM images, it was determined that the monolithic GA were composed of a large number of interconnected macropores with the SSA increased from 280 to 475 m^2 g^{-1}. The enhancement of

SSA can be attributed to the appropriate Polyethylenimine (PEI) polymers covering the surface of GO sheets, which prevent GO sheets from stacking. The monolithic GO–PEI have a smaller SSA when PEI is too high. As PEI content increases, only some polymers will take effect. As far as surface chemistry is concerned, the method appears to be effective, as the FTIR and XPS spectra confirm the presence of PEI polymers on the GO surface, and some PEI chains are covalently linked to the GO surface through amide bonds. Ultimately, they believed that the synthesis method was successful, and that monolithic GO-PEI have a great deal of potential for application in especially in environmental research. Pruna *et al.* developed EDA-functionalized GA through a single-step hydrothermal process, and they investigated the effects of starting graphite material and oxidation conditions (Pruna *et al*., 2019). According to the results, the distribution of oxygen groups and type of GO altered by oxidation conditions and graphite nature result in a different N doping configuration in the modified aerogel, and a higher surface utilization factor for the performance. They also observed that the GO-based aerogel obtained from expanded graphite exhibited the highest performance (2-fold that of the unmodified one), suggesting that this approach has great potential for improving CO_2 adsorption.

Other than insertion of functional groups on the surface or edges of graphene, the doping of sole heteroatoms such as nitrogen, boron, oxygen, and sulfur or the mixture of heteroatoms is also one of the methods used for tuning the favourable properties of nanomaterials and optimizing the performance. In addition, the combination of polymers has also shown beneficial effects in improving the performance especially in CO_2 adsorption. Politakos *et al.* performed the reduction-induced self-assembly process at mild conditions to produced 3D

rGO / polymethylmethacrylate (PMMA) (Politakos *et al*., 2020). The reduction reaction was performed using ascorbic acid as reducing agent; after that, it was placed in an oven at three different temperatures (45, 60, and 90 °C). The BET analysis was performed to define the porous texture of the monoliths, and at temperature 90 °C, the BET surface area was the highest as the reduction reaction took place very fast at higher temperatures compared to temperature 40 and 60 °C. The amount of PMMA can also influence the self-assembly phase of rGO as it can create highly durable structures. In this work, the preparation conditions of the graphene-based adsorbent, *i.e.* the reducing agent amount and the reduction temperature, were crucial for the efficiency of the application. Thus, in this case, the surface area was not the only primary consideration for high performance. Lee and colleagues developed a complex 3D macroporous material which was mechanically flexible with tunable porous morphologies through chemically modified GO platelets (Lee *et al*., 2010). In addition, due to the polymerization process, the 3D complex structure may have formed, where the concentration of precursors and the chain length of grafted polymers played an important role.

Table 2.3 Specific surface area, porosity, density, and applications of GBMs prepared by different methods

Type of 3D GBM	Synthesis approach	Precursor/starting material/reactants	SSA ($m^2 \cdot g^{-1}$)	Porosity	Density ($g.cm^{-3}$)	Application	Ref.
Direct synthesis approach							
3D highly porous graphene	Single-step chemical solid deposition	Carbon source: methane Catalyst precursor: scallop Etching solution: HCl	2720	Pore volume: 1.45 $cm^3\ g^{-1}$	N / A	Methane adsorption	(Mahmoudian *et al*., 2016)
3D porous FLG	Direct CVD growth by porous Cu template	Catalyst precursor: Copper carbonate Etching solution: HCl and hydrogen peroxide (H_2O_2)	1545	Pore volume: 7.30 $cm^3\ g^{-1}$	N / A	Electrochemical energy storage	(Zhao *et al*., 2017)
3D graphene foams	CVD growth of graphene films	Carbon source: Methane; Catalyst precursor: Nickel foam Etching solution: HCl and $FeCl_3$	~ 850	N / A	0.0025-0.007	N / A	(Chen *et al*., 2011)

Table 2.3 Continue

Type of 3D GBM	Synthesis approach	Precursor/starting material/reactants	SSA ($m^2 \cdot g^{-1}$)	Porosity	Density ($g.cm^3$)	Application	Ref.
3D graphene nanowalls	PECVD	Carbon source : methane Catalyst precursor : GA	795	Pore size: 0.56 - 0.62 nm	N / A	N / A	(Zhou *et al*., 2017)
3D graphene macroscopic objects	Direct CVD growth of graphene nanostructure	Carbon source: methane Catalyst precursor: nickel chloride hexahydrate Etching solution: HCl and $FeCl_3$	~ 560	N / A	0.022	Removal of heavy metal	(Li *et al*., 2013)
3D graphene foams	Direct CVD growth by seashell based templete	Catalyst precursor: bagasse Etching solution: HCl	337	Pore size: 2.3- 3.6 nm	0.03	Oil- water separation	(Shi *et al*., 2016)

Table 2.3 Continue

Type of 3D GBM	Synthesis approach	Precursor/starting material/reactants	SSA ($m^2 \cdot g^{-1}$)	Porosity	Density ($g.cm^{-3}$)	Application	Ref.
Self-assembly approach							
3D porous graphene	Self-assembly by hydrothermal reduction and polymer cross-linking	Starting material: GO Type of linker: PEI Reductant: NaOH	476	Pore volume: 0.6−1.3 cm^3 g^{-1}	0.02−0.03	Dye and gas adsorption	(Sui *et al*., 2013)
3D graphene-based macrostructures	Self-assembly by hydrothermal reduction and chemical activation	Starting material: GO Chemical activation: CO_2	~1300	Pore volume: >1 cm^3 g^{-1}	N / A	Gas adsorption (CO_2 capture)	(Chowdhury and Balasubramanian, 2016b)
3D nitrogen doped graphene aerogel	Self-assembly by thermal process	Starting material: GO Reductant: ammonia solution	830	Pore volume: 0.05-0.3 cm^3 g^{-1}	N / A	Supercapacitors electrode and gas adsorption	(Sun *et al*., 2018)

Table 2.3 Continue

Type of 3D GBM	Synthesis approach	Precursor/starting material/reactants	SSA ($m^2 \cdot g^{-1}$)	Porosity	Density ($g.cm^{-3}$)	Application	Ref.
3D GO composite	Self-assembly via chemical cross-linking	Starting material: GO Type of linker: glutaraldehyde, resorcinol, and Borax	~700	N / A	0.02−0.03	Gas storage and adsorption (CO_2 capture)	(Sudeep *et al.*, 2013)
3D graphene aerogel	Self-assembly by chemical function grafting	Starting material: GO Type of linker: lignosulfonate Functional group: amine	627	Pore size: 1 to 40 nm	N / A	Removal of heavy metal	(Singh *et al.*, 2017)
Graphene/cysteamine aerogel	Self- assembly with organic linker	Starting material: GO Type of organic linker: cysteamine	68.11	N / A	N / A	Water purification	(Chen *et al.*, 2018)

Table 2.3 Continue

Type of 3D GBM	Synthesis approach	Precursor/starting material/reactants	SSA ($m^2 \cdot g^{-1}$)	Porosity	Density ($g.cm^{-3}$)	Application	Ref.
3D copolymer/ graphene aerogel	Self-assembly by hydrothermal reduction and polymer cross-linking	Starting material: GO Type of linker: Composite flocculant P(AM-DMDAAC) Reductant: urea	206.591	3.6 - 4.2 nm	0.0114	Oil/water separation	(S. Zhang *et al*., 2019)
3D graphene composite	Self- assembly with organic linker	Starting material: GO Type of organic linker: β-cyclodextrin/poly (l-glutamic acid)	105.50	-	N / A	Water and wastewater treatment	(Jiang *et al*., 2017)
3D N-doped graphene aerogel	Self-assembly by solvothermal reduction	Starting material: GO Type of linker: EDA	156	N / A	0.01	Gas adsorption (CO_2 capture)	(Zhang *et al*., 2013)

2.6 Summary

There has been considerable effort directed toward developing interesting graphene materials over the past few years, as well as a better understanding of graphene formation and properties. However, pristine graphene is extremely hydrophobic, free of functional groups, and difficult to manipulate, which limits its use. An overview of the literature on chemical and physical modifications of 2D GBM surfaces is provided in this chapter. GO and rGO were demonstrated in the past decade as a potential material to be use for environmental application. They have opened up new opportunities to be use as a starting material for synthesis of GBMs because of sufficient oxygen atoms are present on both the basal plane and edge, making them capable of reacting covalently with different compounds. Besides, it also described the state of the art and critical aspects of designing and constructing a series of 3D GBM using different frameworks (for example, hydrogels, aerogels, sponges, and foam). The relationship between 2D graphene and 3D graphene monoliths is also discussed to gain a deeper understanding of the chemistry involved in the modification process. Even though 3D GBM are becoming increasingly popular in various fields, commercial applications will face a number of challenges that need to be addressed. Indeed, the method preparation of 3D GBM is one of the crucial part that need to be considered. In this chapter, different strategies have been discussed in order to create 3D GBMs which are by direct synthesis approach and self-assembly approach. Besides, in this chapter, we highlighted that 3D GBMs are promising new materials with high SSA and outstanding chemical characteristics that can be controlled to provide favourable interactions with reactive species. From the recent literature, it has been shown that keeping the accessible surface morphology of 3D GBMs affects its adsorption

performance, particularly since mater transfer is the limiting factor for adsorption process. Besides, the possibility of chemical surface modifications and their control to design advanced functional materials has been addressed including post-modification, where pure 3D GBMs frameworks are used as skeletons, and different components are chemically added to those frameworks (atoms, molecules, inorganic particles, polymers, carbon nanomaterials, inorganic compounds). The literature has indeed shown that the performance of graphene-based materials in terms of adsorption studies is highly dependent on their properties, especially the SSA, pore volume, and pore size. Further, chemical modification of the surfaces of 2D and 3D graphene may provide a unique opportunity to control the structural properties as well as surface chemistry and the adsorption capacity.

CHAPTER 3

METHODOLOGY

This chapter presents details of the overall experimental study, which includes the description of the used materials and chemicals, equipment setups. The procedures and their optimization applied for the synthesis of the studied graphene-based samples including 2D graphene, their assembly to 3D graphene-based macrostructures (or GBMs) and the 3D alumina/GBM hybrids produced. Additionally, all the used characterization techniques to analyse the samples and the used operating conditions for the performed analysis are described. The measurement process to evaluate the performances of the selected graphene-based materials for CO_2 adsorption or CR dye adsorption are as well described.

For this PhD work conducted in the framework of a bilateral cotutelle program, the experiments including the sample preparation, the performed characterizations and the evaluation of the performances of the prepared adsorbents have been done in two different universities: University Sains Malaysia (Malaysia), USM and University of Lorraine (France), UL. The location where each part of the work has been done is specified in this chapter.

3.1 Materials and Chemicals

There were several chemicals (including liquids and gases) used for the preparation of the studied graphene-based samples (Table 3.1).

Table 3.1 List of chemicals and reagents.

Chemical/Reagent	Purity (%)	Supplier	Purpose of use	Location
Graphite powder	99	Sigma-Aldrich	GO preparation	USM and UL
Sulphuric acid (H_2SO_4)	95-97	Sigma-Aldrich	GO preparation	USM and UL
Sodium nitrate ($NaNO_3$)	-	Sigma-Aldrich	GO preparation	USM and UL
Potassium permanganate ($KMnO_4$)	-	Sigma-Aldrich	GO preparation	USM and UL
Hydrogen peroxide (H_2O_2)	-	Chem-Supply	GO preparation	USM and UL
Hydrochloric acid (HCl)	37	Biolab	GO preparation	USM and UL
Potassium hydroxide (KOH)	85	Sigma-Aldrich	GO preparation	USM and UL
Ascorbic acid (AA)	-	Sigma-Aldrich	GBM preparation	USM and UL
Liquid Nitrogen	99	Air Product	GBM preparation	USM and UL
Trimethylaluminum (TMA)	99	Sigma-Aldrich	Alumina/GBM preparation	UL

Table 3.1 Continue

Chemical/Reagent	Purity (%)	Supplier	Purpose of use	Location
Deionized water (Resistivity =18.2 μΩ)	-	ELGA Pure lab Option Q	GO and GBM preparation	USM and UL
Carbon dioxide (CO_2)	99.9	Air Product	2D graphene activation agent and CO_2 source for adsorption study	USM
Nitrogen (N_2)	99.9	Air Product	N_2 source for adsorption study	USM
Congo red (CR)	99	Sigma Aldrich	Model pollutant	USM

3.2 Equipment

All the equipment used in this study were also be discussed in this section. Table 3.2 provides an overview of all equipment used along with their specifications and functions.

Table 3.2 List of equipment used for preparation of 2D, 3D GBM and 3D Al_2O_3 / GBM hybrid adsorbent.

Equipment	Model	Purpose	Location
Oven	Memert	Drying	USM and UL
Hot plate stirrer	Ika C-Mag H57	Mixing of solution	USM and UL
Weighing balance	Mettler Toledo	Weighing of sample	USM and UL
Stainless steel Teflon-lined autoclave	Swagelok	Hydrothermal preparation	USM
Tubular reactor	-	Activation process	USM
Freeze dryer	-	Freeze dry 3D GBM samples	USM and UL
ALD PICOSUN™ R-200 Advanced reactor	-	Alumina deposition	UL
Thermogravimetric analysis (TGA)	Setaram Setsys evolution 1750 / TA Instrument Q600	To determine a material's thermal stability and the fraction of volatile components / CO_2 sorption study	USM and UL
Scanning electron microscope (SEM)	XL 30 S-FEG and ZEISS Gemini SEM 500	To examine the surface morphology of the samples	UL

Table 3.2 Continue

Equipment	Model	Purpose	Location
Transmission Electron Microscope (TEM)	JEOL JEM-ARM 200F	To examine the surface morphology of the samples	UL
Energy Dispersive X-ray Spectroscopy (EDS)	FEI Quanta 450 FEG Microscope	To confirm the metal deposition on the samples	USM
Fourier Transform Infrared (FTIR)	Thermo Scientific Nicolet iS10 spectrometer	To determine the surface functional group	USM and UL
Raman Spectroscopy	LabRAM HR 800 micros-Raman spectrometer	To measure the defect of the samples	USM and UL
X-ray photoelectron spectroscopy (XPS)	Kratos Axis Ultra	To analyse the surface chemistry of the samples	USM
Brunauer–Emmett–Teller (BET)	Micromeritics Ltd	To determine the specific surface area of the samples	USM and UL

Table 3.2 Continue

Equipment	Model	Purpose	Location
Zeta Potential	Malvern Zetasizer Nano-Z (ZEN 3600, UK)	To measure the effective electric charge on the surface, quantifying the charges.	USM
UV- Vis Spectrophotometer	Model Shimadzu UV- 1800, Japan	To obtain the absorption spectra of a compound in solution	USM

3.3 Experimental steps

The flow of overall experimental activities throughout the PhD work is presented in Figure 3.1. This work is organized with six parts:

1. Preparation of GO as starting materials
2. Modification of GO by physical and chemical activation
3. Study of the CO_2 adsorption capacity
4. Synthesis of 3D GBMs using a hydrothermal approach
5. Modification of 3D GBMs by deposition of alumina via ALD to produce nano porous alumina-based adsorbents.
6. Evaluation of removal of CR dye

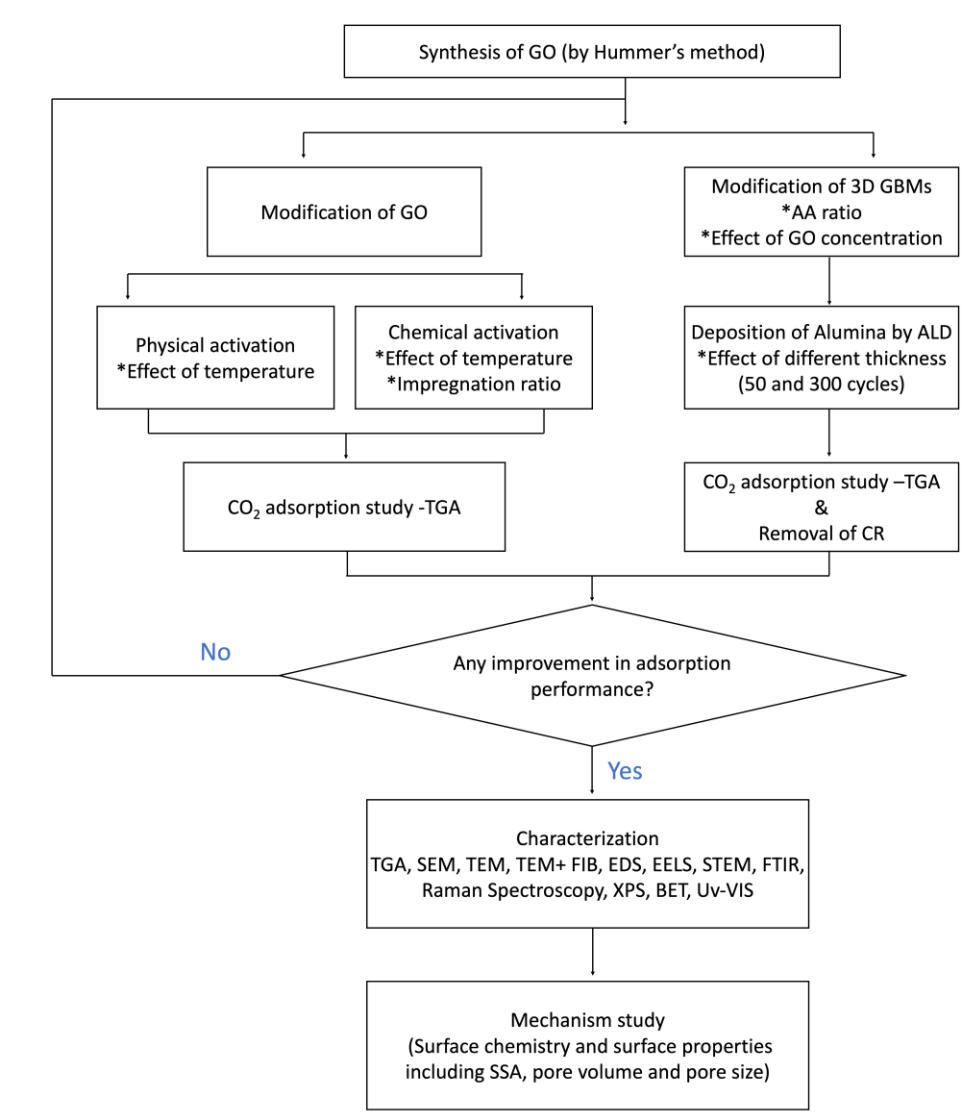

Figure 3.1 Flowchart of the overall experimental activities in the present study.

3.3.1 Preparation of graphene oxide

The modified Hummers' method was used to synthesize graphene oxide (GO) from graphite powder. The typical procedure is as follows: graphite (2 g) and $NaNO_3$ (2 g) were mixed with H_2SO_4 (50 mL) and stirred for 2 h in an ice bath (0–5 °C). Then, 6 g of $KMnO_4$ was slowly added to the resulting solution. The ice bath was removed, and the solution was then stirred at 35 °C for 2 days. An amount of 300 mL of deionized water (DI) was added gently to the solution. Then, 10 mL of H_2O_2 were slowly added to the above solution. The resulting solution was washed

with HCl (400 mL, 10%). Additional washing with DI water provide the GO product under the form of a paste. Subsequently, the concentrated aqueous paste of GO was dried using a freeze dryer and the used GO is produced under the form of powder.

3.3.2 Physical activation of graphene oxide

GO was activated in a simple one-step reaction using CO_2 as the activation agent. In a typical procedure, 0.5 g of the synthesized GO was loaded on a ceramic boat, placed at the center of the tube furnace, and heated under a continuous flow of CO_2 (100 mL min^{-1}) to the desired temperature (500, 600, 700, 800 and 900 °C) at a heating rate of 10 °C min^{-1} and a holding time of 1 h. Following the activation step, the sample was left to cool naturally to room temperature in the furnace under the flow of N_2. The materials thus obtained were labelled as GO-PA X, where X is the activation temperature.

3.3.3 Chemical activation of graphene oxide

In this experiment, 0.5g of GO were soaked in an aqueous KOH solution (1.5 grams in 1 mL) at a ratio of 1:3 of GO:KOH. After 6 h of contact time, the mixture was dried at 110 °C for 24 h. Later, each sample was loaded into the horizontal tube furnace under a flowing N_2 atmosphere (100 mL min^{-1}) and was heated at 10 °C min^{-1} to 500 °C. Once the maximum temperature was reached, a reaction time of 60 min was applied. After the heat treatment, the samples were washed with HCl (1 M), then washed with distilled water until pH 6. This procedure was repeated using a different range of temperature (500, 600, 700, 800 °C). The

materials thus obtained were labelled as GO-CA X, where X is the activation temperature.

3.3.4 Preparation of 3D graphene-based macrostructures

Aqueous suspensions of GO (1, 2, 4, 6 mg mL^{-1}) were prepared with 10 mg of GO dispersing in 5 mL deionized water via ultrasonic treatment for 20 min. Briefly, 10 mg of AA was dissolved in an GO suspension, and the mixed suspension was transferred to Stainless steel Teflon-lined autoclave, heated to 95 ◦C and kept 3 h, leading to the formation of hydrogel. Then, to remove the residual agents, the hydrogel was washed with deionized water for 24 h. Finally, the 3D GBMs sample was achieved by freeze-drying for 24 h with GO to Vit C mass ratio of 1:1. The materials thus obtained were labelled as 3D GBM-X, where X is the GO concentration (1, 2, 4, 6 mg mL^{-1}).

3.3.5 ALD deposition on 3D Al_2O_3 / GBM hybrids

A layer of Al_2O_3 was deposited on 3D GBM by using the ALD PICOSUN™ R-200 Advanced reactor and Trimethylaluminum (98%, Stream Chemicals) as Al precursor and water as co- reactant. TMA precursor and water were kept at 18°C in Peltier-cooled precursor bottles. In this experiment, the reaction chamber pressure was set at 10 kPa, and the substrate temperature at 200°C. The optimal sequence for deposition of 3D GBM samples is 1s of TMA / 30 s of N_2 purge / 1 s of H_2O / 40 s of N_2 purge, resulting in a growth per cycle of 0.2/cycle.

3.4 Characterization techniques

The prepared graphene-based materials have been analysed using several techniques in order to determine their structural, chemical and physicochemical

properties. Each technique and the instrument used is described in a separate subsection.

3.4.1 Scanning Electron Microscopy with Energy Dispersive X-Ray (SEM-EDX)

Surface morphology of 2D graphene were determined by a FEI Quanta 450 FEG (Czech Republik) field emission scanning electron at School of Chemical Engineering, Universiti Sains Malaysia, Penang. The SEM provided images by scanning the samples using secondary electron back-scattering electron imaging (BEI) and Inlens mode. The energy dispersive X-ray spectroscopy was used in conjunction with SEM analysis. Besides, for 3D GBM and 3D Al_2O_3 / GBM hybrids samples, the analysis was carried out at the Institute Jean Lamour (University of Lorraine-CNRS, Nancy, France) using scanning electron microscopy with a ZEISS Gemini SEM 500 equipped with a field emission gun. This apparatus is equipped with Energy Dispersive X-ray Spectrometer.

3.4.2 Transmission electron microscopy (TEM)

Transmission electron microscopy (TEM) analysis was carried out using a JEOL ARM 200F cold FEG (Université de Lorraine, Institut Jean Lamour, France) with field emission apparatus at an operating voltage of 200 kV. For the nanoparticle observation, a small amount of powder is dispersed in ethanol in a low-power sonication bath for a few minutes and deposited on a holey carbon grid (200 mesh size). The structure of the graphene samples was carefully studied under high resolution with selected area electron diffraction (SAED) and fast Fourier transform (FFT) was performed on chosen areas. Besides, scanning transmission electron microscopy (STEM) coupled with electron energy loss spectroscopy (EELS) were

also used in this study to measures the elemental content of atomic and nano atomic scale structures. Additionally, a Focused Ion Beam (FIB) scanning electron microscope (SEM) dual beam system FEI Helios NanoLab 600i was used to prepare the GBM cross section for their TEM observations.

3.4.3 Fourier transform infrared spectroscopy (FTIR)

This analysis was carried out at School of Chemical Engineering, Universiti Sains Malaysia, Penang. In order to determine the surface functional group of the sample, Fourier transform infrared spectroscopy (FTIR) analysis is carried out using Nicolet IS10 instrument. At the beginning, the sample was prepared by pelleting method using KBr powder. Sample was ground together with KBr in the ratio of KBr : adsorbent (1:10) thus pelletized using a hydraulic press machine. Right after the KBr-adsorbent power transforms into a transparent pellet, it was placed on the sample holder prior allowing for the infrared radiation. The spectrum results were recorded over a wavenumber of 4000 – 400 cm^{-1}.

3.4.4 Raman Spectroscopy

Raman spectroscopy is one of the most powerful tools for determining chemical species and providing information about chemical structure, polymorphism, crystallinity, and molecular dynamics. In this study, raman spectra of the prepared samples were measured with a Renishaw inVia Raman microscope (Science and Engineering Research Center, Universiti Sains Malaysia) and LabRAM HR 800 micro-Raman spectrometer at the Institute Jean Lamour using for both an excitation wavelength of 632.8 nm from an argon laser. A range from 1100 to 1800 cm^{-1} of Raman shift was scanned. For the analysis, the powdered samples were dispersed in ethanol thanks to a sonication bath and gently deposited

on a glass slice. For the 3D based graphene materials, a peace of each sample was simply deposited on a glass slice. An X50 objective was used for both kinds of analysed samples. At least three spectra were recorded for each sample. For data analysis, a baseline was first subtracted and the height of the D band was divided by that of the G band to calculate the I_D/I_G intensity ratio.

3.4.5 X-ray photoelectron spectroscopy (XPS)

X-ray photoelectron spectroscopy (XPS) is used to obtain elemental composition within specific sample together with their molecular bonding and chemical state. XPS analysis was used in this work to investigate the oxidised carbon percentage on the 2D graphene, 3D GBMs and 3D Al_2O_3 / GBM hybrid surface and the oxygen-containing functional group. All the apparatus used for sample preparation must be clean well to avoid any contamination that would affect the results of the analysis. The sample will be pressed into a clean, high purity of indium foil. This analysis study was carried out at MIMOS Berhad in Kuala Lumpur using a ULVAC-PHI Quantera II XPS equipped with an Kα X-ray source (hv = 1486.6 eV) (ULVAX-PHI, Inc., Kanagawa, Japan) and Kratos Axis Ultra (Kratos Analytical, UK) spectrometer equipped with a monochromatic Al Kα source (1486.6 eV) respectively. All spectra were recorded at a 90° take off angle, with the analysed area being about 0.7 × 0.3 mm. Survey spectra were acquired with 1.0 eV step and 160 eV analyser pass energy and the high-resolution regions with 0.1 eV step and 20 eV pass energy (instrumental resolution better than 0.5 eV). Curve fitting was performed using a Gaussian/Lorentzian (70/30) peak shape after Shirley's background subtraction and using the X-vision 2.2.11 software.

Table 3.3 Reference used to determine the binding energy (eV) for the C1s components of GO (Chen et al., 2020)

		C-O			
C=C	C-C	C-OH	C-O-C	C=O	COOH/COOR
284.1	284.7		285.5	286.1	288.7
284.7		287.0		288.0	289.2
284.6		286.6		287.8	289.5
284.5		285.9	286.6	287.5	288.9
284.4	285.4	286.3		288.0	289.0

Table 3.4 Reference used to determine the binding energy (eV) for the C1s components of graphene (Chen et al., 2020)

C=C	C-C	C-OH	C-O-C	C=O	COOH/COOR	π-π*
284.3	285.3		286.5	287.9		291.2
284.5		285.4	286.6	288.3		290.5
284.6			285.6	288.2	289.4	
284.6	284.9	285.9	286.9	288.2	289.3	290.6
284.5	285.6	286.7			288.3	

3.4.6 Nitrogen adsorption volumetry

The most important properties that determine the effectiveness of the samples (2D graphene, 3D GBMs and 3D Al_2O_3 / GBM hybrid) is the structural properties. This analysis was carried out at School of Chemical Engineering,

Universiti Sains Malaysia, Penang. The N_2 adsorption-desorption isotherm analysis was used to measure the SSA where Brunauer Emmet-Teller (BET) method was applied by an automated gas adsorption analyser (ASAP 2020 V4 Micromeritics) to determine the SSA. In contrast, Barrett-Joyner-Halenda (BJH) analysis uses adsorption and desorption techniques to calculate pore area and specific pore volume. The N_2 adsorption test was carried out at -196 °C (77 K). The degassing process was compulsory at the beginning of the analysis to ensure all the volatile materials adsorb on the sample's surface will be removed. The weight of three major components was calculated: the weight of the empty vial without sample, the weight of the sample before degassing, and the weight of the sample after degassing. Besides, 0.02 g of the sample was used for this analysis.

3.4.7 Thermogravimetric analysis (TGA)

Thermogravimetric analysis (TGA), an established technique for characterizing carbon nanomaterials, was carried out with a Setaram Setsys Evolution 1750 Thermal Gravimetric Analyzer (University of Lorraine, Institute Jean Lamour, France). Temperature is raised from room temperature to 900 °C at a rate of 5°C/min under dry air or helium (20 mL min^{-1}). Under air, all samples were subjected to a TGA analysis under air in order to determine graphene combustion temperature and the amount of remaining residues: purity of the samples. In order to optimize the accuracy of the analysis, a blank curve corresponding to the weight modification of the empty crucible under the same conditions (due to Archimedes' buoyancy) was systematically subtracted from the TGA thermograms of the samples.

3.4.8 Zeta potential

The 3D alumina/ GBM surface charges can be estimated using its pH at zero-point charge (pH_{pzc}). The zeta potential of the 3D alumina / GBM surface was evaluated in this research utilizing the Malvern Zetasizer Nano-Z. (ZEN 3600, UK) at School of Chemical Engineering, Universiti Sains Malaysia, Penang. The pH at which the zeta potential is zero is referred to as the zero-point charge. Before the analysis, 20 mL of deionized water was adjusted at various pH levels, including 2, 4, 6, 8 and 10 with 0.1M HCl and 0.1M NaOH solution. Then, the measurement was recorded and after three measurements, the average value of the zeta potential was reported. This measurement is used only for the adsorption study of CR.

3.4.9 UV-visible spectrophotometry

UV-Visible (UV-Vis) spectroscopy is a quantitative technique for measuring the amount of light absorbed by chemical substances. In this study, CR concentration was determined at School of Chemical Engineering, Universiti Sains Malaysia, Penang with a UV-vis spectrophotometer (Model Shimadzu UV- 1800, Japan). In order to determine the wavelength of the dye, 10 mg L^{-1} of CR was analyzed, and the maximum absorbance determined as the wavelength. Accordingly, the wavelength of CR was determined to be 498 nm and was used throughout the experiment. A calibration curve relating absorbance value and dye concentration was used to determine the concentration of CR. In Appendix A, a calibration curve for the CR concentration versus peak area is presented.

3.5 Adsorption study

3.5.1 CO_2 adsorption studies in TGA

The CO_2 adsorption performance of the developed adsorbent samples was assessed isothermally in a Thermogravimetric Analyzer (TGA, SDTQ-600, TA Instruments, Eschborn, Germany). For this purpose, around 15 mg of the adsorbent was loaded in the TGA pan and heated at the heating rate of 20 °C min^{-1} to 110 °C under N_2 flow of 75 mL min^{-1}. The sample was kept isothermally at 110 °C for 15 min purposely to remove all the moisture or any pre-adsorbed CO_2 from the sample. The temperature was then equilibrated to temperature 30 °C to prepare for the CO_2 adsorption process. A CO_2 flow of 75 mL min^{-1} was introduced to initiate the CO_2 adsorption and held at this adsorption temperature for 90 min. The weight changes indicated the amount of CO_2 captured were continuously recorded for further calculation of CO_2 adsorption capacity (mg g^{-1}). CO_2 adsorption capacity was referred to the amount of CO_2 gas adsorbed by the adsorbent at a specific time (duration of the CO_2 adsorption test) and was calculated.

3.5.2 Batch equilibrium studies for removal of Congo red (CR) dye

Adsorption of CR on the prepared 3D GBMs and 3D alumina /GBMs were performed by batch equilibrium tests. The effects of CR initial concentration, contact time and solution pH on the removal were investigated. The dye solution of few millilitres was taken at regular intervals at every 15 min for 240 min of adsorption and analysed using a UV–vis spectrophotometer. The concentration of the treated sample was measured at a wavelength of 498 nm. The removal efficiency ξ (%) of CR at period of time, and the equilibrium adsorption capacity q_e (mg g^{-1}) were calculated using (1) and (2), respectively:

$$\xi = \frac{C_0 - C_t}{C_0} \times 100 \qquad (3.1)$$

Where C_0 (mg L^{-1}) is the initial CR concentration and C_t (mg L^{-1}) is the final concentration of CR remaining at time, t.

CHAPTER 4

RESULTS AND DISCUSSSION

In this chapter, we discuss the results and the key findings of the present study. It begins with in section 4.1 with the preparation of GO as starting material and its characterization to verify the success of the synthesis. In section 4.2, the modification of GO by physical and chemical activation are studied. Further characterization for both approaches were performed and the performance towards CO_2 capture by these two approaches is studied and discussed in this section. The possible activation mechanism was also proposed in this section. Section 4.3 presents a finding by using a self-assembling process of 2D GO by chemical reduction using ascorbic acid (AA) into 3D interconnected hierarchical porous networks and the optimization study of the outcome 3D GBMs. In addition, the mechanism of AA reduction is discussed. Lastly, the chemically modified 3D GBMs by ALD by alumina covering is presented in section 4.4. All the morphological and structural characterizations as well as performance towards removal of Congo red are described accordingly.

4.1 Synthesis of graphene oxide as starting material

Today, researchers are eager to discover scalable ways to synthesize covalently linked molecules. Scalability is a crucial component in the synthesis of graphene materials, and the modified Hummer's technique to produce GO is one of the most prevalent ways to graphite exfoliation. In this experiment, KMnO4 was used to improve reaction safety and prevent explosions (Dreyer et al., 2010).

Besides, because of its great efficiency and acceptable reaction safety, the modified Hummers' technique has garnered a lot of attention. In principle, the result demonstrates the presence of a significant number of oxygen-containing functional groups that are put onto both sides of a single graphite sheet to produce GO. The insertion of functional groups overcomes the van der Waals forces between sheets and increases interlayer space. Besides, the oxidation of graphite results in a brown-coloured viscous slurry. The slurry consists of non-oxidized graphitic particles and residual oxidizers, as well as GO and exfoliated sheets. However, several times of continuously washing can removed the slurry produced by the oxidation process. Details of the findings are discussed below. The structure and morphology of the GO samples prepared during this PhD work, including TEM observations with FFT analysis and SEM observations, were characterized to verify the success of the synthesis. Besides, further characterization of the physical and chemical properties was performed using FTIR, Raman spectroscopy, XPS, and BET. The TEM images of GO at different magnifications are shown in Figures 4.1 (a) and (b). GO consists of less than 10 graphene layers stacked together in thin nanosheets. The spacing distances d_{hkl} obtained from the FFT patterns (insert Figure 4.1 (b)) correspond to a graphite structure (P63/mmc, d100 = 2.090 Å, d110 = 1.206 Å). The interspacing of the GO layers of 0.37–0.4 nm is as well consistent with a typical GO structure (Figure 4.2). SEM was used to study the microstructure and morphology of the starting material (GO). The typical thin sheets of GO are well visible by SEM (Figure 4.1c) in agreement with TEM (Figure 4.1a, 4.1b)

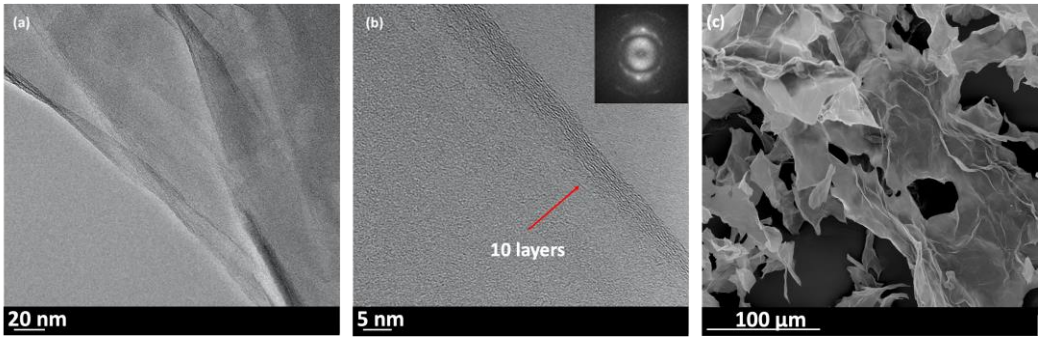

Figure 4.1 TEM images of GO (a) low-magnification (b) high-magnification, insert corresponding to the corresponding FFT; (c) SEM image of GO.

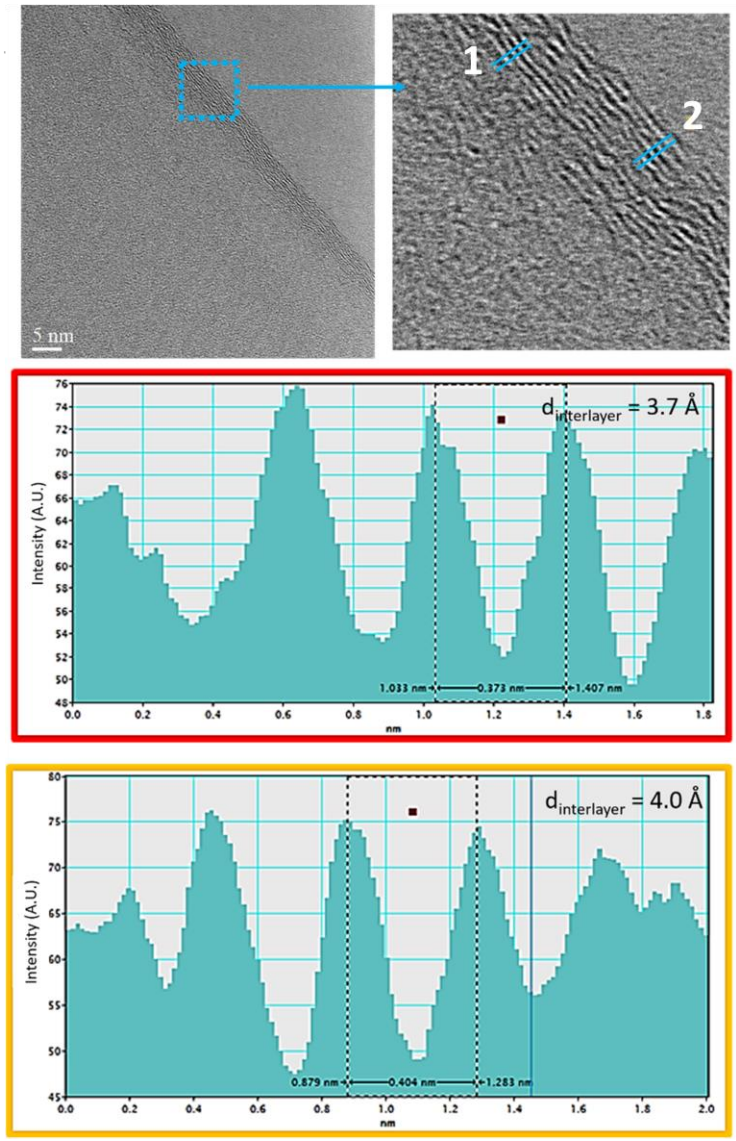

Figure 4.2 Measurement of the interspacing layer of GO from TEM images.

Raman spectroscopy is a prominent tool for characterising carbon nanomaterials because it helps researchers to analyse structural changes in the carbon network caused by chemical treatments. Raman spectroscopy was performed on the produced GO samples (a typical spectrum is shown in Figure 4.3) and compared to graphite flake found in literature (insert of Figure 4.3). Typically, these two carbons nanomaterials exhibit the well-known D and G bands at 1354 and 1584 cm^{-1}, respectively. The ratio of the intensity of the D band to that of the G band (I_D/I_G), considered as a certain signature of the sp^3 defects present in the carbon nanomaterial structure, is calculated to be around 0.3 for the graphite flakes, which indicates fewer defects. The GO sample exhibits a prominent and larger D band, as well as a substantially higher I_D/I_G ratio (1.04 ± 0.05), suggesting the existence of a large number of defects/functional groups due to the strong oxidative conditions during its synthesis, as expected.

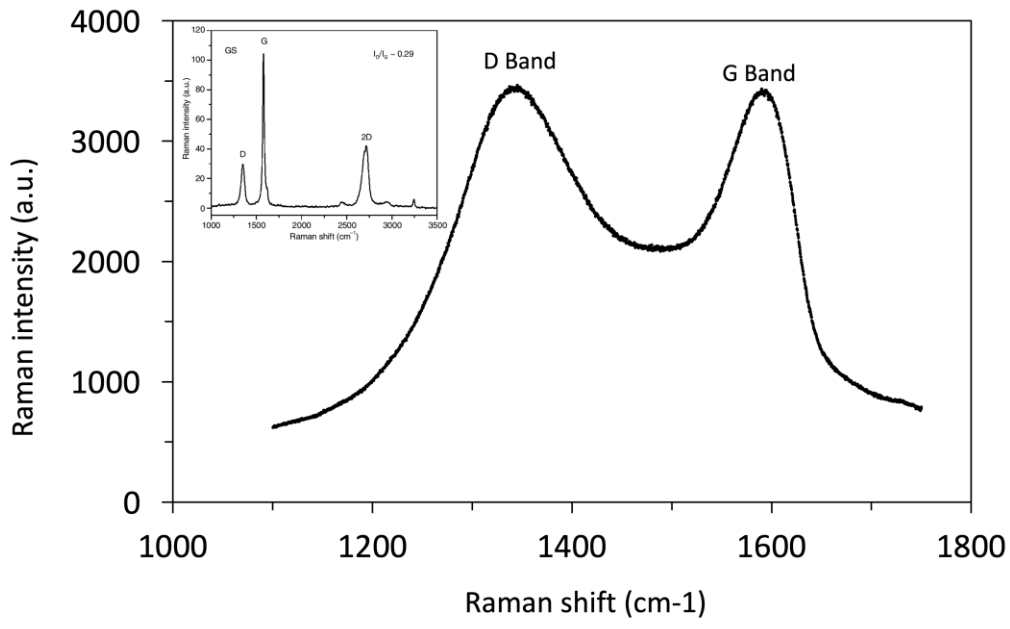

Figure 4.3 Raman spectrum of pristine GO and graphite (inserted image).

FTIR allows to study the effect of thermal/chemical treatment on the eventual nature changes of the grated functional groups. The FTIR spectra of GO is illustrated in Figure 4.4. As predicted for GO, the sharp peak at around 1575-1579 cm^{-1} is the signal of the sp^2 carbon skeleton C=C vibrations in the aromatic ring structure. The wide peak about 3400 cm^{-1} is assigned as O-H stretching vibrations of hydroxyl or carboxyl groups. The band seen at roughly 2900 cm^{-1} corresponds to aliphatic and aromatic sp^3 C-H stretching vibrations in aliphatic and aromatic structure. The C=O stretching vibrations may be responsible for the abrupt unsymmetrical peak at 1744 cm^{-1} of GO.

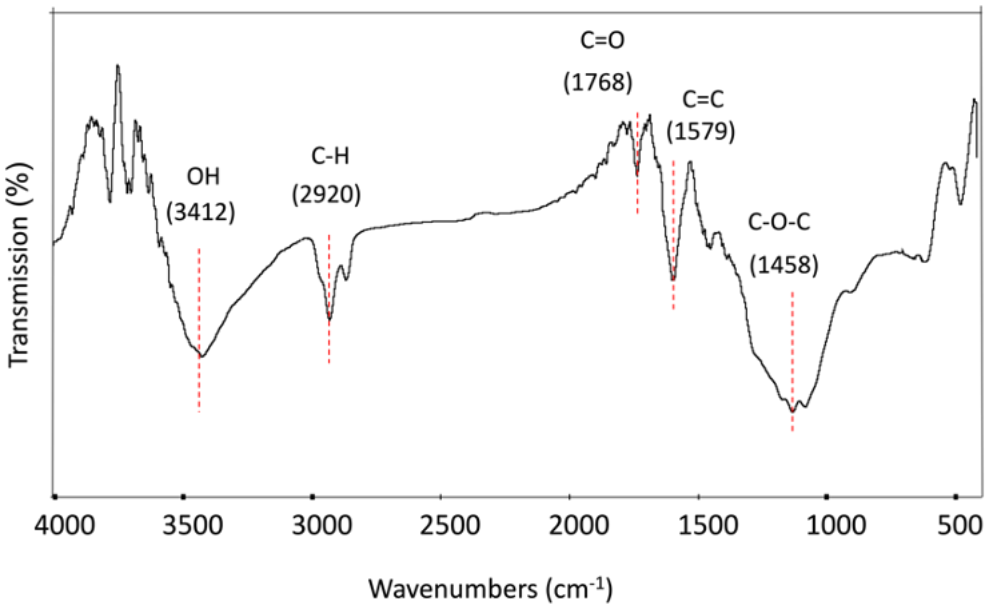

Figure 4.4 FTIR spectrum of pristine GO.

Surface area analysis was performed on the pristine GO sample and the results reveal that the surface area, pore size and pore volume of GO are 219 m^2 g^{-1}, 3.7 nm and 0.007 cm^3 g^{-1}, respectively. Aside from that, Figures 4.5 presents nitrogen adsorption-desorption isotherms of pristine GO. According to IUPAC

classification, GO indicates Type IV isotherms, indicating the presence of mesopores. As a result of its isotherm, the GO sample indicates a H3 hysteresis loop. The hysteresis loop begins in a relative pressure range of 0.5-1, indicating capillary condensation occurrences, which are common in mesoporous materials (ALOthman, 2012). Hysteresis is basically a condition where the adsorption and desorption curves do not overlap, associated with the capillary condensation phenomenon that takes place in mesoporous structures during desorption process.

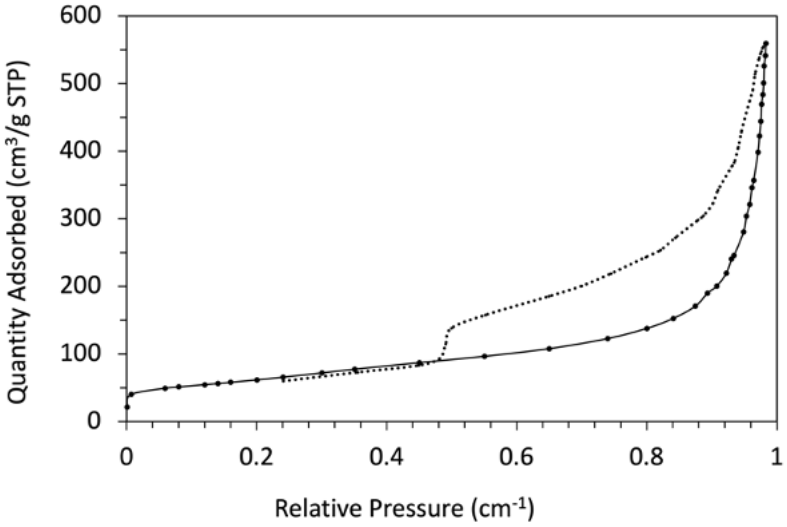

Figure 4.5 N_2 adsorption-desorption isotherms of the prepared pristine GO.

The XPS technique is of paramount importance for characterization of carbon-based materials, as it allows one to determine the chemical environment of elements. As shown in Figure 4.6 (a), a clear presence of carbon (C1s) and oxygen (O1s) is seen in the survey scan and sulfur (S1s) is detected as an impurity probably resulting from H_2SO_4 synthesis. In general, XPS is not a purely quantitative technique, however, the atomic ratio of oxygen over carbon, O/C, from the survey scan gives a rough idea of the oxygen content in the samples (O/C = 0.46), as expected for GO. The deconvoluted contributions of each signal (C1s and O1s) are

given in Tables 4.1 and 4.2. The deconvoluted high resolution C1s region spectra of GO is presented in Figure 4.6 (b). The contribution at 284.2–284.8 eV is assigned to the sp^2/sp^3 carbon atoms in C=C graphene network and/or carbon atoms belonging to C-H bonds (Abdelnabi et al., 2021; Shulga et al., 2021). Higher C1s binding energy can be assigned to carbon linked to oxygen: C-O around 286 eV, C=O around 287 eV, and O=C-O at 287–289 eV (Table 4.1). The results of the XPS analysis have shown that there has been a significant correlation between carbon and oxygen bonds in the sample, which is in line with the results of the FTIR analysis. In contrast, high resolution spectra in the O 1s peak were acquired to know more about the presence of oxygen in the synthesis products. Following deconvolution, there are three distinct peaks: (1) 532.2 eV, (2) 534.4 eV and (3) 533.94 eV. Based on literature, it is evident that the first peak corresponds to the carbonyl group, O=C, the second peak corresponds to the group C-OH, and the last peak corresponds to O-C (Al-Gaashani et al., 2019; Chen et al., 2020). This result is consistent with the O1s spectral regions shown in Figure 4.6 (c) and Table 4.2.

A comprehensive characterization of GO has been conducted and based on the results we conclude that the modified Hummers method via oxidation of graphite powder may be a viable method for producing GO on a large scale. Further, FTIR and XPS analyses revealed that the oxidation process enhanced the compatibility of matrix composites by providing evidence of functional groups. Simultaneously, these functional groups can be served as sites for chemical modification or functionalization of GO sheet, in order to easily apply in many other aspects. Furthermore, the polar oxygen functional groups in GO sheet render it strongly hydrophilic, which gave GO good dispersibility in many solvents, particularly in water.

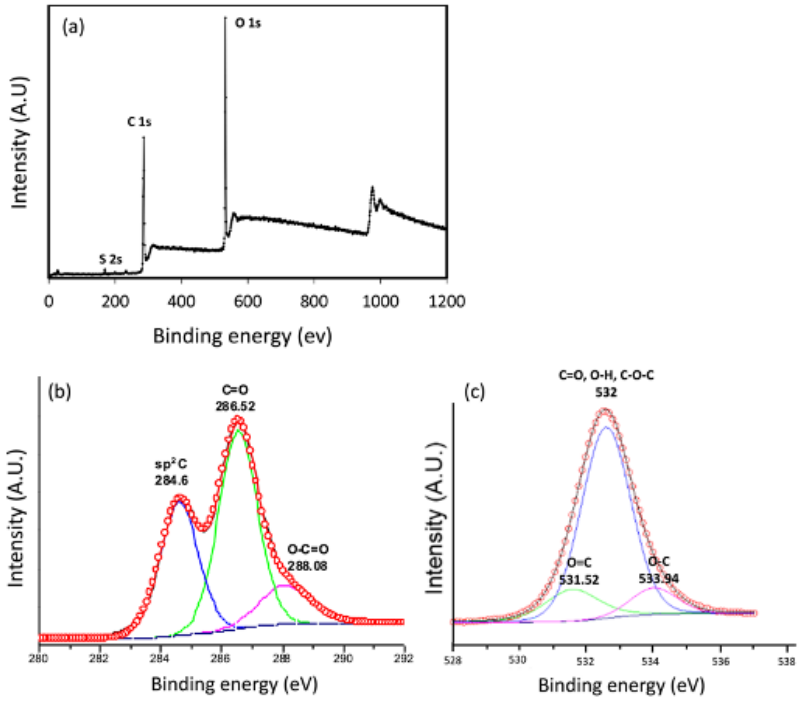

Figure 4.6 XPS spectra of the used pristine GO (a) wide range scan, (b) C1s and (c) O1s XPS features.

Table 4.1 Deconvolution of C1s features of GO

	C=C, C-H	**C=O**	**O-C=O**
Position (eV)	284.60	286.52	288.08
Concentration (%)	34.79	51.81	13.39

Table 4.2 Deconvolution of O1s features of GO

	O=C	**O=C, C-O-C**	**O-C**
Position (eV)	531.52	532.53	533.94
Concentration (%)	10.79	79.64	9.57

4.1.1 Mechanism of graphene oxide formation

In general, this work reveals that the preparation of GO by the modified Hummers' method involving four steps, and each step has an independent chemical reaction as shown in Figure 4.7. By utilizing the primary oxidant, Mn2O7, oxygen molecules are broken down and react with graphite. The first stage involves thermochemically intercalating sulfuric and nitric acids between the layer of graphite layers to order to generate to generate graphite intercalation compounds (GICs). During this phase, intercalating H_2SO_4 molecule is challenging since H_2SO_4 molecules have a diameter of around 0.39 nm, which is larger than the gap between graphite lamellar layers (Tjong, 2014). Thus, to achieve the intercalation of formed HNO_3−H_2SO_4−GIC, $NaNO_3$ must be added to react with concentrated sulfuric acid to form HNO_3. This process subsequently produces small oxygen atoms, oxidises carbon atoms at the margins of graphite, and opens graphite lamellar channels, which eventually diffuse into graphite sheets via molecular thermal motion. Further, the reaction of potassium permanganate with concentrated sulfuric acid yields Mn_2O_7, which is then intercalated between graphite layers by molecular convection diffusion, restore part of the sulfuric acid molecules to generate Mn_2O_7−H_2SO_4−GIC compounds. In the third step, Mn_2O_7 is decomposed by exothermal reaction, and oxygen atoms are generated to oxidize the defects in the graphite layer to pristine GO. Finally, the solution is rinsed with 10% HCl multiple times. In principle, Cl^-, which has a small molecular diameter, is used in the washing process to facilitate intercalation into oxidised graphite layers, hence restoring sulphate and manganese ions between graphite oxide layers.

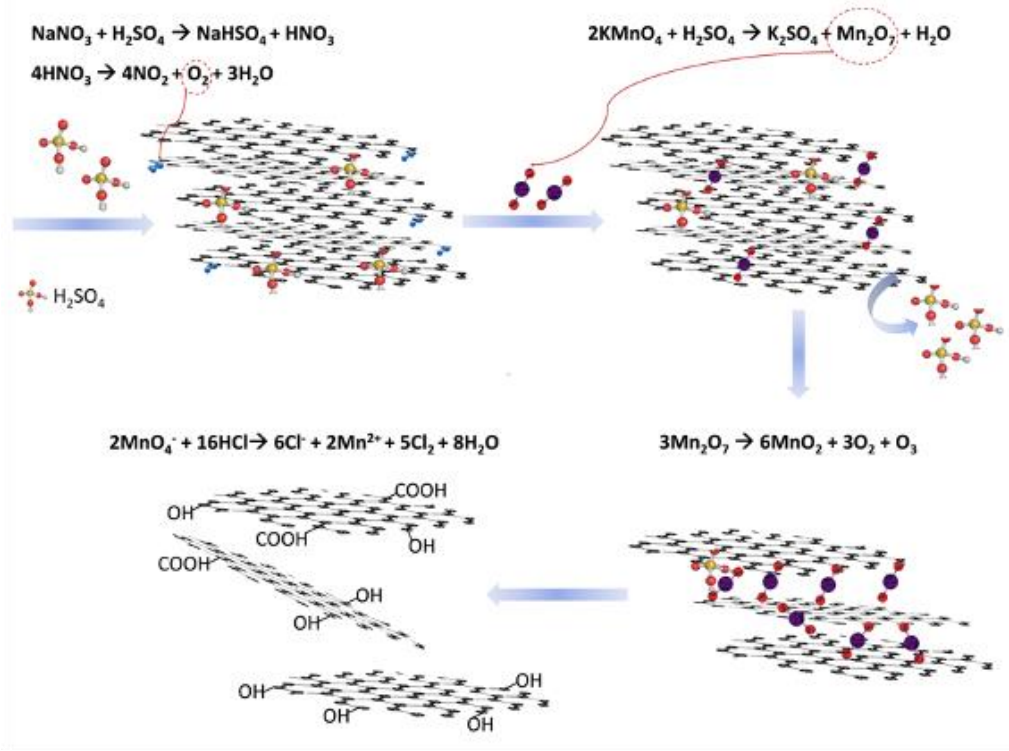

Figure 4.7 Reaction mechanism of the conversion of graphite flakes into GO by a chemical oxidation process

4.2 Activation of graphene oxide by chemical and physical approaches

The objective of activation is to enhance the structural properties (SSA and pore volume). Furthermore, activation can change or modify the surface chemistry or chemical composition of activated graphene, giving it distinct properties. Since the physicochemical properties of carbons are highly affected by the existence of chemical compounds on their surface and their chemical characteristics, understanding the surface chemistry of activated graphene is critical in adsorption study. In this study, both physical and chemical activation approaches have been applied to GO as starting material. CO_2 and KOH-based activation methods have been used as physical and chemical activation, respectively. The structural and the chemical properties of the prepared activated GOs have been deeply characterized by means of complementarily techniques: SEM, TEM, Raman spectroscopy, FTIR,

XPS and nitrogen adsorption. The impact of the used temperature for the activation towards the CO_2 adsorption capacity has been investigated and discussed by means of a proposed mechanism.

4.2.1 Structural and chemical modifications of graphene oxide through activation

The starting material which is GO was characterized once again together with the physical and chemical activated GO. According to Raman spectroscopy shown in Figure 4.8 (a), the two main peaks detected for all spectra at 1370 and 1620 cm^{-1} reflect the defects/sp^3 (D-band) and crystalline/sp^2 (G-band) carbon structures, respectively. When defects are introduced into the sp^2 carbon network, the intensity of the D band (in comparison to the G band) is known to increase (Xiao et al., 2021a). Figure 4.8 (b) depicts the computed I_D / I_G for the starting material, GO and all the treated GO samples including both chemically and physically activated at different temperatures. The pristine GO sample possesses high I_D/I_G ratio, indicating the existence of defects/functional groups due to the strong oxidative conditions during its synthesis, as expected. After both activation treatment, the I_D/I_G ratio is not significantly modified, meaning that, in average, activation does not impact the structural quality of the activated GOs which have already a highly defected structure. The nature of the functional groups was next studied by FTIR for all the activated GO samples.

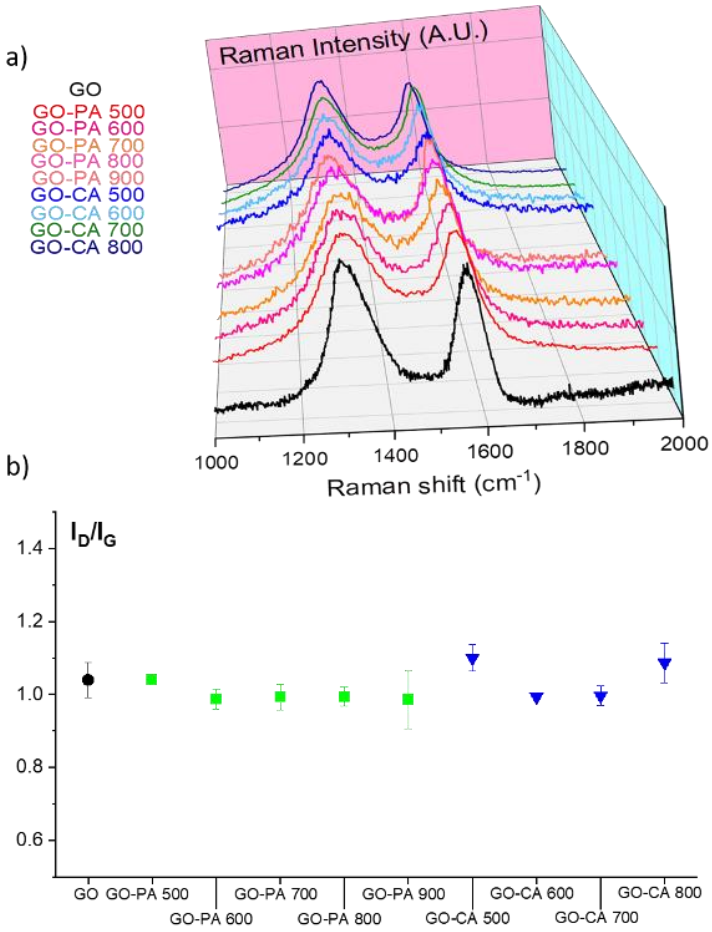

Figure 4.8 (a) Raman spectra and (b) corresponding I_D/I_G of pristine GO and the activation GO by both the chemical and the physical activation methods.

Figure 4.9 displays the FTIR spectra of all the samples. There are five main peaks shown in spectra: 3421 cm^{-1}, 2923 cm^{-1}, 1705 cm^{-1}, 1575 cm^{-1}, 1359 cm^{-1} which assign to the stretching mode of O-H, C-H, C=O, bending vibration of OH groups of water molecules and C-OH group respectively (Khalili, 2016). The bonds associated with oxygen-containing groups in GO were considerably decreased and some of these bonds disappeared after GO was activated. A significant factor in achieving a good CO_2 adsorption capacity is the surface chemistry, which reflects the basicity of the adsorbent. Hence, from the FTIR result, it revealed that the properties associated with carbon-oxygen bonds become less intense as the

activation temperature for both chemical and physical activation rises. When compared to physical activated and GO, the O-H peak for chemically activated GO is less intense, which might suggest that it was undergoing strong reduction process. As reduction increases, the surface chemistry of the adsorbent changes, resulting in a more basic adsorbent.

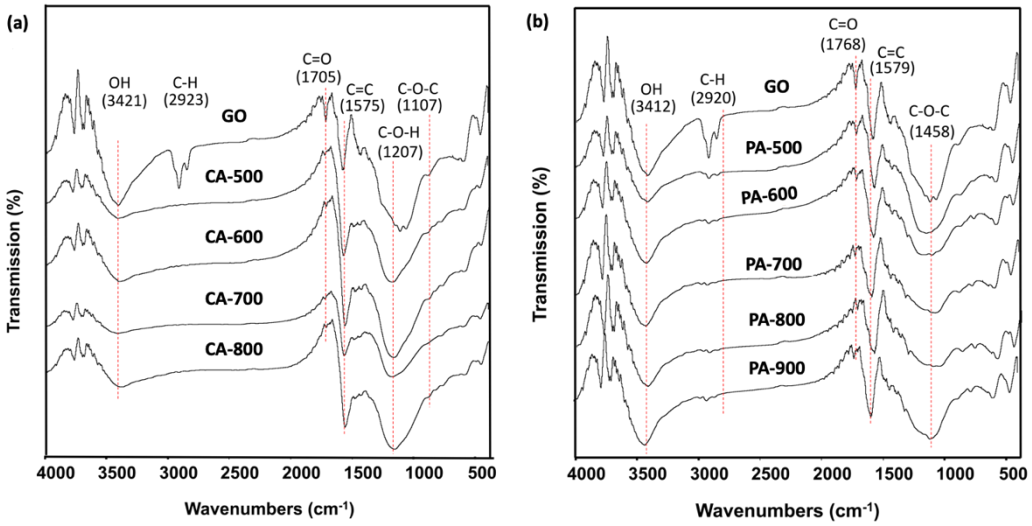

Figure 4.9 FTIR spectra of (a) physical activation and (b) chemical activation of GO at different temperatures.

Beside, these FTIR analysis also revealed that activated GO has undergone a reduction process, which is consistent with prior studies indicating that activation treatment resulted in an effective decrease of GO (Xiao et al., 2021a). Raman spectroscopy is not a technique that is sensitive to the type of functional groups, hence no effect of reduction process is expected. A similar I_D/I_G between the treated samples and pristine GO indicates that the number of defects have not been impacted by the applied activation approaches neither towards defect curing, nor over damaging.

4.2.2 CO_2 adsorption on physically and chemically activated graphene oxide

The impact of both chemical and physical activation approaches conducted at different temperatures to prepare graphene-based adsorbents for CO_2 capture were examined. A difference in activation temperatures (physical activation: 500 to 900 °C) and (chemical activation: 500 to 800 °C), resulted in almost similar adsorption trends, in which rapid adsorption was observed within the first 20 min. Then, the adsorption rate gradually slowing down, and a plateau was reached after 40 min, indicating equilibrium in the adsorption process. The adsorption of CO_2 on activated graphene was sustained until saturation was reached. In general, the adsorption capacity increases when the activation temperature for physical and chemical increases from 500 to 900 °C and from 500 to 800 °C, respectively, as shown in Figures 4.10 (a) and (b). However, temperatures higher than 900 and 800 °C for physical and chemical activation, respectively cannot not be sustained by the samples that are too much damaged and even partly burnt off. Thus, to conclude, based on a comparison of the adsorption curves, the adsorption of CO_2 molecules increased with an increase in activation temperature.

According to the findings (Table 4.3), physical activation leads to an improvement of the adsorption capacity of pristine GO by a factor of 6.5, from 4.2 to 27.2 mg g^{-1}. From chemical activation, the adsorption capacity is enhanced by a factor of 9 from 4.3 to 38.9 mg g^{-1}. The CO_2 adsorption capacities of both activated GO was presented in Table 4.3.

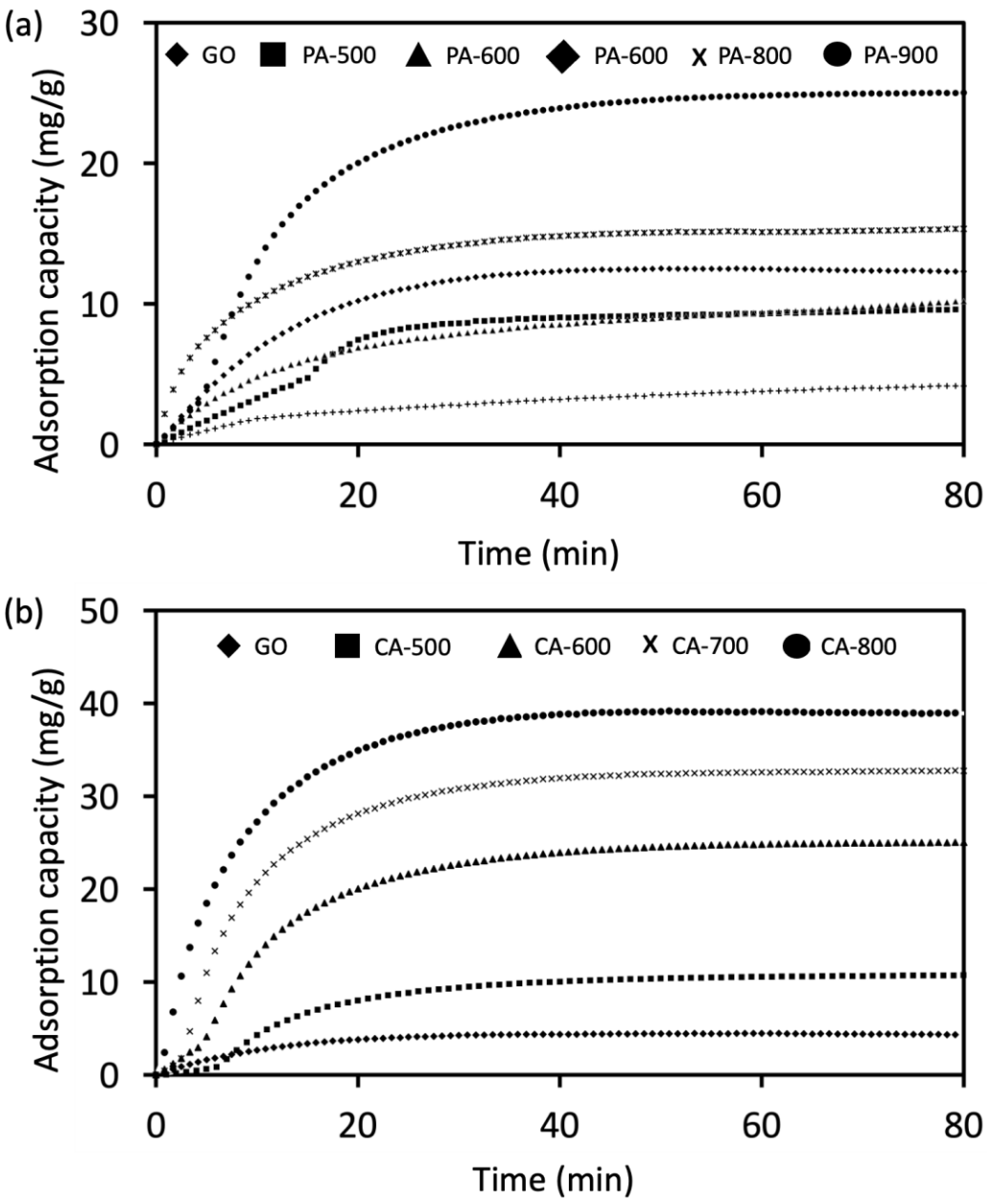

Figure 4.10 CO_2 adsorption isotherms of GO after (a) physical activation and (b) chemical activation at different temperatures.

Table 4.3 CO_2 adsorption capacity of pristine and activated GO via different activation approaches.

Approaches	**Samples**	**Adsorption capacity ($mg\ g^{-1}$)**
Physical activation	GO	4.2
	GO-PA 500	9.6
	GO-PA 600	10.2
	GO-PA 700	12.3
	GO-PA 800	15.3
	GO-PA 900	27.2
Chemical activation	GO	4.3
	GO-CA 500	10.8
	GO-CA 600	25.0
	GO-CA 700	32.8
	GO-CA 800	38.9

4.2.3 Morphological and structural characteristics of physically and chemically activated graphene oxide

An in-depth characterization of activated GO samples which have led to the best CO_2 capture properties (GO-PA 900 and GO-CA 800) were conducted by SEM to examine their microstructure and morphology. Figure 4.11 illustrates the light and porous structure of both GO-PA 900 and GO-CA 800. The meso-macropores of the GO-PA 900 with a diameter ranging from several μm to larger than 50 μm are obtained from the BET surface area analysis & BJH pore size analysis. The macroporosity of the GO-PA 900 remains intact even after CO_2 activation. Figure 4.12 shows nitrogen adsorption-desorption isotherms of the three samples: GO, GO-PA 900 and GO-CA 800. The main difference form isotherm curves is the significantly increased in adsorbed quantity after activation.

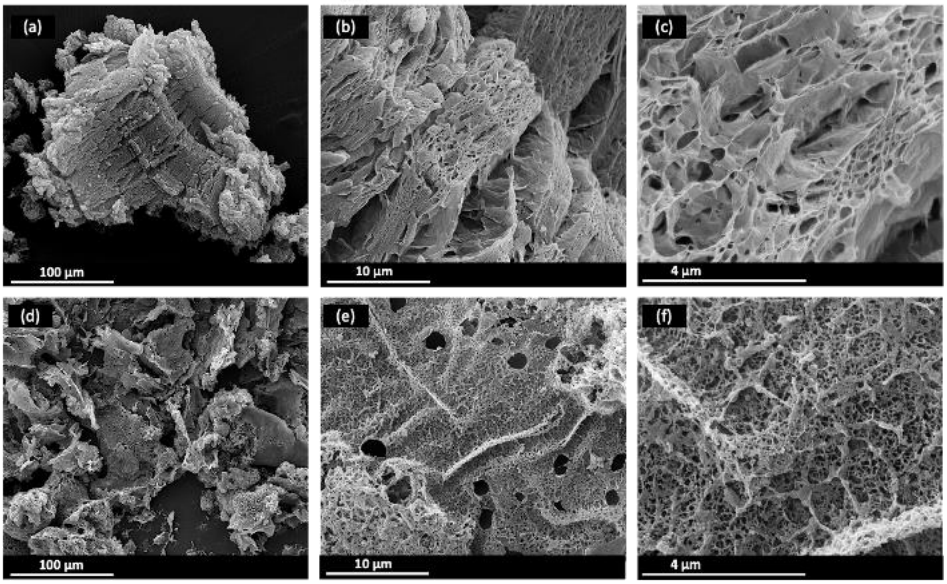

Figure 4.11 SEM images of GO-PA 900 at different magnifications (a-c) and of GO-CA 800 different magnifications (d-f).

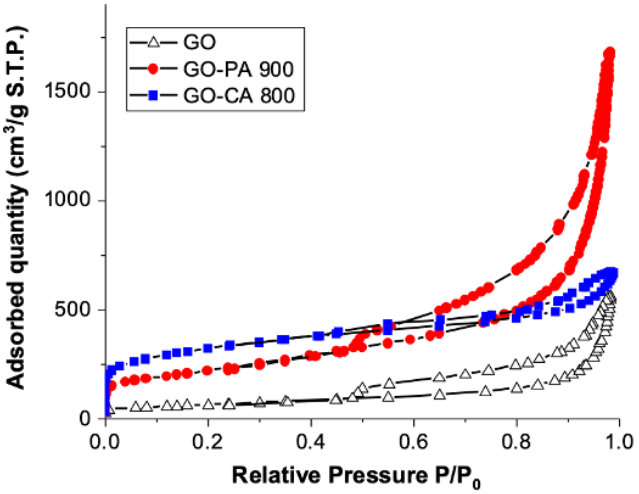

Figure 4.12 N_2 adsorption-desorption isotherms of the pristine GO, GO-PA 900, and GO-CA 800.

Similar to GO, GO-PA 900 indicates Type IV isotherm, showing the existence of mesopores (ALOthman, 2012). High temperatures aid in the formation

of mesoporosity in the sample. Furthermore, micropores and mesopores were observed in sample GO-CA 800, indicating Type I and Type IV isotherms. Additionally, Type I isotherms can also be found in activated carbon, molecular sieve zeolites, MOFs, and certain porous oxides (Kruk and Jaroniec, 2001). Type IV isotherms are distinguished by their hysteresis loop, which is related to capillary condensation in mesopores, and their limiting uptake across a wide range of high P/P_0 values. The isotherm among all samples indicates H3 hysteresis loop which much more arrow for the activated GO compared to GO probably due to a reduced amount of mesopores after activation. The quantitative results from adsorption analysis are shown in Table 4.4. Besides, the appearance of H4 hysteresis loop was clearly spotted in sample GO-CA 800, indicating the existence of micro-mesopore structure.

Table 4.4 SSA, total pore volume and pore size of GO, GO-PA 900 and GO-CA 800 determined from the measured isotherms.

Sample	**SSA** ($m^2\ g^{-1}$)	**Total pore volume** ($cm^3\ g^{-1}$)	**Pore size** (nm)
GO	219.3	0.79	13.67
GO-PA 900	762.5	2.31	12.14
GO-CA 800	1060.5	0.99	3.65

BET surface area analysis results reveal that GO has the lowest SSA, whereas KOH activation at 800 °C appears to be the most effective in increasing surface area and porosity with the highest SSA (1060.5 $m^2\ g^{-1}$), followed by CO_2 activation at 900 °C (762.5 $m^2\ g^{-1}$). Furthermore, the pore size decreases

significantly after chemical activation, from 13.67 nm to 3.65 nm and in a lower extent to 12.14 nm after physical activation. Since CO_2 has a relatively small kinetic diameter of 0.33 nm, it is widely known that microscopic pores are required for its efficient gas molecule diffusivity into the adsorbent framework (Zubbri et al., 2021).

Similarly, Ma *et al.* found that after activating graphene oxide sheets with KOH, the SSA of activated graphene increased by a factor of 3.7, along with the formation of micropore structure, as compared to pristine graphene. Wu *et al.* discovered that as well that at higher activation temperatures, micropores were fully developed (Wu et al., 2016). Theoretically, metallic potassium can be formed at high temperature during the redox reaction between GO and KOH, causing intercalation on the graphitic type layers and, therefore, allowing the graphitic layers to split and degrade, resulting in the development of microporosity (Raymundo-Piñero et al., 2005). However, at low temperature, the pore development is likely incomplete, which can cause a large pore diameter. Multi-porous property can be useful in the development of some materials to facilitate diffusion and accessibility within the internal surface, however, for gas adsorption, micropores and narrow mesopores are recommended.

XPS was especially investigated on the two activated GOs, which show the best CO_2 adsorption performances; namely GO-PA 900 and GO-PA 800. Table 4.5 gives the O/C atomic ratio of GO, GO-PA 900 and GO-CA 800. As shown in the previous section, GO shows high oxygen content and after both chemical and physical activation, a distinct decrease in oxygen content is observed meaning that the oxygen-containing groups (carboxyl, epoxide, or other functional groups) are

decomposed or reduced by the activation approaches. The atomic percentage of oxygen was decreased from around 46 % to less than 17 % after chemical activation and down to 5 % after physical activation. However, the 17 % oxygen content in GO-CA 800 does not only correspond to oxygen linked to carbon atoms (oxygen-containing groups), but it also originates from additional oxygen contribution from the activation treatment with KOH.

Table 4.5 O/C atomic ratio from XPS survey spectra of GO, GO-PA 900 and GO-CA 800.

Sample	O/C (atomic ratio)
GO	0.46
GO-PA 900	0.05
GO- CA 800	0.17

As observed, depending on the reduction method and the used experimental conditions, the C/O atom ratio from XPS is not necessarily accompanied by I_D/I_G decrease. It is explained by the fact that even if the nature of the functional groups, especially elimination of COOH functional groups, is modified upon the reduction reaction, the sp^2 carbon atom hybridization (from sp^3) is not necessarily reached. Indeed, as expected, the creation of these hydrogenated carbon atoms (C-H) or other defect types (vacancies, holes, dangling bond, etc.) does not increase the sp^2 ratio content after reduction since the defects are not cured and the C=C double bonds are not restored (Díez-Betriu et al., 2013; King et al., 2016). The C1s spectral region

was analysed for the activated GO. The deconvoluted high resolution C1s region spectra of GO-PA 900 and GO-CA 800 are presented in Figure 4.13.

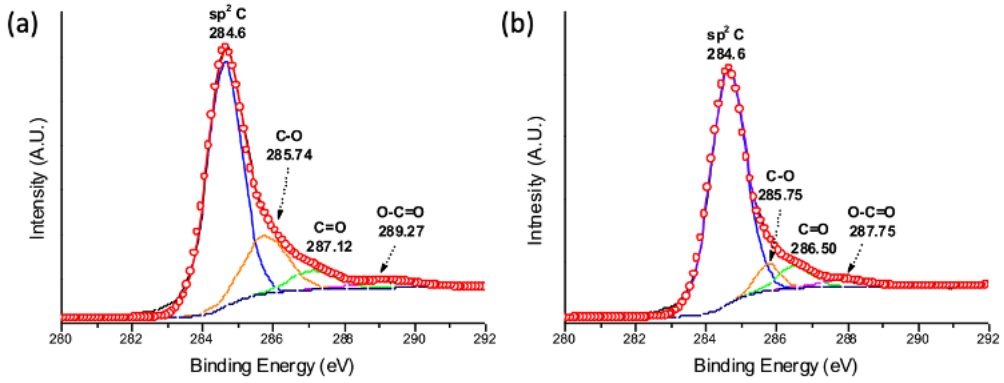

Figure 4.13 C1s XPS spectra for (a) GO-PA 900 and (b) GO-CA 800.

The fitting parameters including contribution assignment, Full Width at Half Maximum (FWHM) and the different contributions used to deconvolution of the C1s signal of GO-PA 900 and GO-CA 800 are given in Table 4.6. For GO, GO-CA 800, and GO-PA 900, the concentration of C=C / C-H contribution is 34.79, 78.65, and 75.57%, respectively, while the total contribution concentration relative to C bond to oxygen is 65.2, 24.43, and 21.35% for GO, GO-CA 800, and GO-PA 900, respectively. Besides, the C=C/C-H contribution is observed to be significantly increased while the features assigned to oxygen linked with the carbon network are decreased for the two activated GOs (GO-PA 900 and GO-CA 800). The concentration of C=C/C-H contribution is 34.79 %, 78.65 % and 75.57 % for GO, GO-CA 800 and GO-PA 900, respectively. The total contribution concentration relative to C bond to oxygen is 65.2 %, 24.43 % and 21.35 % for GO, GO-CA 800 and GO-PA 900, respectively. These results from XPS, in agreement with FTIR (Figure 4.9), indicate that both physical and chemical activations lead to a reduction reaction of the starting GO. Similarly, Yang *et al.* reported that after the

reduction of GO, the intensity of all C1s peaks of hydroxyl, carbonyl, and carboxyl carbon atoms, including C-OH, decreased significantly (J. Yang et al., 2015).

Table 4.6 Deconvolution of C1s features of GO-PA 900 and GO-CA 800.

GO-PA 900	**C=C/C-H**	**C-O**	**C=O**	**O=C-O**
Position (eV)	284.81	285.88	286.69	287.93
FWHM	1.18	1.11	1.37	1.63
Concentration (%)	75.57	12.37	8.11	3.95
GO-CA 800	**C=C/C-H**	**C-O**	**C=O**	**O=C-O**
Position (eV)	284.80	286.02	287.16	288.65
FWHM	1.15	1.28	1.38	1.50
Concentration (%)	78.65	12.92	5.44	2.99

4.2.4 Mechanism of activation

From the TEM analysis, a thin layer of pure GO flakes with around 5–7 layers (thickness of around 2 nm) were observed (Figures 4.1 (a) and (b)). The smooth surface of GO was visible in the TEM pictures before activation, which is consistent with the SEM observations. The surface of activated GOs displayed a visible pore structure after both activation processes, indicating that KOH and CO_2 may work as activators — particularly KOH forming many pores. FTIR and XPS of activated GO by both physical and chemical activation have shown a significant reduction in oxygen-containing group content. Concerning microporosity development by chemical activation, the increase in SSA appears to be significant,

with an increase of a factor of 5 for GO-CA 800, confirming the exceptional porous structure of the activated GO by the KOH-based method conducted at 800 °C. Moreover, the hysteresis loops for the sample are type H3, suggesting that the pores formed are irregular and open, with high connection between intragranular pores with parallel, slit-like, and open-ended tubes, which are favourable to gas transfer (Bensalah et al., 2020).

In this study, physical activation of graphenic materials, particularly GO, is carried out using heat treatment at temperature greater than 600 °C in a partly oxidizing medium of CO_2 and N_2 with the main goal of maximizing internal surface area. Shen *et al.* further supported this, claiming that graphitic materials exhibited endothermic reactions above 700 °C, and breakdown of the carbon framework happening in this temperature range (Shen et al., 2020). Furthermore, greater temperatures would be required for decomposition, resulting in improved chemical and physical activation efficiency (Lillo-Rodenas et al., 2003). Figure 4.14 represents the mechanisms of chemical activation (top) and physical activation of GO (bottom).

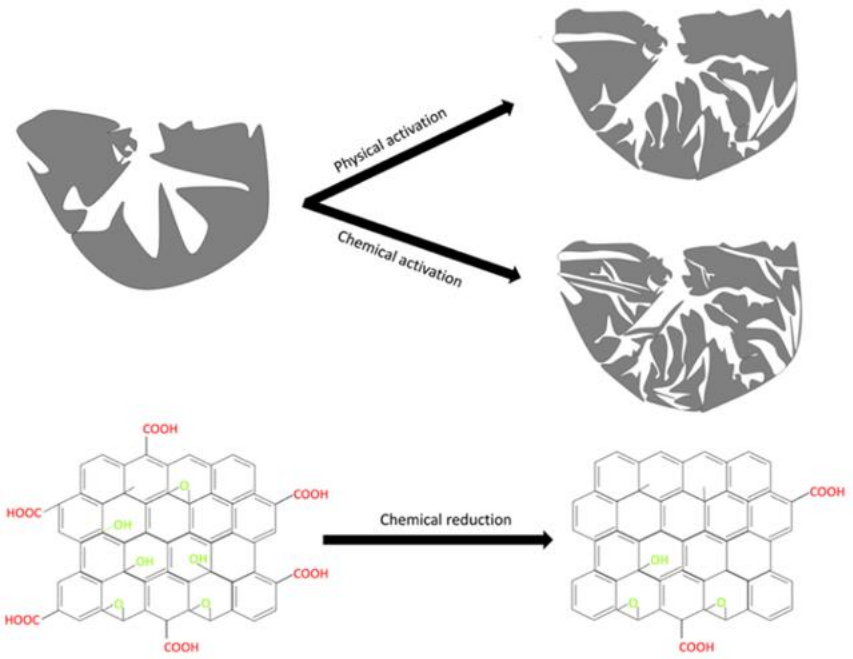

Figure 4.14 Mechanism of chemical and physical activation approaches in GO; top: modification of pore structure of GO by activation; bottom: modification of the functional groups on GO surface by activation.

The mechanism of GO activation with CO_2 normally involves the Boudouard reaction (Equation (4.1)) (Lahijani et al., 2015). The CO_2 undergoes dissociative chemisorption on the carbon surface as a result of the reaction, forming a surface oxide and carbon monoxide (as described in Equation (4.2)). The surface oxide, C(O), is then desorbed from the surface by Equation (4.3), allowing the pore structure to grow further (as shown in Figure 4.13). Additionally, the CO in the gaseous product can potentially be deposited on the carbon active sites and delay the gasification process (Equation (4.4)).

$$C + CO_2 \rightarrow CO \qquad (4.1)$$

$$C + CO \rightarrow C(O) + CO \qquad (4.2)$$

$$C(O) \rightarrow CO \qquad (4.3)$$

$$C + CO \rightarrow C(CO) \quad (4.4)$$

On the other hand, following chemical activation with KOH, the morphology of the GO gradually degrades as the imposed activation temperature increases, and the structure of the activated GO appears to become less dense, with a rougher surface and many more holes as a result of the activation process. First, KOH reacts with H_2O coming from the impregnation process. The formation of pores on the GO surface after activation can be related to the reaction between KOH and C in an inert atmosphere at high temperatures during the activation process, where some species such as potassium oxide (K_2O), potassium carbonate (K_2CO_3), and potassium (K) metal begin to diffuse within the structure of the GO, thereby forming new pores and opening existing ones. As shown, the formation of pores on activated GO may be explained by a series of simultaneous and sequential reactions (Acik et al., 2011; Xiao et al., 2021b):

$$2KOH.4H_2O \rightarrow K_2O + 5H_2O \quad (4.5)$$

$$C + 5H_2O \rightarrow CO + 5H_2 \quad (4.6)$$

$$CO + 5H2O \rightarrow CO_2 + 5\ H_2 \quad (4.7)$$

$$K_2O + CO_2 \rightarrow K_2CO_3 \quad (4.8)$$

$$K_2O + H_2 \rightarrow 2K + H_2O \quad (4.9)$$

$$K_2O + CO \rightarrow 2K + CO_2 \quad (4.10)$$

$$6KOH + 2C \rightarrow 2K + 3\ H_2 + 2\ K_2CO_3 \quad (4.11)$$

$$K_2CO_3 \rightarrow K_2O + CO_2 \quad (4.12)$$

$$K_2CO_3 + C \rightarrow K_2O + 2\ CO_2 \qquad (4.13)$$

$$K_2O + C \rightarrow 2K + CO \qquad (4.14)$$

$$2K + CO_2 \rightarrow K_2O + CO \qquad (4.15)$$

In general, in this section 4.2, chemical activation by KOH appears to be more efficient than physical activation in terms of developing high surface areas and porous graphene-based adsorbents. There are few aspects that have been taken into consideration in order to achieve a good adsorption capacity. The aspects include surface area, pore volume, pore size and chemical reduction of GO investigated in this work. For the first aspect, which is surface area, GO-CA 800 exhibits higher SSA compared to GO-PA 900 (762.5 $m^2\ g^{-1}$) which is 1060.5 $m^2\ g^{-1}$. Secondly, GO-PA 900 shows higher pore volume (2.31 $cm^3\ g^{-1}$) compared to GO-CA 800 (0.99 $cm^3\ g^{-1}$). Thirdly, GO-CA 800 exhibits lower pore size which is 3.65 nm as compared to GO-PA 900 (12.14 nm). Even though the pore volume of GO-PA 900 seems to be much higher but, we believe that since CO_2 has a relatively small kinetic diameter of 0.33 nm, it is widely known that microscopic pores are required for its efficient gas molecule diffusivity into the adsorbent framework. As a final point, based on Table 4.6 from XPS, GO-CA 800 undergoes greater reduction efficiency than that observed for GO-PA 900, which reduces acidity at the surface and improves CO_2 capture. Overall, GO-CA 800 shows a more positive result for the highlighted aspects, showing that chemical modification would be a better choice for the CO_2 adsorption efficiency.

4.3 Development of 3D graphene-based macrostructures

In this section, the results for the preparation, the properties, and the surface modification of 3D hierarchical GBMs by using the prepared GO as the starting material are described. This study utilized a simple one-step hydrothermal technique to synthesize 3D GBMs by incorporating AA as a reductant. The hydrothermal process begins with a solution of GO in which the GO nanosheets are homogeneously dispersed thanks to hydrogen bonds with water or electrostatic force. In this study, the GO dispersion was hydrothermally treated and freeze-dried to obtain the studied GBMs. As discussed in the following, the effect of the GO concentration of the starting GO dispersion was particularly investigated since they can impact both the fragility and the porosity of the GBMs. The prepared GBMs were characterized using adsorption volumetry, Raman spectroscopy, TEM, SEM and FTIR techniques.

4.3.1 Effect of graphene oxide concentration

In this study, different GO concentrations, *e.g.* 1, 2, 4, and 6 mg mL^{-1}, have been used of GO to prepare GBMs. For the fabrication of the 3D GBMs, these GO dispersions have been subjected to a hydrothermal process at 90 ^{o}C for 4 h in the presence of AA. Figures 4.15 (a) and 4.15(b) show digital photos of GO before and after undergoing the hydrothermal process, respectively. The as-prepared samples exhibit different macroscopic appearances with the presence of AA, and after 4 h of the hydrothermal treatment they have formed as a monolithic bulk with a cylindrical shape. In addition, AA is beneficial to the fabrication of the 3D GBMs, yielding a light (porous) monolith.

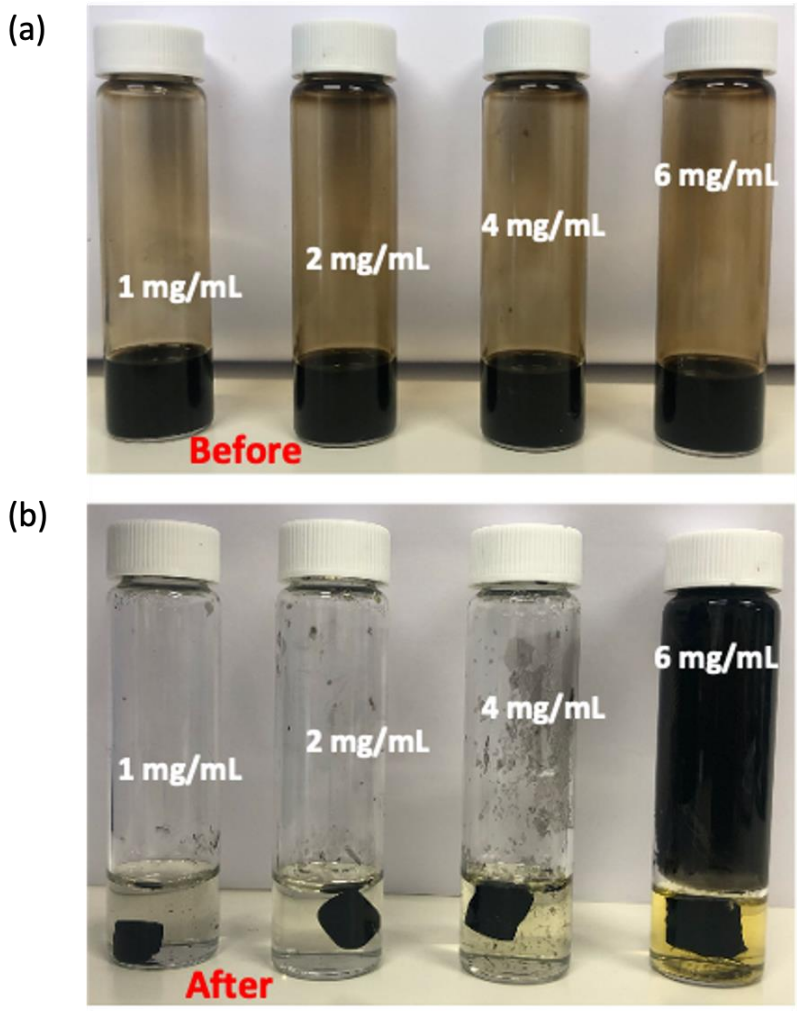

Figure 4.15 Photographs of (a) different initial GO concentration before undergoing chemical reduction process (b) formation of 3D GBMs after undergoing chemical reduction process

The formation of graphene network is driven by attractive interactions between graphene nanosheets. These interactions can be either π–π stacking interactions or van der Waals attractive forces. GO experiences a reduction reaction, as validated subsequently by the conducted characterizations, and as expected when introducing AA to drive the 3D assembly process. As a result of the decrease in oxygen-containing functional groups, the GO platelets become more hydrophobic, and rGO gel develops gradually. Furthermore, graphene platelets evidently connect,

squeezing out water and, it is proposed, completing the reduction of the GO gel as well as subsequent shrinking. Finally, the graphene hydrogel was removed from the enclosed reactor and freeze-dried for 24 h, causing the wet gel to shrink even further. The 3D GBM formation is sensitively dependent on the concentration of GO. When the concentration of the rGO dispersion was low (e.g., 0.05 mg g^{-1}), precipitates were not produced (Jo et al., 2015; Xu et al., 2010a). This hypothesis is supported by the other study, which found that the initial concentration of GO dispersion cannot be less than 1 mg mL^{-1} while constructing aerogel materials.

From this experiment, when the GO concentration is higher than 2 mg mL^{-1}, the 3D structure seems to be mechanically stable. However, when the concentration is lower than 2 mg mL^{-1}, the outcome 3D GBMs became more fragile in term of mechanically handling by observation during manual manipulation. The reason for this may be that π–π bonds are weak and the formation between rGO sheets may not be efficient or even impossible at low concentrations, due to the large distance between rGO sheets and the low interaction rate between rGO sheets and AA. Consequently, the rGO sheets were not interconnected enough, and formation of 3D GBMs become fragile. The appropriate concentration selection to prepare these 3D GBMs is particularly eventful. In the following, a deep characterization is conducted the GO concentration series and for the following of the study, the optimized GO concentration of 2 mg mL^{-1} has been chosen to prepare the alumina/GBM hybrids.

4.3.2 Structural characterization of 3D graphene-based macrostructures

In Figure 4.16, the Raman spectra exhibited typical G and D bands in the range of 1000 to 2000 cm^{-1}. The calculated I_D/I_G ratio of GO was 1.04, while those

of 3D GBM-1, 3D GBM-2, 3D GBM-4, and 3D GBM-6 were 1.41, 1.44, 1.40, and 1.41, respectively. The I_D/I_G ratios of all 3D GBMs samples were quite similar for the whole GBM series and higher than that of GO. The effect of GO concentration on structural quality of 3D GBMs does not appear to be significant as expected for the reduction reaction undergone since only the nature of the functional groups is modified, not their number meaning that the structural disorder of GO is expected to be roughly similar to that of rGO. To ascertain the surface chemistry of the 3D GBMs, further analyses such as FTIR were conducted.

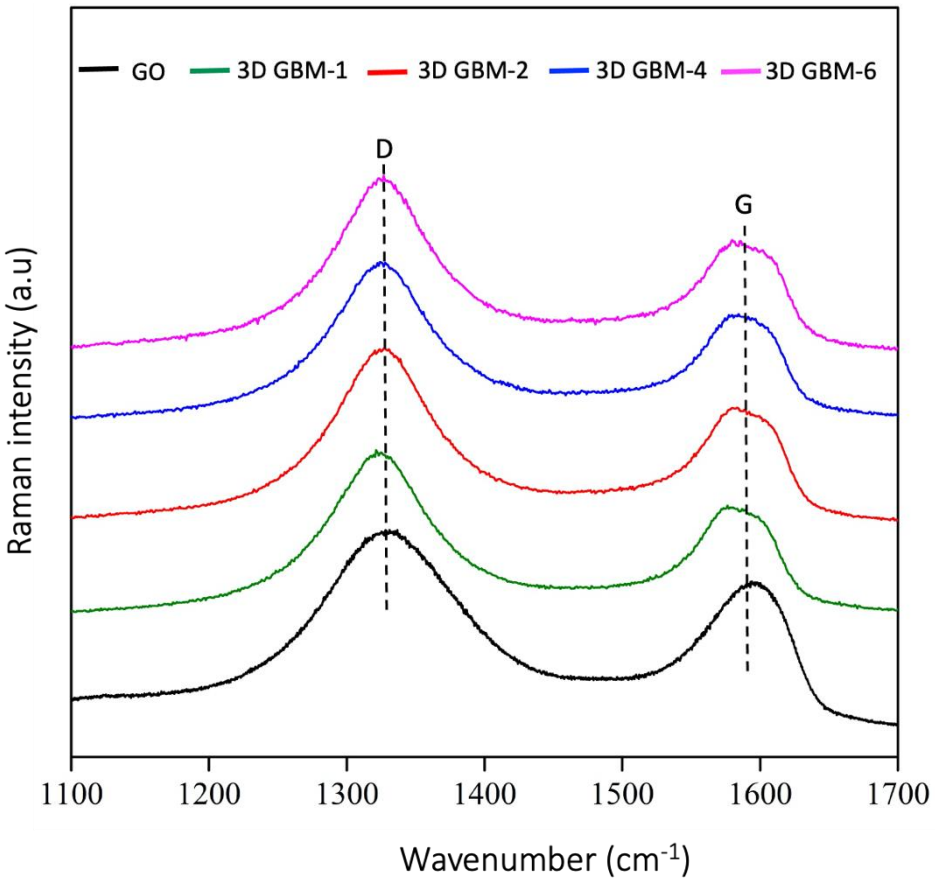

Figure 4.16 Raman spectra of 3D GBM prepared with starting GO solutions of different concentrations: 1 mg mL^{-1} (3D GBM-1), 2 mg mL^{-1} (3D GBM-2), 4 mg mL^{-1} (3D GBM-4), and 6 mg mL^{-1} (3D GBM-6).

Figure 4.17 presents the FTIR spectra of GO and all the 3D GBM samples (3D GBM-1, 3D GBM-2, 3D GBM-4, and 3D GBM-6). For all samples, the characteristic peaks of carbon materials can be observed at 1600 cm^{-1} for aromatic sp^2 C=C stretching and 2921 cm^{-1} for C-H bending. For all samples, the FTIR results clearly show the typical signature of rGO with remaining O-H functional groups, O–H stretching at 3440 cm^{-1} and C-O bond signature, C–O stretching at 1050 cm^{-1} (Emiru and Ayele, 2017).

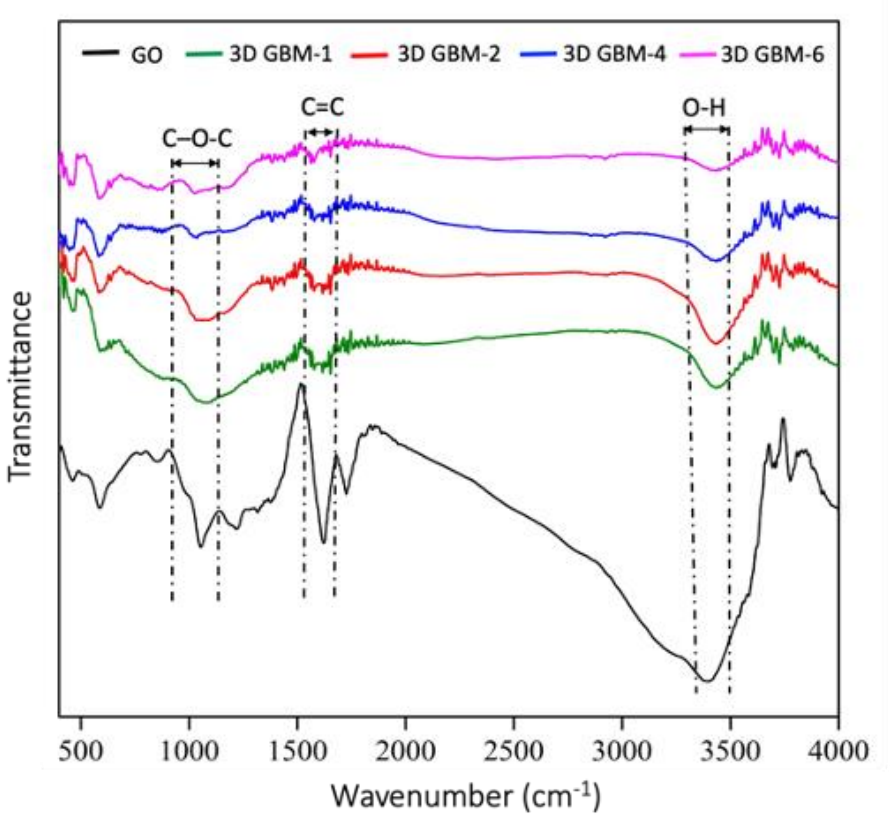

Figure 4.17 FTIR spectra of the 3D GBMs prepared with starting GO solutions of different concentrations: 1 mg mL^{-1} (3D GBM-1), 2 mg mL^{-1} (3D GBM-2), 4 mg mL^{-1} (3D GBM-4), and 6 mg mL^{-1} (3D GBM-6).

The intensity of the features related to oxygen presence in the remaining oxygen-containing groups is more pronounced for the 3D GBM-4 and 3D GBM-6, compared to GBMs prepared with lower GO concentration. As the AA/GO ratio

remains constant for all the used GO concentrations (and other parameters such as temperature and duration), the observed less efficient reduction for solutions with the highest concentrations of GO may be the result of the viscosity of the solution (observed by naked eyes), which reduces the diffusion of the reductant to the surface of the GO.

The textural properties, including SSA, pore volume, and pore size of the GBMs prepared with different concentration of GO are given in Table 4.7. The 3D GBMs exhibit a significant improvement in textural properties compared to the starting GO powder. The highest SSA and total pore volume values of 331.00 $m^2 g^{-1}$ and 0.80 $cm^3 g^{-1}$ are found for the GBM prepared with a GO solution of 2 mg mL^{-1}. In contrast, the 3D GBM prepared with low GO concentration shows the lowest SSA and total pore volume of 44.09 $m^2 g^{-1}$ and 0.16 $cm^3 g^{-1}$, respectively.

Table 4.7 SSA, pore volume, and pore size of GBMs prepared with a starting GO solution with a concentration of 1 mg mL^{-1} (3D GBM-1), 2 mg mL^{-1} (3D GBM-2), 4 mg mL^{-1} (3D GBM-4), and 6 mg mL^{-1} (3D GBM-6) determined by N_2 adsorption volumetry technique.

Sample	**SSA** ($m^2 g^{-1}$)	**Total pore volume** ($cm^3 g^{-1}$)	**Pore size** (nm)
GO	219.30	0.79	13.67
3D GBM-1	44.09	0.16	11.53
3D GBM-2	331.00	0.80	9.880
3D GBM-4	243.45	0.47	7.66
3D GBM-6	201.35	0.50	9.62

At low concentration of GO, larger pores are formed (11.53 nm) probably due to the higher distance between the graphene nanosheets as the GO concentration is reduced. Besides, as GO concentration increases, the distance between the GO nanosheets at the beginning of the assembly process will become closer, which will increase van der Waals attraction and more densely connected network leading to smaller pores. Regarding the 3D GBM surface, increase in GO concentration of the starting solution induces a tendency of the surface to be decreased but it remains quite high around 200 $m^2 g^{-1}$. As observed for the surface area evolution, the total pore volume and the micropore volume as well decrease as the GO concentration increase in the starting GO solution. From the literature, the optimum concentration is always higher than 1 mg mL^{-1} (Zhou et al., 2009).

In the study by Xu *et al.* GO concentrations of 0.5 mg mL^{-1} resulted in only precipitation with hydrothermal treatment, whereas concentrations of 1 mg mL^{-1} resulted in weak assembly (Xu et al., 2010a). Furthermore, from our results, higher GO concentrations seem to result in increased graphene nanosheet congestion, Furthermore, larger GO concentrations resulted in increased graphene nanosheet congestion, which increase the thickness of the sheets in the porous 3D structure and hinders site exposure. However, the formation of 3D GBMs at high concentrations of GO may not be suitable for some applications, particularly adsorption, as agglomeration could cause block sliding and interfere the continuous pore structures. This statement can be proven by the work of Shen *et al.* where they found that the adsorption rate increased with decrease of the GO building block concentration because less stacking favoured the diffusion of pollutants molecules. Consequently, 3D GBMs have a lower threshold concentration for assembly, but an optimum concentration is still required to achieve complete contact and

connection between nanosheets (Shen et al., 2016). In our preparation conditions, the optimized GO concentration is of 2 mg mL^{-1} and this concentration (3D GBM-2) was selected to prepare 3D GBM/alumina hybrids (section 4.4).

4.3.3 Performance of 3D GBMs in CO_2 adsorption

The GBM prepared with different concentrations of GO have been tested towards CO_2 capture, the measured adsorption capacities are gathered in Table 4.8. The 3D GBMs undergo a reduction which reduce the acidity at the adsorbent surface which is responsible for the observed enhancement of the CO_2 capture. As concentration of GO is increased in the starting solution, SSA decreases probably due to occurrence of restacking of the graphene nanosheets impacting negatively CO_2 adsorption capacity. According to the findings, 3D GBM-2 shows good optimization of two effects: limitation of restacking and surface reduction, which improves CO_2 capture by a factor of 17 compared to GO, from 4.2 mg g^{-1} to 74 mg g^{-1}. Based on BET findings, these surface properties provide an attractive alternative for CO_2 adsorption, as SSA and total pore volume significantly increase after chemical reduction of the initial concentration of 2 mg ml^{-1} (3D GBM-2). In addition, the pore size is reduced to 9.880 nm for 3D GBM-2. As CO_2 has a relatively small kinetic diameter of 0.33 nm, it is widely known that microscopic pores are required to ensure that the gas molecules are able to diffuse into an adsorbent framework in an efficient manner (Zubbri et al., 2021).

Table 4.8 CO_2 adsorption capacity of different concentration of GO

Samples	Adsorption capacity (mg g^{-1})
GO	4.2
3D GBM-1	10.2
3D GBM-2	74.0
3D GBM-4	17.2
3D GBM-6	15.3

4.3.4 Mechanism of self-assembly of graphene oxide under hydrothermal by ascorbic acid

GO may create colloidal suspension particles based on colloid chemistry due to the significant electrostatic repulsions (depending on the pH) from the ionised oxygen-containing groups, that could resist the attractive interactions of the van der Waals forces from the carbon structure. Based on FTIR results, the possible mechanism is presented in Figure 4.18. The carboxyl groups on GO are reduced by AA to hydroxyl groups under hydrothermal conditions, and the epoxy bond dehydrate the water molecules by nucleophilic ring-opening, thus restoring the conjugate system of C=C. Graphene sheets interweave with each other through hydrogen bonding and stacking interaction to form a 3D network. In theory, altering the balance toward more favourable interactions, for example, reducing structural features or altering the GO interaction, might help in the attachment of graphene nanosheets.

The mechanism in this work begins with as the pH is adjusted to 10, homogeneous dispersion of GO sheets occurs, which are distributed by repulsive

electrostatic forces arising from ionization of surface functional groups such as carboxyl groups. In the GO solution at pH 10, GO sheets naturally move in a random direction due to Brownian motion without aggregating (Sandhya et al., 2021). Following the addition of AA, these charged functional groups undergo chemical alteration (reduction), which eliminates these repulsive interactions, resulting in the formation of GBMs based on rGO nanosheets (Yuan and Su, 2006). In this study, AA causes partial decrease of oxygen-containing hydrophilic groups in certain areas, leading them to become hydrophobic and not able to disperse in water, causing graphene dispersion to be destabilised and large sheet deformation as the undispersed regions attach to each other. Furthermore, the mechanism is believed to be triggered by the phase separation of GO sheets from a liquid, and a continuing liquid phase working as a separator, or a continuous template facilitates in the formation of an interconnected pore network and the final 3D structure.

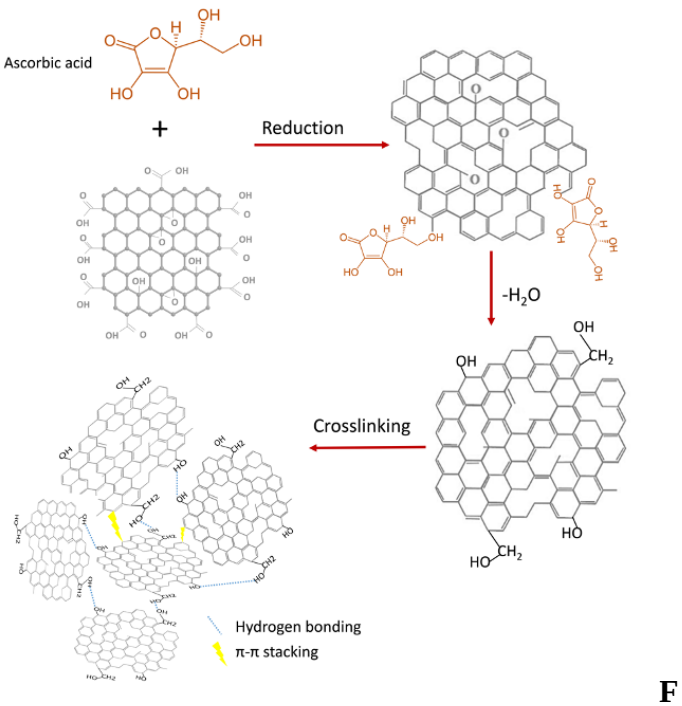

F

Figure 4.18 Working mechanism of AA reduction and crosslinking.

4.4 Chemically modified 3D graphene-based macrostructures by alumina coating: synthesis of porous alumina / graphene-based macrostructures hybrids

4.4.1 Alumina deposit on 3D graphene-based macrostructures by Atomic Layer Deposition

The studied 3D Al_2O_3/GBM hybrids have been synthesized by a two-step approach by first self-assembling GO to form porous 3D GBM and then deposit the Al_2O_3 coating by ALD (Figure 4.19). As discussed later in this sub-chapter, ALD is an advanced deposition technique that is intrinsically versatile and can be used to form conformal coatings at atomic-scale precision.

In accordance with previous statements, GO was used as the starting material because it is easier to synthesis in large quantities, less expensive, safer, and more environmentally friendly. In brief, GO was initially synthesised by a modified Hummers' method (section 4.1) and the GO nanosheets (2 mg mL^{-1} at pH 10) were assembled through a reactive hydrothermal process to form 3D GBM-2 (section 4.3). The SEM observations of 3D GBM show a hierarchical structure with interconnected channels and pores. Figure 4.20 shows representative SEM images of the 3D GBM at different magnifications. Figures 4.20 (a) and (b) illustrate how the aerogel is composed of rippled nanosheets of graphene, which are randomly oriented, leaving macropores between them. At high magnification, the as-prepared material has visible macropores with quite homogeneous sizes of 4-5 μm, these pores seem to be connected via large channels (Figures 4.20 (c) and (d)). In the SEM images (Figure 4.20), the walls of the 3D GBM appear thin, indicating low overlapping between the graphene nanosheets.

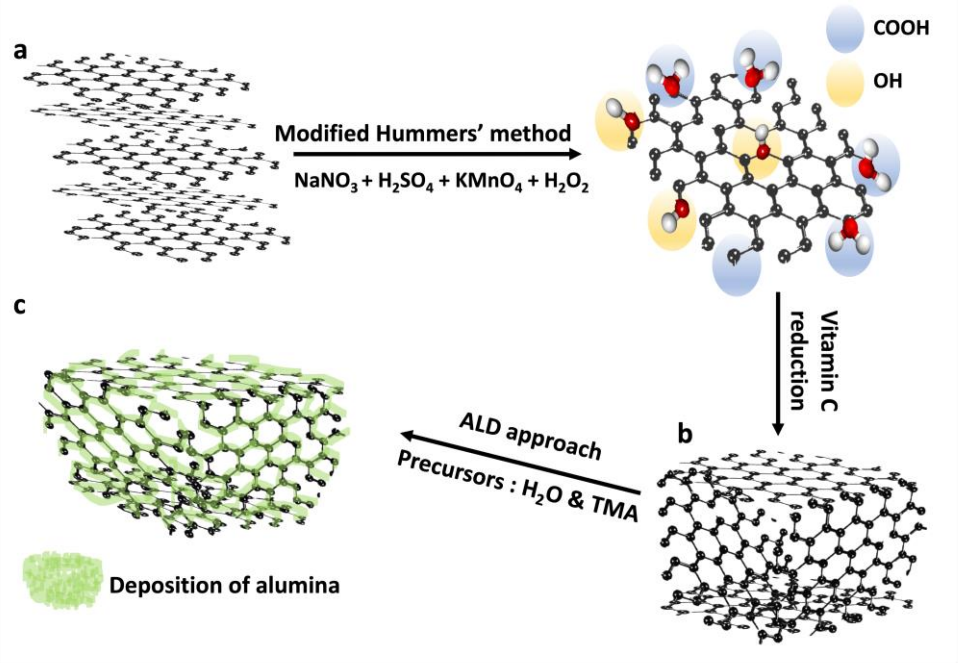

Figure 4.19 Schematic 3D Al_2O_3 / GBM hybrid synthesis: (a & b) steps involved in the synthesis of alumina 3D GBM process; (c) one "half-reaction" for the TMA-pulse and one for the water-pulse; (d) coated alumina on 3D GBM.

The second step of the hybrid preparation (Fig. scheme d→ c) consists of deposit an alumina coating on the graphene walls of these 3D GBM by using the ALD technique. ALD has been chosen because of it is a gas phase deposition technique with particular good ability to cover complex surfaces. However, since ALD is based on a chemical process for deposition, the efficiency of the process depends on the chemical properties of the surface where the coating is deposited. During deposition, the most accessible sites will be covered first, then it will gradually penetrate deeper into the inner pore structure. However, the difficulty of coating is largely caused by the low sticking probability of reactant molecules in reaction limited growth.

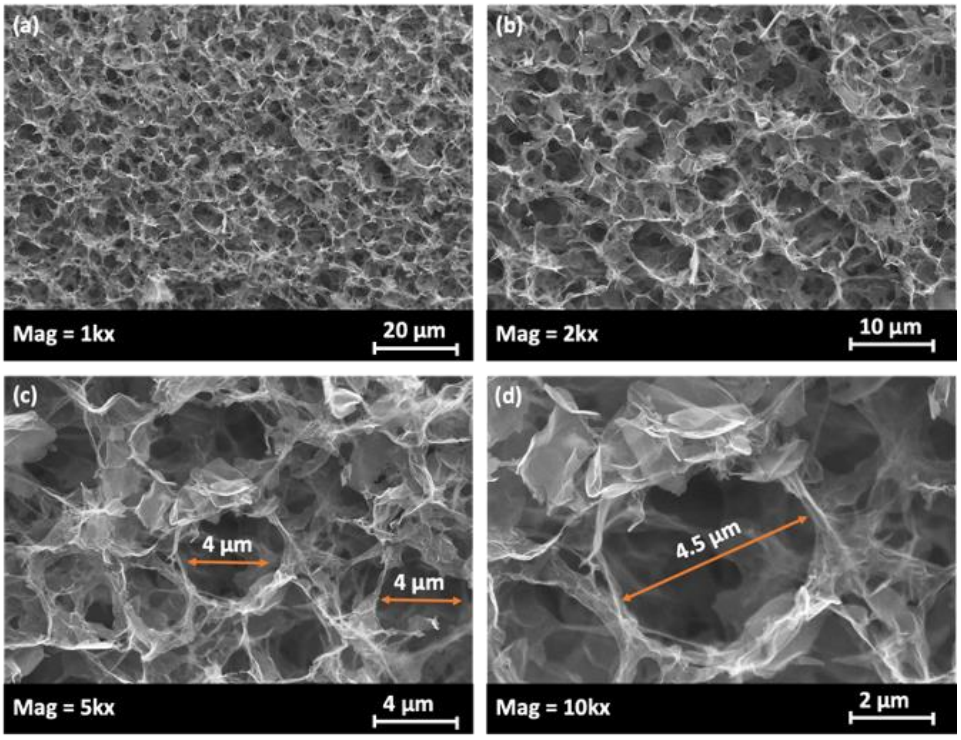

Figure 4.20 Representative SEM images of graphene aerogels prepared starting from GO dispersion at 95 °C for 4h: (a; b) low magnification (c; d) High magnification

4.4.2 Conformal deposit of alumina 3D graphene-based macrostructures hybrids

This section presents an in-depth morphological characterization of the prepared 3D Al_2O_3/GBM hybrids by standard (SEM) and advanced methods (TEM/STEM/EELS analysis on thin lamella prepared by FIB). In this work, the coating on 3D GBM was successfully achieved due to reduced GO forming the porous aerogel providing sufficient seeding sites for alumina formation, as confirmed by SEM images. Among the inorganic nanomaterials, alumina is chosen to be deposited on 3D GBM because of the ideally self-terminating nature of the adsorption process and inertness of the reaction. In addition, alumina have high

decontamination efficiency and low manufacturing costs. Thus, to investigate the mechanism of alumina deposition on these prepared 3D GBM surfaces, two ALD durations (number of cycles; 50 and 300 cycles) were employed while the other operating parameters remained constant. For both ALD conditions, low magnification SEM images of the prepared 3D Al_2O_3/GBM-50 and 3D Al_2O_3/GBM-300 reveal interconnected 3D graphene network architectures resembling of the starting pristine graphene aerogels (Figures 4.21 (a) and (b)) respectively.

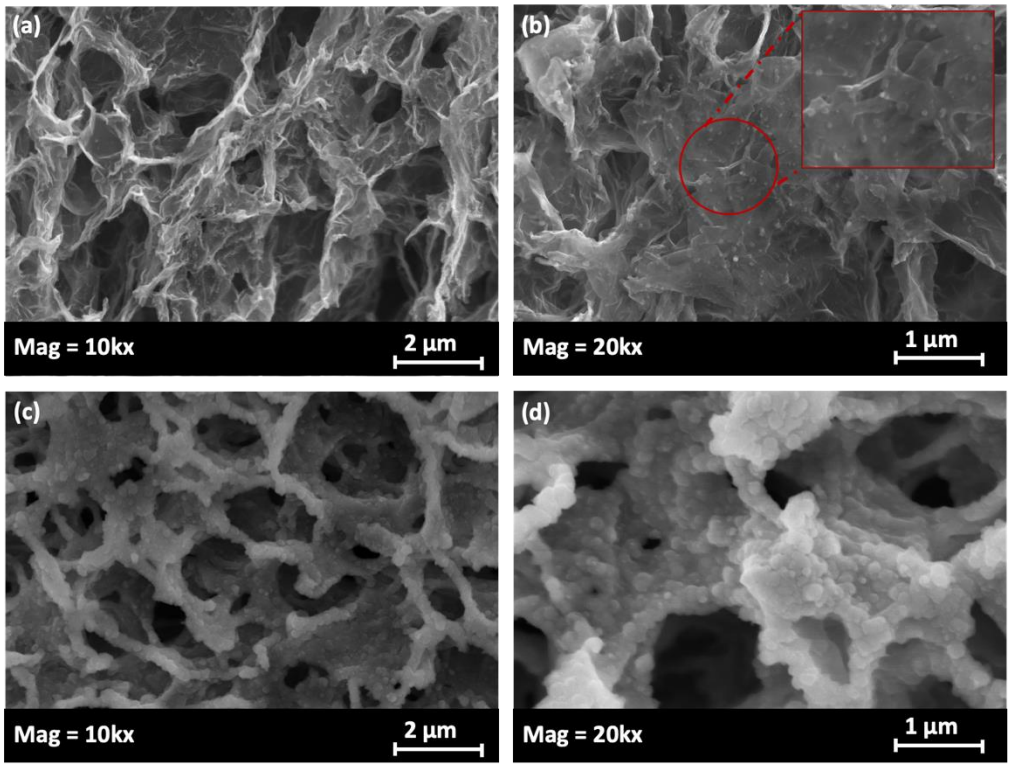

Figure 4.21 Representative SEM images of 3D Al_2O_3/GBM with coating of (a; c) 50 ALD cycles and (b; d) 300 ALD cycles.

Successful deposition is obvious for the 300 cycle-deposition condition with a thick layer visible covering the porous structure. At higher magnification, the alumina coating of 50 cycles appears to have formed particles or islands on the

graphene surface. In addition, SEM observations on the fracture surfaces of the 3D Al_2O_3/GBM-50 in Figures 4.21 (c) showed homogeneous particle dispersion, whereas the thickest alumina layer (3D Al_2O_3/GBM-300) seems to cover the graphene surface continuously in Figure 4.21. (d). However, EDS mapping indicates that these particles are protrusions on the surface of a thin continuous layer, as illustrated in Figure 4.22.The deposition process by ALD indeed strongly depends on the nature of the substrate onto which the deposit is implemented and especially the number of available sites for the ALD precursor chemisorption (Park et al., 2017). From the ALD mechanism, the ALD deposition successfully occurs if the chemisorption energy of the precursor exceeds than that involves in its physical desorption from the substrate. In the case of a weak adsorption energy on the 2D surface, a non-uniform film will grow. Whereas pristine graphene surface is unfavorable to ALD nucleation and a full graphene surface coverage, the presence of defects/functional groups on basal plane of rGO provides here favorable early stages for the alumina nucleation process.

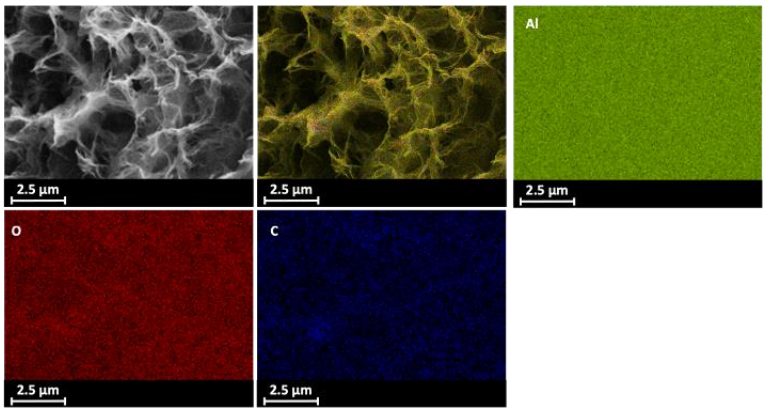

Figure 4.22 EDS mapping of 3D Al_2O_3 / GBM hybrids of 300 ALD cycles.

The growth mechanism on the graphene surface is certainly initiated by a directly reaction between TMA and reactive sites at graphene surface groups like –

OH and C=O (Figure 2.12). The adsorption of $Al(CH_3)_3$ with hydroxyl-OH groups initiates the first half-reaction. When $Al(CH_3)_2$ was adsorbed onto all available OH atoms by a spontaneous coordination between Al and O, a Al-O bond was formed.

In the second half-reaction, H_2O molecules react with the surface intermediates of $Al(CH_3)_2$ to produce CH_4 species as a product. TMA and H_2O molecules are thus trapped in the subsurface and forms nucleation clusters. The subsequent cycle numbers will fill the space between 3D graphene pore which eventually coalesce and close the space to be nearly continuous. By increasing the cycle number, the clusters will fill the region among the porous frameworks which eventually connected each other and close the space to be continuously covered by ALD material clusters with a subsequent certain roughness of the film (Wilson et al., 2005). This statement is highly supported by the evidence shown in the SEM images in Figure 4.20 confirming the preservation of the interconnected 3D graphene network architecture. The structural and chemical analysis of the inner part of the prepared 3D Al_2O_3/GBM hybrids (300 cycles) has been investigated by means of TEM/STEM performed on a thin foil lamella of several microns depth prepared by FIB (Figure 4.23 (a)). Interconnection is as well obvious in these hybrid materials as well confirmed by the technical feasibility to prepare such FIB lamellas of high porous samples. EDS mapping has been performed to check the diffusion of aluminium and oxygen precursors within the internal porosity of the 3D GBMs. Carbon, aluminium and oxygen elements from the deposited alumina film, with a faultless matching in position, are obviously well deposited within the entire 3D GBMs with a perfect coverage of the graphene sheets (Figure 4.23 (b-d)).

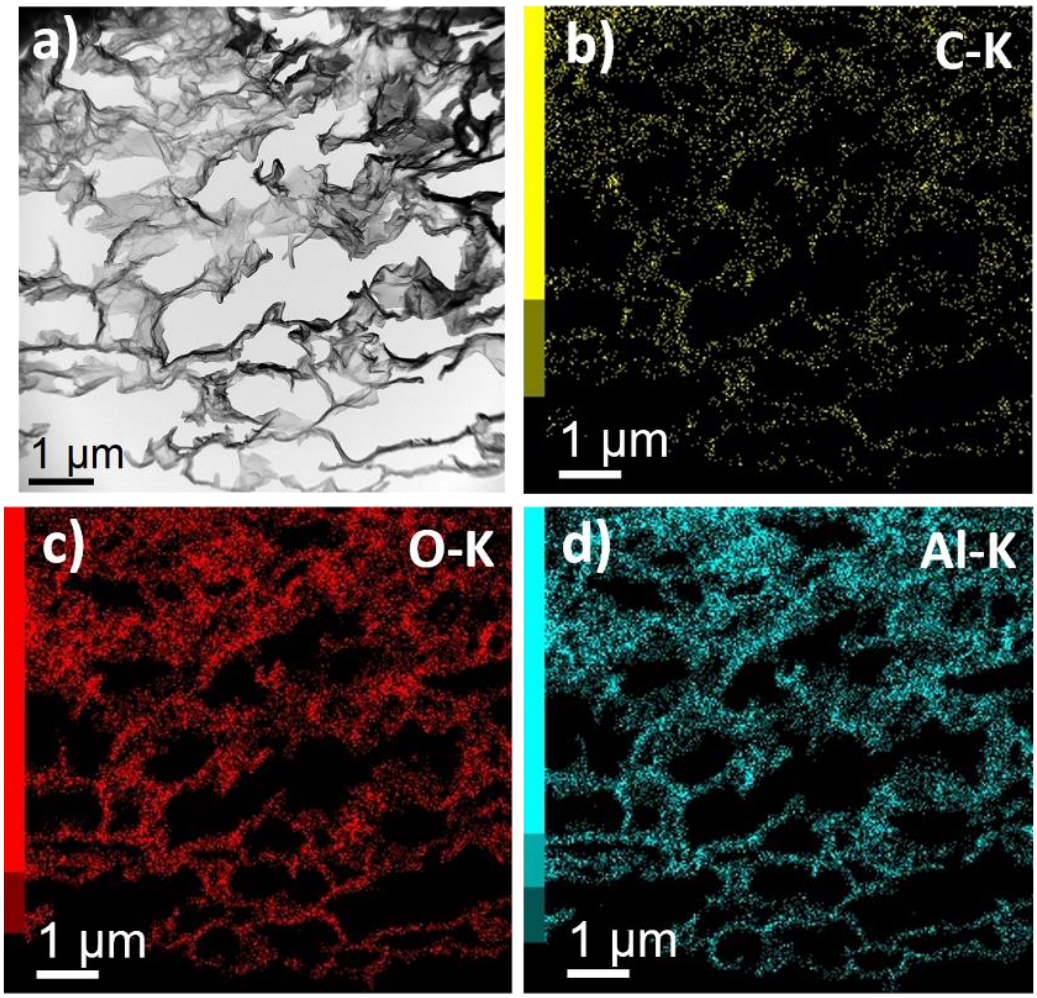

Figure 4.23 (a) STEM bright field image of the 3D graphene sample covered by an alumina ALD layer, (b), (c) and (d) EDS mapping of carbon, aluminum and oxygen, respectively.

High resolution TEM/STEM observations (Figure 4.24) and EELS mapping (Figure 4.25) performed at internal areas of the FIB lamella taken from the 3D Al_2O_3 / GBM hybrid reveal the graphene layers sandwiched in between two layers of Al_2O_3 which covers well both sides of a graphene nanosheet. The electron microscopy study of the prepared 3D ALD Al_2O_3/GBM hybrids have shown that the gaseous precursors are able to diffuse within the 3D network and that their seeding on the graphene surface is efficient enough to make grow an homogenous

layer of alumina in the whole porous material. The thickness of the alumina layer is estimated to be of approx. 7 – 8 nm (from EELS mapping and HRTEM; Figure 4.24 and Figure 4.25 respectively) whereas that of alumina deposited during the same ALD run on a silicon substrate was measured to reach approx. 59 nm.

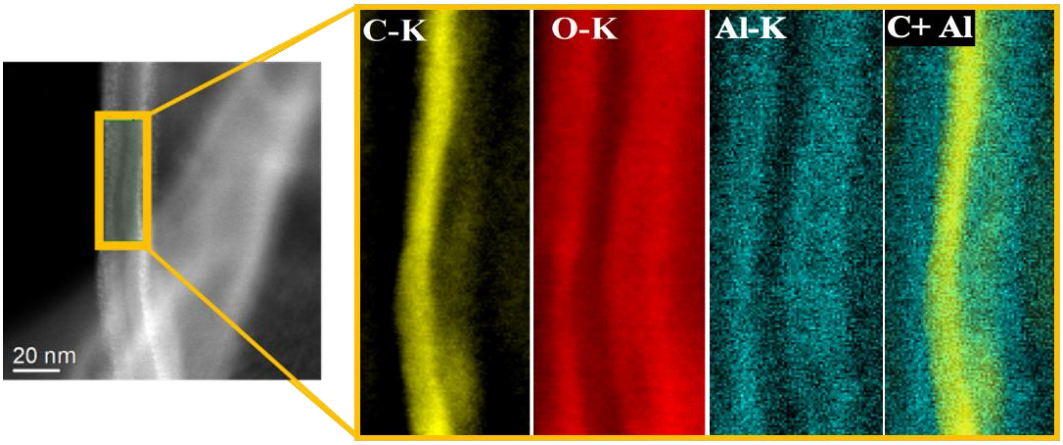

Figure 4.24 High resolution STEM bright field image of a folding edge evidencing the Al_2O_3 film deposited on both surfaces of the 3D Al_2O_3 / GBM-50 hybrid and EELS mapping of the zone highlighted by the orange rectangle.

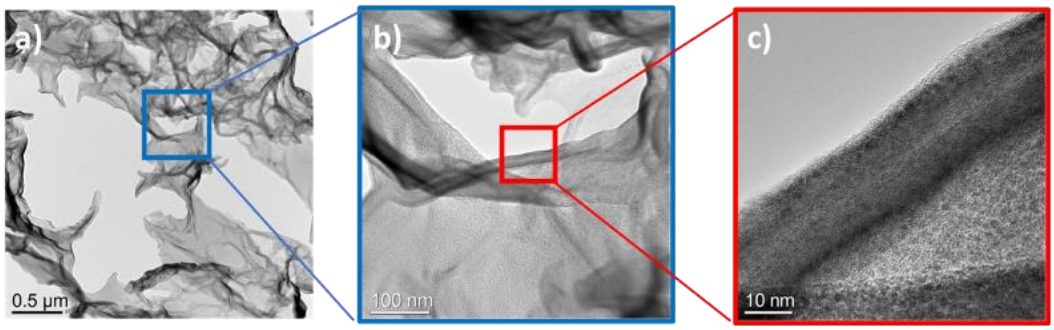

Figure 4.25 (a) TEM bright field image of a FIB cross section of the 3D graphene sample covered by an Al_2O_3 thin film, (b) TEM bright field image of the region highlighted by the blue square in image and (c) high resolution image of the region highlighted by the red square in image b.

The surface area and porosity of the prepared 3D GBMs including both pristine and hybrids were determined using nitrogen adsorption volumetry. Surface area and pore size and volume are gathered in Table 4.9 and Figure 4.26.

Table 4.9 Surface area, pore volume, and pore size of pristine 3D GBM and the 3D Al_2O_3/GBM hybrids (50 and 300 cycles) prepared with two different ALD deposit durations.

Sample Name	**Surface area** ($m^2\ g^{-1}$)	**Total pore volume** (cm^3/g)	**Pore size** (nm)
3D GBM	331	0.80	9.88
3D Al_2O_3 / GBM-50	284	0.37	5.04
3D Al_2O_3 / GBM-300	32	0.07	7.64

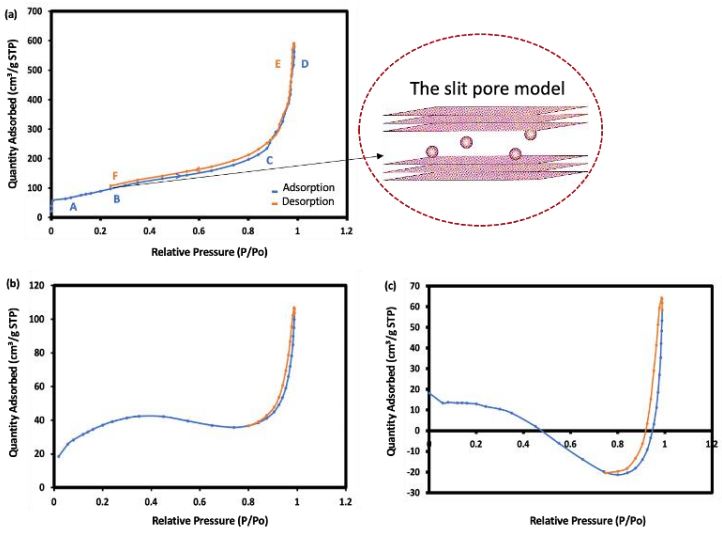

Figure 4.26 BET and BJH analysis of (a) pristine 3D GBM, red circles indicate the slit pore model; (b) 3D Al_2O_3 / GBM-50 (50 cycles); (c) 3D Al_2O_3 / GBM-300 (300 cycles).

The BET surface area of the developed pristine 3D GBM is as high as 331 $m^2\ g^{-1}$. When thickness of Al_2O_3 is increased GBM surface (ALD cycle number increased), the surface area is decreased due to the presence of the covering layer; 284 and 32 $m^2\ g^{-1}$ for 3D Al_2O_3 / GBM-50 and 3D Al_2O_3 / GBM hybrid-300, respectively. As expected, this effect is dramatically pronounced for 3D Al_2O_3 / GBM-300, having a much more thicker alumina layer at its surface. According to George *et al.* they found that all ALD overcoated supports lost surface area due to filling of pores and/or interstitial voids within the porous material (George et al., 2020). After the 50 cycle-ALD, the pore volume is reduced by a factor of 2 from 0.80 to 0.37 $cm^3\ g^{-1}$. The ALD process on the developed GBM is accompanied of a reduction of surface and pore volume due to the presence of the alumina layer at the graphene wall surface but also an increase of the available alumina surface due to the additional roughness as discussed earlier. If the alumina layer is too thick (300 cycles), the gain in surface due to the created roughness does not balance the lost in surface due to the filling of the porosity. The subsequent cycle numbers will fill the space between 3D graphene pore which eventually coalesce and close the space to be nearly continuous. By increasing the cycle number, the clusters will fill the region among the porous frameworks which eventually connected each other and close the space to be continuously covered by ALD material clusters (Wilson et al., 2005). However, interestingly, for 3D Al_2O_3 / GBM-50, the resulting surface remains as high as 284 $m^2\ g^{-1}$ leading to high alumina surface available for a further adsorption process. As shown in Table 4.10, the SSA of the 3D alumina / GBM developed in this study is comparable with other studies and even in the high range.

Table 4.10 Surface area of porous alumina-based materials and their performances for environmental applications from literature.

Sample Name	Surface area (m^2 g^{-1})	Synthesis Method	Application	Reference
3D Al_2O_3 / GBM-50	284	Alumina deposition by ALD	Removal of CR	This study
3D Al_2O_3 / GBM-300	32			
Hybrid layered double hydroxides/mesoporous alumina (LDH/MA)	278	Surfactant-assisted self-assembly method + Co-precipitation method	CO_2 capture	(Wu et al., 2022)
Ordered Mesoporous Alumina	305	Evaporation-induced self-assembly	CO_2 capture and dye separation	(Seah et al., 2021)
Bead-Shaped Mesoporous Alumina	267	Template-assisted sol–gel reaction of alumina with chitosan as a template.	Adsorption of ammonia	(Kim et al., 2020)
Mesoporous alumina	95 - 289	Evaporation Induced Self Assembly (EISA) method.	Adsorption of ammonia	(Vo et al., 2020)
Porous γ-alumina nanoshells	218	Condensed layer deposition (CLD) technique	Removal of CR	(Al-Salihi et al., 2022)

TGA is a quantitative technique, commonly used for carbon nanomaterials. When submitted to an oxidative (oxygen alone or air), carbon nanomaterials undergo combustion phenomenon from which the combustion temperature depends on the structural quality of the carbon materials. For example, amorphous carbon burns off at much lower temperature (250-350 °C) (Saputra et al., 2022) than graphite (600-800 °C) (Bratten et al., 2021). For GBMs a defect-free graphene derivative can withstand stronger (higher temperature) oxidative conditions than highly defected/functionalized graphene, like GO (Farivar et al., 2021). In the low temperature range, the present functional groups can be detached from the carbon surface. In the case of metal-based compounds in the carbon nanomaterial samples, their relatively good stability compared to carbon species allows to quantify their content in impure or hybrid samples.

The TGA profiles of GO, 3D GBM, 3D Al_2O_3 / GBM-50 and 3D Al_2O_3 / GBM-300 are shown in Figure 4.27. The first observation about these TGA profiles is that GO behaves differently from the other samples since it loses weight in two steps before the combustion occurrence at around 500°C. For GO, the 10 % of weight loss at round 100 °C correspond to elimination of adsorbed water molecules due to the hydrophilic nature of GO. A more dramatic mass loss of around 20 % is observed around 200 °C. This is commonly associated with the thermally-induced decomposition of oxygen-containing functional groups. In the high temperature region (>300 °C), the mass losses in GO were continuous, reaching up to 50 %. This behaviour is expected as the materials undergo further carbonization and more stable groups such as carbonyls are eliminated (Alazmi et al., 2016).

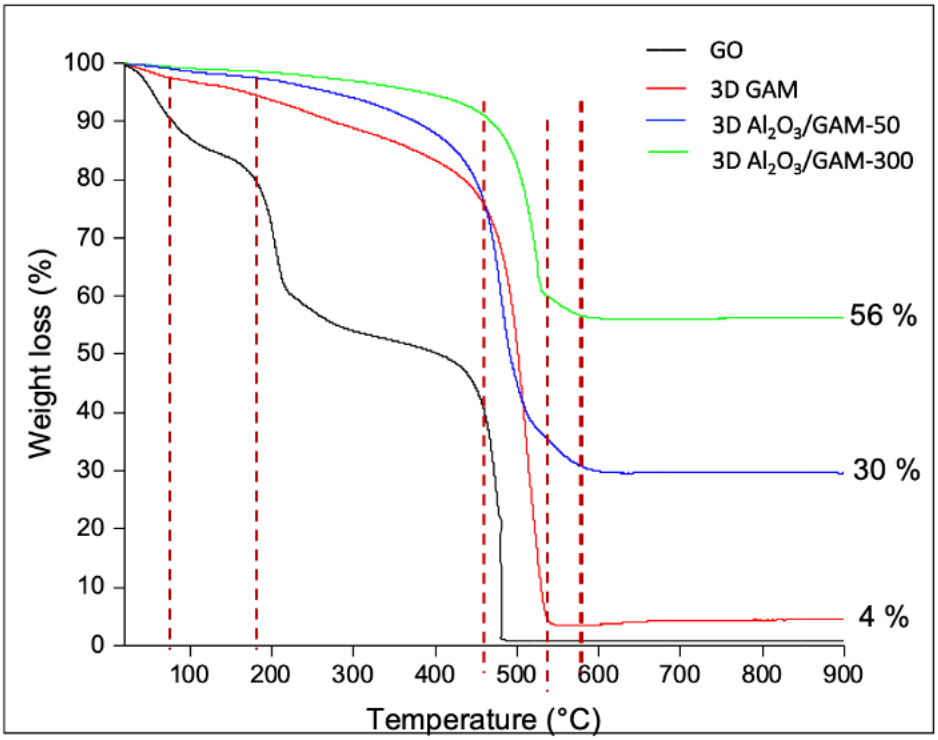

Figure 4.27 TGA profile diagram of GO, 3D GBM, 3D Al_2O_3 / GBM-50 and 3D Al_2O_3 / GBM-300.

The remaining mass after combustion of the carbon species above 500°C is very low (less than 1 wt.%) meaning that almost no residues remains in GO. 3D GBM shows a higher combustion temperature, around 450 °C, which is in agreement with the fewer amount of oxygenated functional groups after the reduction reaction under the hydrothermal process. Additionally, the residual mass of inorganic contamination after combustion above 600°C is less than 4 wt.%, implying that only slight residues remain in the 3D GBM. For the two alumina / GBM hybrids (3D Al_2O_3 / GBM-50 and 3D Al_2O_3 / GBM-300), the graphene combustion temperature remains in the 500-550°C range and the residual weight are 30 % and 56 % for the 3D Al_2O_3 / GBM-50 and 3D Al_2O_3 / GBM-300, respectively. In addition to the thickness analysis, the estimated thicknesses for 50 and 300 cycles on the silicon surface were 9.8 and 59 nm measured by optical

profilometry, respectively. Even if the measurement of the thickness by STEM/EELS mapping is certainly not accurate, the thickness of alumina on the 3D GBM seems quite reduced compared to silicon: *i.e.* 7-8 nm for 3D alumina/GBM-300 and 59 nm for the silicon wafer. Silicon wafer is normally covered by SiO_2 layer which offers a lot of reactive sites for alumina growth by ALD (Arl et al., 2020). For rGO within the 3D GBM to cover, as discussed earlier, the seeding sites are present but alumina growth is less favourable than for surfaces like silica or other substrate like WSe_2 for which the alumina layer is under the form of a continuous film (Park et al., 2017). On the prepared 3D GBMs, alumina growth occurs as nanoparticles instead of a continuously homogeneous film, this is as well the reason why the alumina thickness on the 3D GBMs is difficult to determine. However, from SEM / EDS mapping, it seems that alumina has a quite good covering on the graphene surface within the 3D GBMs (Figure 4.22).

4.4.3 3D Al_2O_3 / graphene-based macrostructures for water treatment application

3D Al_2O_3 / GBM-50 has been shown to possess a quite good covering of its surface with alumina under the form of nanoparticles and/or thin film and from TGA and N_2 adsorption volumetry analysis, 3D Al_2O_3/GBM-50 potentially provide then an excellent candidate to be tested as adsorbent for water treatment. The surrounding pH in the polluted medium is an important factor which can dramatically impact the adsorption process because it affects the surface charge of both the adsorbent and the adsorbate. In an aqueous solution, electrostatic interactions between charged surface and ionized species can powerful attractive or repulsive forces. This is the reason why, Zeta Potential analysis was first investigated to determine the point of zero charge (pH_{PZC}) for the charge

characteristics of the adsorbent (Figure 4.28). The point of zero charge, pH_{PZC}, 3D Al_2O_3/GBM-50 is around 6.0 with a surface positively charged at pH < pH_{PZC}, and negatively charged at pH > pH_{PZC}. CR is an anionic standard dye at its natural pH (pH 5) whose adsorption efficiency will increase with decreasing pH of the dye solution (Litefti et al., 2019).

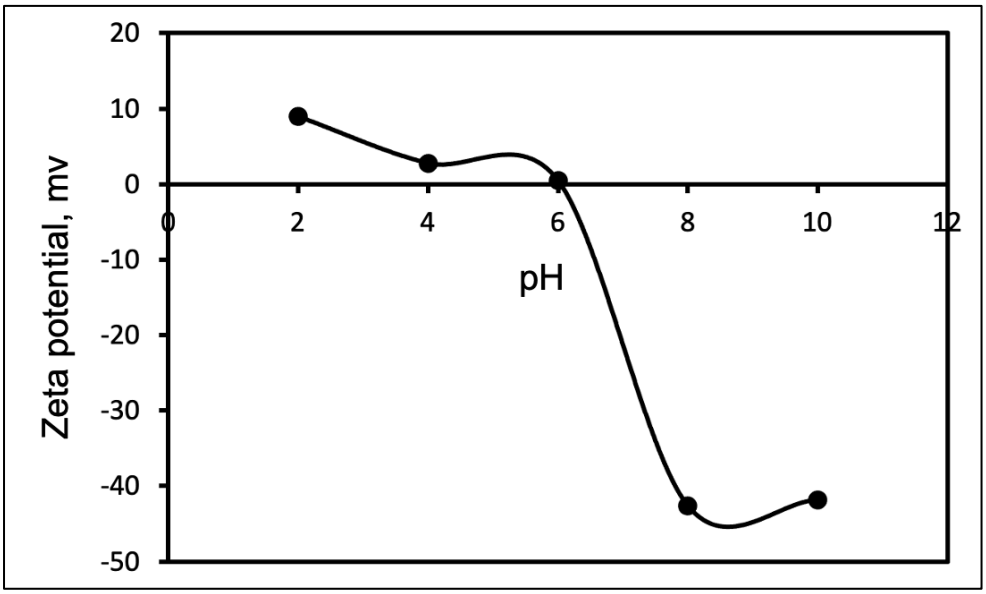

Figure 4.28 Zeta potential plots for ALD 3D Al_2O_3 / GBM -50 with point of zero charge

In this work, both pristine 3D GBM and 3D Al_2O_3/GBM-50 hybrid adsorbents have been tested for the removal of CR at pH 5 (Figure 4.29). For both the first (Figure 4.28(a)) of CR removal, the adsorption of CR on 3D Al_2O_3 / GBM-50 hybrid is more rapid than for pristine 3D GBM and reaches equilibrium in 15 min with removal of CR 87 % while CR adsorb less rapidly and less efficiently on pristine 3D GBM. At the second cycle, 98 % of CR removal are even performed by the porous hybrid nanomaterial for the second cycle. The pristine 3D GBM has a lower rate of CR adsorption with only about 20 % at the first cycle with no adsorption occurring at the second cycle. The performance of our 3D alumina/GBM

is tentatively compared to similar materials reported in the literature. However, dye adsorption and especially CR removal by this kind of hybrids is a relatively new subject. A recent study by Al Salihi *et al.* synthesised highly porous g-Al_2O_3 nanoshells from alumina coated carbon black (CB) by method called Condense Layer Deposition (CLD). They studied CR adsorption (initial concentration range: 20-160 mg L^{-1} at pH range: 4-10) for porous g-Al_2O_3 nanoshells and they found that equilibrium for CR adsorption was reached in 30 min, much longer compare to our graphene-based hybrid. That can be the sign of a good mater diffusion in our hybrid adsorbent. They did not performed any cycling study and they obtained a removal adsorption capacity for porous g-Al_2O_3 nanoshells of 98.6 % which is comparable with our study.

Clearly, the developed ALD 3D Al_2O_3 / GBM-50 hybrid shows higher adsorption capacity than pristine 3D GBM thanks to favourable interactions between alumina surface and CR in the used conditions, which is the dominant mechanism in the adsorption process of CR dye (Al-Salihi et al., 2022). Moreover, mass transfer of CR dye molecules between liquid solution and alumina surface is as well certainly not a limiting factor due to the multi-porosity offered by the hybrid guaranteeing a ease of access to the adsorption sites.

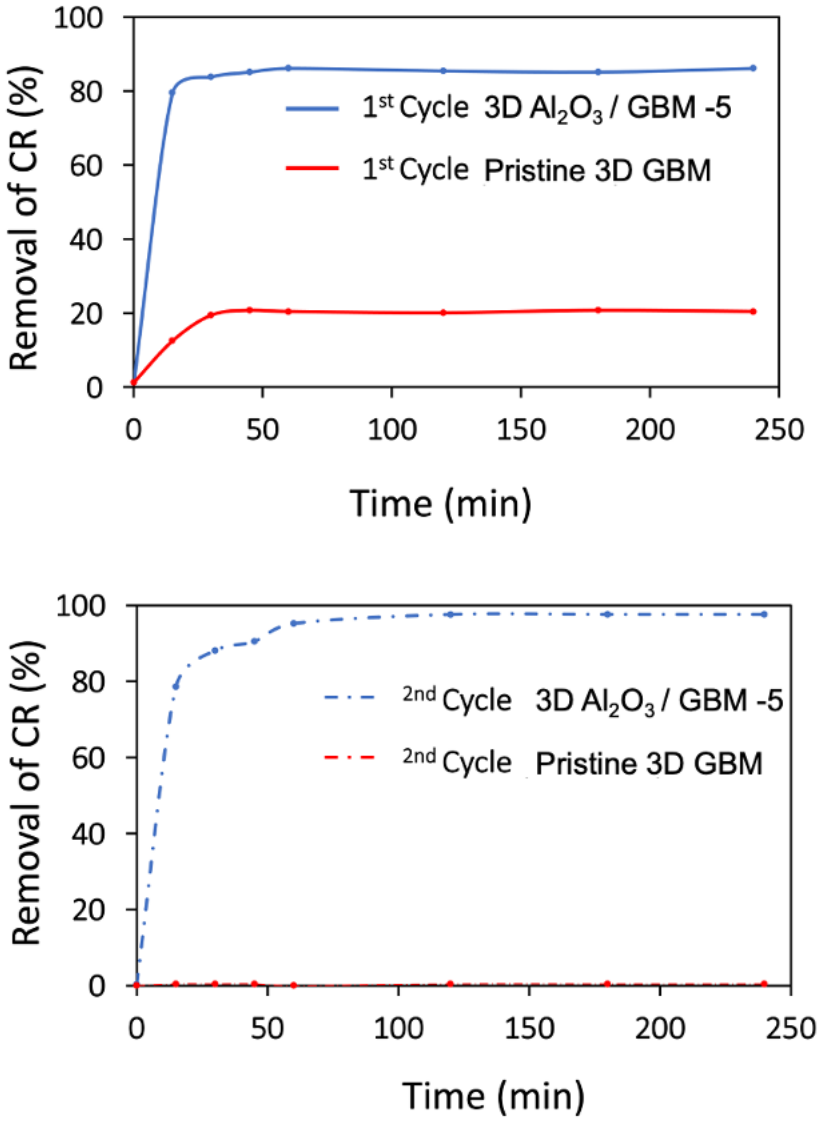

Figure 4.29 Adsorption isotherms for pristine 3D GBM and 3D Al_2O_3 / GBM -50 hybrid (a) first cycle and (b) second cycle. Initial CR concentrations of 10 mg L^{-1}, pH 5

CHAPTER 5

CONCLUSION AND RECOMMENDATIONS

5.1 Conclusion

The first objective of this study was achieved by synthesising and characterizing GO to be used as starting materials for preparation of 2D and 3D graphene-based adsorbents. GO is synthesised and used as starting material because it can be produced using graphite (since it is inexpensive) with high amount production (grams) with exceptional cost-efficiency. Secondly, GO is very dispersible in water and can form stable aqueous suspensions which can serve as the starting material to be assembled into macroscopic structures with cheaper solution processes. Through the oxidation process, oxygen-containing functional groups are attached to the surface of graphite and thus converting the graphite to GO after a chemical exfoliation process. In this study, the surface modification of GO is modified using a modified Hummers' method and all the surface characterization analysis of GO is performed by using a set of complementary techniques. The overall structural properties of this graphene derivative remain preferable for environmental applications especially in adsorption regardless of some defects on the surface and GO can potentially be used as a starting material for subsequent modifications of 2D and 3D GBMs based on the results of the analysis.

The second objective for this work is to study the structural and the chemical properties of activated GO by chemical and physical activation and analyse their performance for CO_2 capture application. Four different aspects have been highlighted including (i) surface area; (ii) pore volume; (iii) pore size and (iv)

chemical reduction. According to the results, first, GO-CA 800 has a higher SSA compare to GO-PA 900 which is 1060.5 m^2 $g^{-1}$and 762.5 m^2 g^{-1},respectively. Secondly, GO-PA 900 (2.31 cm^3 g^{-1}) exhibits higher pore volume than GO-CA 800 (0.99 cm^3 g^{-1}). Thirdly, GO-CA 800 has smaller pores than GO-PA 900, at 3.65 nm and 12.14 nm respectively. Lastly, greater reduction efficiency is experienced by GO-CA 800 compare to GO-PA 900, which lowers surface acidity and enhances CO_2 capture. Consequently, the results for the highlighted characteristics are better for GO-CA 800, indicating that chemical activation by KOH is more effective for generating high surface and porous structure as well as altering the surface chemistry of activated graphene, thereby promoting adsorption.

For the third objective, the work focus on modification of 2D graphene into 3D macroscopic self-assemblies of graphenes for CO_2 capture. The hydrothermal process begins with a solution of GO (pH 10) in which the GO nanosheets are homogeneously dispersed due to the electrostatic forces. The reduced GO nanosheet assembled in a 3D interconnected network are formed after incorporating with AA, which alters these functional groups chemically by a reduction reaction. By using FTIR measurement, the reduction of GO into 3D GBMs was verified. Besides, it is also noteworthy that the reduction reaction appears not to have a drastic impact on the structural quality of 3D GBMs as predicted,

The forth objective is to chemically modify by alumina coating on the graphene walls of the 3D GBM using ALD technique for the removal of CR dye. From the findings, the 3D Al_2O_3 / GBM-50 (50 ALD cycles) has been shown to possess a quite good covering of its surface with alumina under the form of nanoparticles and from TGA and N_2 adsorption volumetry analysis, 3D Al_2O_3 / GBM-50 hybrid

potentially provide then an excellent structural properties, making it a good adsorbent for CR removal. The adsorption study shows that the developed ALD 3D Al_2O_3 / GBM-50 hybrid shows higher adsorption capacity than pristine 3D GBM thanks to favorable interactions between alumina surface and CR in the used conditions, which is the dominant mechanism in the adsorption process of CR dye.

The last objective was about to investigate and propose advanced and suitable techniques for an in-depth morphological characterization of the 3D GBMs and 3D porous alumina / GBM hybrids which are nanomaterials difficult to analysed especially because of the complexity of their three-dimensional structure. In this work, the characterization techniques used were quite standard like SEM and much more technically advanced like TEM/STEM/EELS analysis on thin lamella prepared by FIB. FIB / TEM coupling approach on this kind of materials has not been reported in literature to the best of our knowledge. SEM images of 3D GBMs coated by Al_2O_3 have shown that the gaseous precursors are able to diffuse into the 3D network and can form homogenous alumina layer on the graphene sheets. Besides, the TEM and EELS mapping analysis on the folding edge of a graphene sheet also confirms that graphene is both sides covered by alumina even at the inner part of the 3D alumina / GBM hybrids. Furthermore, by ALD technique, which is a technique little used yet for modification of 3D graphene networks, the compositional control as well as conformal coating of complex geometries can be achieved. Besides, these characteristics, combined to the low synthesis temperature and the versatility in term of materials that can be deposited, make ALD a highly suitable technique for the synthesis of 3D Al_2O_3 / GBM hybrids for improved adsorption performance.

5.2 Recommendations

This thesis has accomplished its main objectives which concerns very new graphene-based materials and it opens opportunities for new research studies that can be conducted in the following directions: 2D and 3D graphene have characteristics of large specific surface area, small particle size, and high adsorption efficiency. From this findings, we found that, in developing an ideal adsorbent, there are two major factors that give an impact towards the efficiency of the adsorption process which are structural (surface and porosity) properties and surface chemistry. Thus, there are few strategies that can be further explored in order to enhance properties of these GBMs in order to be used in the adsorption study: (1) in-depth study are needed in term of surface functionalization regulation, (2) morphology and structure control (3) material composite.

Functional groups are primarily responsible for the surface chemistry of graphene. Recent studies on functional adsorbents with O/N/S-containing groups on GBMs have demonstrated good adsorption performance for environmental pollutants. Besides, GBMs surfaces with nitrogen function might change the surface chemistry because it promotes a higher functional basicity, which increases adsorption capacity. Additionally, another way to regulate surface functionalization is to chemically modify GBMs surfaces by doping heteroatoms, metal or metal oxide, and coating organic polymers on the surface. Based on the characteristics of surface structures of GBMs, it is suggested to study a simple semiquantitative model in order to describe the intrinsic adsorption behaviour of GO and targeted pollutant. We expected that by the adsorption mechanism, discussion in details can be achieved at molecular levels. For example, the contribution coefficients derived

from the proposed model is expected to indicate that the most preferential interactions between GO and the targeted pollutant.

The methods for regulating the morphology and structure of GBMs mainly include fold structure control, pore structure control, and size control. Furthermore, 3D GBMs with 3D porous structure retain the inherent excellent characteristics of graphene, exhibiting the characteristics of large specific surface area, high mechanical strength, fast mass transfer rate and strong electron transmission capacity. The structural characteristics of 3D GBMs make it easy to be separated from water in practical operation, as such, it becomes an ideal material for the treatment of pollutants. Hydrothermal-reduction-induced self-assembly technology is the common method used for the preparation of 3D GBMs. However, in-depth understanding of the specific mechanism of each assembly method is important at this stage, not only for realizing full control of the assembly process and microstructure of 3D GBMs but also for clarifying common points (intersheet interaction) across different assemblies. Thus, phase separation and liquid spacers should be consider for the 3D assembly of GO or rGO in various cases, and clearer theoretical explanations are needed in order to have a very reasonable understanding of the assembly. Besides, the properties of the GO precursor are sensitive to the experimental conditions. So, effects of parameter study like GO sheet size, shape, thickness, surface chemistry and defects and traces of impurities need to be study in depth in order to clarify the interactions between GO or rGO during the assembly process.

In addition, a series of GBMs composite materials can be studied in more depth. For example, novel 3D GBMs were developed in this study using chemically

modified ALD. We found that from TEM and EELS images, aluminium and oxygen precursors are able to diffuse into the 3D network of graphene and can be adsorbed on the growing surfaces, inducing a perfect coverage of the graphene sheets. However, the exact mechanism of ALD remains unclear among researches because these GO / rGO surface are complicated to know precisely (especially in term of number and exact nature of the functional groups) and future studies in terms of the deposition of the metal oxide by adjusting conditions such as pressure, temperature, purge time, concentration, etc. are necessary and need to be coupled with an in-depth characterization of the deposits formed. The ALD process also offers quite a large variety of materials to be used, however, not all materials can be used; therefore, simulations are recommended to determine and predict which effective reaction pathways are most appropriate. This experimental/theoretical approach can be an important consideration when designing future ALD recipes for 3D materials.

REFERENCES

Abdelnabi, M.M.S., Izzo, C., Blundo, E., Betti, M.G., Sbroscia, M., Di Bella, G., Cavoto, G., Polimeni, A., García-Cortés, I., Rucandio, I., Moroño, A., Hu, K., Ito, Y., Mariani, C., 2021. Deuterium Adsorption on Free-Standing Graphene. Nanomaterials **11**, 130.

Abooalizadeh, Z., Gong, P., Sudak, L., Egberts, P., 2021. Layer dependent out-of-plane elastic modulus of graphene. Appl. Phys. Lett. **118,** 263101.

Acik, M., Lee, G., Mattevi, C., Pirkle, A., Wallace, R.M., Chhowalla, M., Cho, K., Chabal, Y., 2011. The Role of Oxygen during Thermal Reduction of Graphene Oxide Studied by Infrared Absorption Spectroscopy. J. Phys. Chem. C **115**, 19761–19781.

Adegoke, K.A., Oyedotun, K.O., Ighalo, Joshua.O., Amaku, J.F., Olisah, C., Adeola, A.O., Iwuozor, K.O., Akpomie, K.G., Conradie, J., 2022. Cellulose derivatives and cellulose-metal-organic frameworks for CO_2 adsorption and separation. Journal of CO_2 Utilization **64**, 102163.

Aghel, B., Behaein, S., Wongwises, S., Shadloo, M.S., 2022. A review of recent progress in biogas upgrading: With emphasis on carbon capture. Biomass and Bioenergy **160**, 106422.

Ahvenniemi, E., Akbashev, A.R., Ali, S., Bechelany, M., Berdova, M., Boyadjiev, S., Cameron, D.C., Chen, R., Chubarov, M., Cremers, V., Devi, A., Drozd, V., Elnikova, L., Gottardi, G., Grigoras, K., Hausmann, D.M., Hwang, C.S., Jen, S.-H., Kallio, T., Kanervo, J., Khmelnitskiy, I., Kim, D.H., Klibanov, L., Koshtyal, Y., Krause, A.O.I., Kuhs, J., Kärkkänen, I., Kääriäinen, M.-L., Kääriäinen, T., Lamagna, L., Łapicki, A.A., Leskelä, M., Lipsanen, H., Lyytinen, J., Malkov, A., Malygin, A., Mennad, A., Militzer, C., Molarius, J., Norek, M., Özgit-Akgün, Ç., Panov, M., Pedersen, H., Piallat, F., Popov, G., Puurunen, R.L., Rampelberg, G., Ras, R.H.A., Rauwel, E., Roozeboom, F., Sajavaara, T., Salami, H., Savin, H., Schneider, N., Seidel, T.E., Sundqvist, J., Suyatin, D.B., Törndahl, T., van Ommen, J.R., Wiemer, C., Ylivaara, O.M.E., Yurkevich, O., 2017. Review Article: Recommended

reading list of early publications on atomic layer deposition—Outcome of the “Virtual Project on the History of ALD.” Journal of Vacuum Science & Technology A: Vacuum, Surfaces, and Films **35**, 010801.

Ajibade, F.O., Adelodun, B., Lasisi, K.H., Fadare, O.O., Ajibade, T.F., Nwogwu, N.A., Sulaymon, I.D., Ugya, A.Y., Wang, H.C., Wang, A., 2021. Environmental pollution and their socioeconomic impacts, in: Microbe Mediated Remediation of Environmental Contaminants. Elsevier, pp. 321–354.

Akeeb, O., Wang, L., Xie, W., Davis, R., Alkasrawi, M., Toan, S., 2022. Post-combustion CO_2 capture via a variety of temperature ranges and material adsorption process: A review. Journal of Environmental Management **313**, 115026.

Alazmi, A., Rasul, S., Patole, S.P., Costa, P.M.F.J., 2016. Comparative study of synthesis and reduction methods for graphene oxide. Polyhedron **116,** 153–161.

Al-Gaashani, R., Najjar, A., Zakaria, Y., Mansour, S., Atieh, M.A., 2019. XPS and structural studies of high-quality graphene oxide and reduced graphene oxide prepared by different chemical oxidation methods. Ceramics International **45**, 14439–14448.

Al-Ghussain, L., 2019. Global warming: review on driving forces and mitigation: Global Warming: Review on Driving Forces and Mitigation. Environ. Prog. Sustainable Energy **38**, 13–21.

Almoisheer, N., Alseroury, F.A., Kumar, R., Almeelbi, T., Barakat, M.A., 2019. Synthesis of Graphene Oxide/Silica/Carbon Nanotubes Composite for Removal of Dyes from Wastewater. Earth Syst Environ **3**, 651–659.

ALOthman, Z., 2012. A Review: Fundamental Aspects of Silicate Mesoporous Materials. Materials **5**, 2874–2902.

Al-Salihi, S., Jasim, A.M., Fidalgo, M.M., Xing, Y., 2022. Removal of Congo red dyes from aqueous solutions by porous γ-alumina nanoshells. Chemosphere **286**, 131769.

Alvim-Ferraz, M.C.M., Gaspar, C.M.T.B., 2005. Impregnated Active Carbons to Control Atmospheric Emissions: Influence of Impregnation Methodology and Raw Material on the Catalytic Activity. Environ. Sci. Technol. **39**, 6231–6236.

Anwar, A., Mohammed, B.S., Wahab, M.A., Liew, M.S., 2020. Enhanced properties of cementitious composite tailored with graphene oxide nanomaterial - A review. Developments in the Built Environment **1**, 100002.

Arl, D., Rogé, V., Adjeroud, N., Pistillo, B.R., Sarr, M., Bahlawane, N., Lenoble, D., 2020. SiO_2 thin film growth through a pure atomic layer deposition technique at room temperature. RSC Adv. **10**, 18073–18081.

Bandosz, T.J., Seredych, M., Rodríguez-Castellón, E., Cheng, Y., Daemen, L.L., Ramírez-Cuesta, A.J., 2016. Evidence for CO_2 reactive adsorption on nanoporous S- and N-doped carbon at ambient conditions. Carbon **96**, 856–863.

Barquilha, C.E.R., Braga, M.C.B., 2021. Adsorption of organic and inorganic pollutants onto biochars: Challenges, operating conditions, and mechanisms. Bioresour. Technol. Rep. **15**, 100728.

Benítez, A., Caballero, A., Morales, J., Hassoun, J., Rodríguez-Castellón, E., Canales-Vázquez, J., 2019. Physical activation of graphene: An effective, simple, and clean procedure for obtaining microporous graphene for high-performance Li/S batteries. Nano Res. **12**, 759–766.

Bensalah, H., Younssi, S.A., Ouammou, M., Gurlo, A., Bekheet, M.F., 2020. Azo dye adsorption on an industrial waste-transformed hydroxyapatite adsorbent: Kinetics, isotherms, mechanism and regeneration studies. J. Environ. Chem. Eng. **8**, 103807.

Berradi, M., Hsissou, R., Khudhair, M., Assouag, M., Cherkaoui, O., El Bachiri, A., El Harfi, A., 2019. Textile finishing dyes and their impact on aquatic environs. Heliyon **5**, e02711.

Bratten, A., Duan, J., Hoffman, A., Wen, H., He, X., Stempien, J.D., 2021. Effects of microstructure on the oxidation behavior of A3 matrix-grade graphite. J. Am. Ceram. Soc. **104**, 584–592.

Busetty, S., 2019. Environmental Treatment Technologies: Adsorption, in: Hussain, C.M. (Ed.), Handbook of Environmental Materials Management. Springer International Publishing, Cham, pp. 1367–1397.

Chen, C., Zhu, X., Chen, B., 2018. Covalently cross-linked graphene oxide aerogel with stable structure for high-efficiency water purification. J. Chem. Eng. **354**, 896–904.

Chen, W., Yan, L., 2011. In situ self-assembly of mild chemical reduction graphene for three-dimensional architectures. Nanoscale **3**, 3132-3137.

Chen, X., Wang, X., Fang, D., 2020. A review on C1s XPS-spectra for some kinds of carbon materials. Fuller. Nanotub. Carbon Nanostructures **28**, 1048–1058.

Chen, Z., Ren, W., Gao, L., Liu, B., Pei, S., Cheng, H.-M., 2011. Three-dimensional flexible and conductive interconnected graphene networks grown by chemical vapour deposition. Nature Mater. **10**, 424–428.

Chowdhury, S., Balasubramanian, R., 2016a. Highly efficient, rapid and selective CO_2 capture by thermally treated graphene nanosheets. Journal of CO_2 Utilization **13**, 50–60.

Chowdhury, S., Balasubramanian, R., 2016b. Three-Dimensional Graphene-Based Porous Adsorbents for Postcombustion CO_2 Capture. Ind. Eng. Chem. Res. **55**, 7906–7916.

Deng, F., Luo, X.-B., Ding, L., Luo, S.-L., 2019. Application of Nanomaterials and Nanotechnology in the Reutilization of Metal Ion from Wastewater, in:

Nanomaterials for the Removal of Pollutants and Resource Reutilization. Elsevier, pp. 149–178.

Díez-Betriu, X., Álvarez-García, S., Botas, C., Álvarez, P., Sánchez-Marcos, J., Prieto, C., Menéndez, R., de Andrés, A., 2013. Raman spectroscopy for the study of reduction mechanisms and optimization of conductivity in graphene oxide thin films. J. Mater. Chem. C **1**, 6905.

Dindi, A., Quang, D.V., Vega, L.F., Nashef, E., Abu-Zahra, M.R.M., 2019. Applications of fly ash for CO_2 capture, utilization, and storage. J. CO_2 Util. **29**, 82–102.

Dreyer, D. R., Park, S., Bielawski, C. W., & Ruoff, R. S. (2010). The chemistry of graphene oxide. Chemical society reviews, 39(1), 228-240.

Elgarahy, A.M., Elwakeel, K.Z., Mohammad, S.H., Elshoubaky, G.A., 2021. A critical review of biosorption of dyes, heavy metals and metalloids from wastewater as an efficient and green process. Cleaner Engineering and Technology **4**, 100209.

Emiru, T.F., Ayele, D.W., 2017. Controlled synthesis, characterization and reduction of graphene oxide: A convenient method for large scale production. Egypt. j. basic appl. sci. **4**, 74–79.

Fang, Q., Zhou, X., Deng, W., Liu, Z., 2016. Ordered self-assembly of amphipathic graphene nanosheets into three-dimensional layered architectures. Nanoscale **8**, 197–203.

Farivar, F., Lay Yap, P., Karunagaran, R.U., Losic, D., 2021. Thermogravimetric Analysis (TGA) of Graphene Materials: Effect of Particle Size of Graphene, Graphene Oxide and Graphite on Thermal Parameters. C **7**, 41.

Farjadian, F., Abbaspour, S., Sadatlu, M.A.A., Mirkiani, S., Ghasemi, A., Hoseini-Ghahfarokhi, M., Mozaffari, N., Karimi, M., Hamblin, M.R., 2020. Recent Developments in Graphene and Graphene Oxide: Properties, Synthesis, and Modifications: A Review. Chemistry Select **5**, 10200–10219.

Firdaus, R.M., Desforges, A., Rahman Mohamed, A., Vigolo, B., 2021. Progress in adsorption capacity of nanomaterials for carbon dioxide capture: A comparative study. J. Clean. Prod. **328**, 129553.

García-Bordejé, E., Víctor-Román, S., Sanahuja-Parejo, O., Benito, A.M., Maser, W.K., 2018. Control of the microstructure and surface chemistry of graphene aerogels *via* pH and time manipulation by a hydrothermal method. Nanoscale **10**, 3526–3539.

Gayle, A.J., Berquist, Z.J., Chen, Y., Hill, A.J., Hoffman, J.Y., Bielinski, A.R., Lenert, A., Dasgupta, N.P., 2021. Tunable Atomic Layer Deposition into Ultra-High-Aspect-Ratio (>60000:1) Aerogel Monoliths Enabled by Transport Modeling. Chem. Mater. **33**, 5572-5583.

Geim, A.K., Novoselov, K.S., 2010. The rise of graphene. Nat Mater. **6**, 183-91.

George, C., Littlewood, P., Stair, P.C., 2020. Understanding Pore Formation in ALD Alumina Overcoats. ACS Appl. Mater. Interfaces **12**, 20331–20343.

Ghorani-Azam, A., Riahi-Zanjani, B., Balali-Mood, M., 2016. Effects of air pollution on human health and practical measures for prevention in Iran. J Res Med Sci. **21**, 65.

Gregory, P., 1990. Classification of Dyes by Chemical Structure, in: Waring, D.R., Hallas, G. (Eds.), The Chemistry and Application of Dyes. Springer US, Boston, MA, pp. 17–47.

Guo, X., Qu, L., Tian, M., Zhu, S., Zhang, X., Tang, X., Sun, K., 2016. Chitosan/Graphene Oxide Composite as an Effective Adsorbent for Reactive Red Dye Removal. water environ. res. **88**, 579–588.

Hao, J., Huang, C., Wu, H., Qiu, Y., Gao, Q., Hu, Z., Kan, E., Zhang, L., 2015. A promising way to open an energy gap in bilayer graphene. Nanoscale **7**, 17096–17101.

Hasan, M.M.F., First, E.L., Boukouvala, F., Floudas, C.A., 2015. A multi-scale framework for CO_2 capture, utilization, and sequestration: CCUS and CCU. Computers & Chemical Engineering **81**, 2–21.

Hassan, M.M., Carr, C.M., 2018. A critical review on recent advancements of the removal of reactive dyes from dyehouse effluent by ion-exchange adsorbents. Chemosphere **209**, 201–219.

Hu, C., Liu, D., Xiao, Y., Dai, L., 2018. Functionalization of graphene materials by heteroatom-doping for energy conversion and storage. Prog. Nat. Sci.: Mater. Int. **28**, 121–132.

Jiang, L., Liu, Y., Liu, Shaobo, Hu, Xinjiang, Zeng, G., Hu, Xi, Liu, Simian, Liu, Shaoheng, Huang, B., Li, M., 2017. Fabrication of β-cyclodextrin/poly (l -glutamic acid) supported magnetic graphene oxide and its adsorption behavior for 17β-estradiol. J. Chem. Eng. **308**, 597–605.

Jing, J., Qian, X., Si, Y., Liu, G., Shi, C., 2022. Recent Advances in the Synthesis and Application of Three-Dimensional Graphene-Based Aerogels. Molecules **27**, 924.

Jo, H., Noh, H., Kaviany, M., Kim, J.M., Kim, M.H., Ahn, H.S., 2015. Tunable, self-assembled 3D reduced graphene oxide structures fabricated via boiling. Carbon **81**, 357–366.

Julbe, A., Drobek, M., Ayral, A., 2019. About the role of adsorption in inorganic and composite membranes. Curr. Opin. Chem. Eng. **24**, 88–97.

Kamil Kadhim Lawi, Z., Ameen Merza, F., Rabeea Banoon, S., AlSaady, M.A.A.J., AlAbboodi, A., 2021. Mechanisms of Antioxidant Actions and their Role in many Human Diseases: A Review. Journal of Chemical Health Risks 45-57.

Karthik, V., Selvakumar, P., Senthil Kumar, P., Vo, D.-V.N., Gokulakrishnan, M., Keerthana, P., Tamil Elakkiya, V., Rajeswari, R., 2021. Graphene-based materials for environmental applications: a review. Environ. Chem. Lett. **19**, 3631–3644.

Khalili, D., 2016. Graphene oxide: a promising carbocatalyst for the regioselective thiocyanation of aromatic amines, phenols, anisols and enolizable ketones by hydrogen peroxide/KSCN in water. New J. Chem. **40**, 2547–2553.

Kim, J., Lee, H., Vo, H.T., Lee, G., Kim, N., Jang, S., Joo, J.B., 2020. Bead-Shaped Mesoporous Alumina Adsorbents for Adsorption of Ammonia. Materials **13**, 1375.

King, A.A.K., Davies, B.R., Noorbehesht, N., Newman, P., Church, T.L., Harris, A.T., Razal, J.M., Minett, A.I., 2016. A New Raman Metric for the Characterisation of Graphene oxide and its Derivatives. Sci. Rep. **6**, 19491.

Kruk, M., Jaroniec, M., 2001. Gas Adsorption Characterization of Ordered Organic−Inorganic Nanocomposite Materials. Chem. Mater. **13**, 3169–3183.

Kumar, R., Sahoo, S., Joanni, E., Singh, R.K., Tan, W.K., Kar, K.K., Matsuda, A., 2019. Recent progress in the synthesis of graphene and derived materials for next generation electrodes of high-performance lithium ion batteries. Prog. Energy Combust. Sci. **75**, 100786.

Lahijani, P., Zainal, Z.A., Mohammadi, M., Mohamed, A.R., 2015. Conversion of the greenhouse gas CO_2 to the fuel gas CO via the Boudouard reaction: A review. Renew. Sust. Energ. Rev. **41**, 615–632.

Lau, L.C., Tan, K.T., Lee, K.T., Mohamed, A.R., 2009. A comparative study on the energy policies in Japan and Malaysia in fulfilling their nations' obligations towards the Kyoto Protocol. Energy Policy **37**, 4771–4778.

Laxmi, V., Kaushik, G., 2020. Toxicity of Hexavalent Chromium in Environment, Health Threats, and Its Bioremediation and Detoxification from Tannery Wastewater for Environmental Safety, in: Saxena, G., Bharagava, R.N. (Eds.), Bioremediation of Industrial Waste for Environmental Safety. Springer Singapore, Singapore, pp. 223–243.

Le Quéré, C., Moriarty, R., Andrew, R.M., Peters, G.P., Ciais, P., Friedlingstein, P., Jones, S.D., Sitch, S., Tans, P., Arneth, A., Boden, T.A., Bopp, L.,

Bozec, Y., Canadell, J.G., Chini, L.P., Chevallier, F., Cosca, C.E., Harris, I., Hoppema, M., Houghton, R.A., House, J.I., Jain, A.K., Johannessen, T., Kato, E., Keeling, R.F., Kitidis, V., Klein Goldewijk, K., Koven, C., Landa, C.S., Landschützer, P., Lenton, A., Lima, I.D., Marland, G., Mathis, J.T., Metzl, N., Nojiri, Y., Olsen, A., Ono, T., Peng, S., Peters, W., Pfeil, B., Poulter, B., Raupach, M.R., Regnier, P., Rödenbeck, C., Saito, S., Salisbury, J.E., Schuster, U., Schwinger, J., Séférian, R., Segschneider, J., Steinhoff, T., Stocker, B.D., Sutton, A.J., Takahashi, T., Tilbrook, B., van der Werf, G.R., Viovy, N., Wang, Y.-P., Wanninkhof, R., Wiltshire, A., Zeng, N., 2015. Global carbon budget 2014. Earth Syst. Sci. Data **7**, 47–85.

Lee, S.H., Kim, H.W., Hwang, J.O., Lee, W.J., Kwon, J., Bielawski, C.W., Ruoff, R.S., Kim, S.O., 2010. Three-Dimensional Self-Assembly of Graphene Oxide Platelets into Mechanically Flexible Macroporous Carbon Films. Angew. Chem. Int. Ed. **49**, 10084–10088.

Li, W., Gao, S., Wu, L., Qiu, S., Guo, Y., Geng, X., Chen, M., Liao, S., Zhu, C., Gong, Y., Long, M., Xu, J., Wei, X., Sun, M., Liu, L., 2013. High-Density Three-Dimension Graphene Macroscopic Objects for High-Capacity Removal of Heavy Metal Ions. Sci. Rep. **3**, 2125.

Li, W., Yang, H., Jiang, X., Liu, Q., 2016. Highly selective CO_2 adsorption of ZnO based N-doped reduced graphene oxide porous nanomaterial. Appl. Surf. Sci. **360**, 143–147.

Li, Z., Lin, J., Li, B., Yu, C., Wang, H., Li, Q., 2021. Construction of heteroatom-doped and three-dimensional graphene materials for the applications in supercapacitors: A review. Journal of Energy Storage **44**, 103437.

Lillo-Rodenas, M.A., Cazorla-Amoros, D., Linares-Solano, A., 2003. Understanding chemical reactions between carbons and NaOH and KOH An insight into the chemical activation mechanism. Carbon **41**, 267-275.

Lin, D., Liu, Y., Liang, Z., Lee, H.-W., Sun, J., Wang, H., Yan, K., Xie, J., Cui, Y., 2016. Layered reduced graphene oxide with nanoscale interlayer gaps as a stable host for lithium metal anodes. Nature Nanotech. **11**, 626–632.

Lin, Y., Liu, F., Casano, G., Bhavsar, R., Kinloch, I.A., Derby, B., 2016. Pristine Graphene Aerogels by Room-Temperature Freeze Gelation. Adv. Mater. **28**, 7993–8000.

Lin, Z., Karthik, P., Hada, M., Nishikawa, T., Hayashi, Y., 2017. Simple Technique of Exfoliation and Dispersion of Multilayer Graphene from Natural Graphite by Ozone-Assisted Sonication. Nanomaterials **7**, 125.

Litefti, K., Freire, M.S., Stitou, M., González-Álvarez, J., 2019. Adsorption of an anionic dye (Congo red) from aqueous solutions by pine bark. Sci. Rep. **9**, 16530.

Liu, B., Yao, S., Liu, X., Li, X., Krishna, R., Li, G., Huo, Q., Liu, Y., 2017. Two Analogous Polyhedron-Based MOFs with High Density of Lewis Basic Sites and Open Metal Sites: Significant CO_2 Capture and Gas Selectivity Performance. ACS Appl. Mater. Interfaces **9**, 32820–32828.

Liu, H., Qiu, H., 2020. Recent advances of 3D graphene-based adsorbents for sample preparation of water pollutants: A review. J. Chem. Eng. **393**, 124691.

Liu, S., Peng, W., Sun, H., Wang, S., 2013. Physical and chemical activation of reduced graphene oxide for enhanced adsorption and catalytic oxidation. Nanoscale, **6**, 766-771.

Liu, Y., Guo, C., Zhang, D., Shang, Y., 2014. One-pot synthesis of 3D framework graphene via electrochemical method. Materials Letters **115**, 25–28.

Liu, Z., Lu, Y., Wang, P., Wang, T., Liu, S., Johnson, A.C., Sweetman, A.J., Baninla, Y., 2017. Pollution pathways and release estimation of perfluorooctane sulfonate (PFOS) and perfluorooctanoic acid (PFOA) in central and eastern China. Sci. Total Environ. **580**, 1247–1256.

Long, D., Li, W., Ling, L., Miyawaki, J., Mochida, I., Yoon, S.-H., 2010. Preparation of Nitrogen-Doped Graphene Sheets by a Combined Chemical and Hydrothermal Reduction of Graphene Oxide. Langmuir **26**, 16096-16102.

Lyu, J., Kudiiarov, V., Lider, A., 2020. An Overview of the Recent Progress in Modifications of Carbon Nanotubes for Hydrogen Adsorption. Nanomaterials **10**, 255.

Ma, Y., Jang, H., Kim, S.J., Pang, C., Chae, H., 2015. Copper-Assisted Direct Growth of Vertical Graphene Nanosheets on Glass Substrates by Low-Temperature Plasma-Enhanced Chemical Vapour Deposition Process. Nanoscale Res. Lett. **10**, 308.

Madejski, P., Chmiel, K., Subramanian, N., Kuś, T., 2022. Methods and Techniques for CO_2 Capture: Review of Potential Solutions and Applications in Modern Energy Technologies. Energies **15**, 887.

Magne, T.M., de Oliveira Vieira, T., Alencar, L.M.R., Junior, F.F.M., Gemini-Piperni, S., Carneiro, S.V., Fechine, L.M.U.D., Freire, R.M., Golokhvast, K., Metrangolo, P., Fechine, P.B.A., Santos-Oliveira, R., 2022. Graphene and its derivatives: understanding the main chemical and medicinal chemistry roles for biomedical applications. J Nanostruct. Chem. **12**, 693–727.

Mahmoodi, N.M., Maroofi, S.M., Mazarji, M., Nabi-Bidhendi, G., 2017. Preparation of Modified Reduced Graphene Oxide nanosheet with Cationic Surfactant and its Dye Adsorption Ability from Colored Wastewater. J Surfact. Deterg. **20**, 1085–1093.

Mahmoudian, L., Rashidi, A., Dehghani, H., Rahighi, R., 2016. Single-step scalable synthesis of three-dimensional highly porous graphene with favorable methane adsorption. J. Chem. Eng. **304**, 784–792.

Malygin, A.A., Drozd, V.E., Malkov, A.A., Smirnov, V.M., 2015. From V. B. Aleskovskii's "Framework" Hypothesis to the Method of Molecular Layering/Atomic Layer Deposition. Chem. Vap. Deposition **21**, 216–240.

Manisalidis, I., Stavropoulou, E., Stavropoulos, A., Bezirtzoglou, E., 2020. Environmental and Health Impacts of Air Pollution: A Review. Front. Public Health **8**, 14.

Manzoor, J., Sharma, M., 2020. Impact of Textile Dyes on Human Health and Environment:, in: Wani, K.A., Jangid, N.K., Bhat, A.R. (Eds.), Advances in Human Services and Public Health. IGI Global, pp. 162–169.

Mohd Firdaus, R., Berrada, N., Desforges, A., Mohamed, A.R., Vigolo, B., 2020. From 2D Graphene Nanosheets to 3D Graphene-based Macrostructures. Chem. Asian J. **15**, 2902–2924.

Mortazavi, B., 2017. Ultra high stiffness and thermal conductivity of graphene like C_3N. Carbon **118**, 25–34.

Mukhopadhyay, S., Batra, S., 2019. Applications of Sodium Nitrite in Organic Synthesis: Applications of Sodium Nitrite in Organic Synthesis. Eur. J. Org. Chem. **2019**, 6424–6451.

Munnik, P., de Jongh, P.E., de Jong, K.P., 2015. Recent Developments in the Synthesis of Supported Catalysts. Chem. Rev. **115**, 6687–6718.

Orts, F., del Río, A.I., Molina, J., Bonastre, J., Cases, F., 2018. Electrochemical treatment of real textile wastewater: Trichromy Procion HEXL®. Journal of Electroanalytical Chemistry **808**, 387–394.

Papageorgiou, D.G., Kinloch, I.A., Young, R.J., 2015. Graphene/elastomer nanocomposites. Carbon **95**, 460–484.

Park, T., Kim, Hoijoon, Leem, M., Ahn, W., Choi, S., Kim, J., Uh, J., Kwon, K., Jeong, S.-J., Park, S., Kim, Y., Kim, Hyoungsub, 2017. Atomic layer deposition of Al_2O_3 on MoS_2 , WS_2 , WSe_2 , and h-BN: surface coverage and adsorption energy. RSC Adv. **7**, 884–889.

Politakos, N., Barbarin, I., Cordero-Lanzac, T., Gonzalez, A., Zangi, R., Tomovska, R., 2020. Reduced Graphene Oxide/Polymer Monolithic Materials for Selective CO_2 Capture. Polymers **12**, 936.

Pruna, A., Cárcel, A.C., Benedito, A., Giménez, E., 2019. Effect of synthesis conditions on CO_2 capture of ethylenediamine-modified graphene aerogels. Appl. Surf. Sci. **487**, 228–235.

Purba, A., Widana, I.D.K.K., Hadi Sumantri, S., Kurniadi, A., Mayori, E., 2022. Community Resilience to Disaster and Climate Change to Support Sustainable Development in and After The Covid-19 Pandemic. TSSJ **33**, 479–491.

Qiao, H., Huang, Z., Liu, S., Tao, Y., Zhou, H., Li, M., Qi, X., 2019. Novel Mixed-Dimensional Photocatalysts Based on 3D Graphene Aerogel Embedded with TiO_2 /MoS_2 Hybrid. J. Phys. Chem. C **123**, 10949–10955.

Rathi, B.S., Kumar, P.S., 2021. Application of adsorption process for effective removal of emerging contaminants from water and wastewater. Environmental Pollution **280**, 116995.

Raymundo-Piñero, E., Azaïs, P., Cacciaguerra, T., Cazorla-Amorós, D., Linares-Solano, A., Béguin, F., 2005. KOH and NaOH activation mechanisms of multiwalled carbon nanotubes with different structural organisation. Carbon **43**, 786–795.

Robinson, T., Marchant, R., Nigam, P., 2001. Remediation of dyes in textile effluent: a critical review on current treatment technologies with a proposed alternative. Bioresour. Technol. **77**, 247-255.

Rodríguez-García, S., Santiago, R., López-Díaz, D., Merchán, M.D., Velázquez, M.M., Fierro, J.L.G., Palomar, J., 2019. Role of the Structure of Graphene Oxide Sheets on the CO_2 Adsorption Properties of Nanocomposites Based on Graphene Oxide and Polyaniline or Fe_3O_4 -Nanoparticles. ACS Sustain. Chem. Eng. **7**, 12464-12473.

Rodríguez-Mata, V., González-Domínguez, J.M., Benito, A.M., Maser, W.K., García-Bordejé, E., 2019. Reduced Graphene Oxide Aerogels with Controlled Continuous Microchannels for Environmental Remediation. ACS Appl. Nano Mater. **2**, 1210–1222.

Rout, D.R., Jena, H.M., 2021. Removal of malachite green dye from aqueous solution using reduced graphene oxide as an adsorbent. Materials Today: Proceedings **47**, 1173–1182.

Sahoo, T.R., Prelot, B., 2020. Adsorption processes for the removal of contaminants from wastewater, in: Nanomaterials for the Detection and Removal of Wastewater Pollutants. Elsevier, pp. 161–222.

Saleem, M.R., Ali, R., Khan, M.B., Honkanen, S., Turunen, J., 2014. Impact of Atomic Layer Deposition to Nanophotonic Structures and Devices. Frontiers in Materials **1**, 18.

Samadaei, F., Salami-Kalajahi, M., Roghani-Mamaqani, H., Banaei, M., 2015. A structural study on ethylenediamine- and poly(amidoamine)-functionalized graphene oxide: simultaneous reduction, functionalization, and formation of 3D structure. RSC Adv. **5**, 71835–71843.

Samsami, S., Mohamadizaniani, M., Sarrafzadeh, M.-H., Rene, E.R., Firoozbahr, M., 2020. Recent advances in the treatment of dye-containing wastewater from textile industries: Overview and perspectives. Process Saf. Environ. Prot. **143**, 138–163.

Sandhya, M., Ramasamy, D., Sudhakar, K., Kadirgama, K., Samykano, M., Harun, W.S.W., Najafi, G., Mofijur, M., Mazlan, M., 2021. A systematic review on graphene-based nanofluids application in renewable energy systems: Preparation, characterization, and thermophysical properties. Sustain. Energy Technol. Assess. **44**, 101058.

Santhiran, A., Iyngaran, P., Abiman, P., Kuganathan, N., 2021. Graphene Synthesis and Its Recent Advances in Applications—A Review. C **7**, 76.

Saputra, N.A., Darmawan, S., Efiyanti, L., Hendra, D., Wibowo, S., Santoso, A., Djarwanto, Gusmailina, Komarayati, S., Indrawan, D.A., Yuniawati, Nawawi, D.S., Maddu, A., Pari, G., Syafii, W., 2022. A Novel Mesoporous Activated Carbon Derived from Calliandra calothyrsus via Physical Activation: Saturation and Superheated. Energies **15**, 6675.

Saravanan, A., Kumar, P.S., Srinivasan, S., Jeevanantham, S., Vishnu, M., Amith, K.V., Sruthi, R., Saravanan, R., Vo, D.-V.N., 2022. Insights on synthesis and applications of graphene-based materials in wastewater treatment: A review. Chemosphere **298**, 134284.

Saravanan, A., Senthil Kumar, P., Jeevanantham, S., Karishma, S., Tajsabreen, B., Yaashikaa, P.R., Reshma, B., 2021. Effective water/wastewater treatment methodologies for toxic pollutants removal: Processes and applications towards sustainable development. Chemosphere **280**, 130595.

Saxena, R., Saxena, M., & Lochab, A. (2020). Recent progress in nanomaterials for adsorptive removal of organic contaminants from wastewater. Chemistry Select, **5**, 335-353.

Seah, G.L., Wang, L., Tan, L.F., Tipjanrawee, C., Sasangka, W.A., Usadi, A.K., McConnachie, J.M., Tan, K.W., 2021. Ordered Mesoporous Alumina with Tunable Morphologies and Pore Sizes for CO_2 Capture and Dye Separation. ACS Appl. Mater. Interfaces **13**, 36117–36129.

Shahdeo, D., Roberts, A., Abbineni, N., Gandhi, S., 2020. Graphene based sensors, in: Comprehensive Analytical Chemistry. Elsevier, pp. 175–199.

Sharma, B., Dangi, A.K., Shukla, P., 2018. Contemporary enzyme-based technologies for bioremediation: A review. J. Environ. Manage. **210**, 10–22.

Shen, Y., Fang, Q., Chen, B., 2015. Environmental Applications of Three-Dimensional Graphene-Based Macrostructures: Adsorption, Transformation, and Detection. Environ. Sci. Technol. **49**, 67–84.

Shen, Y., Maurizi, L., Magnacca, G., Boffa, V., Yue, Y., 2020. Tuning Porosity of Reduced Graphene Oxide Membrane Materials by Alkali Activation. Nanomaterials **10**, 2093.

Shen, Y., Zhu, X., Chen, B., 2016. Size effects of graphene oxide nanosheets on the construction of three-dimensional graphene-based macrostructures as adsorbents. J. Mater. Chem. A **4**, 12106–12118.

Shi, L., Chen, K., Du, R., Bachmatiuk, A., Rümmeli, M.H., Xie, K., Huang, Y., Zhang, Y., Liu, Z., 2016. Scalable Seashell-Based Chemical Vapor Deposition Growth of Three-Dimensional Graphene Foams for Oil–Water Separation. J. Am. Chem. Soc. **138**, 6360–6363.

Shulga, Y.M., Kabachkov, E.N., Korepanov, V.I., Khodos, I.I., Kovalev, D.Y., Melezhik, A.V., Tkachev, A.G., Gutsev, G.L., 2021. The Concentration of C(sp^3) Atoms and Properties of an Activated Carbon with over 3000 m^2/g BET Surface Area. Nanomaterials **11**, 1324.

Singh, D.K., Kumar, V., Mohan, S., Hasan, S.H., 2017. Polylysine Functionalized Graphene Aerogel for the Enhanced Removal of Cr(VI) through Adsorption: Kinetic, Isotherm, and Thermodynamic Modeling of the Process. J. Chem. Eng. Data **62**, 1732–1742.

Singh, J., Bhunia, H., Basu, S., 2019. Synthesis of sulphur enriched carbon monoliths for dynamic CO_2 capture. J. Chem. Eng. **374**, 1–9.

Singh, J., Bhunia, H., Basu, S., 2018. Synthesis of porous carbon monolith adsorbents for carbon dioxide capture: Breakthrough adsorption study. J. Taiwan Inst. Chem. Eng. **89**, 140–150.

Slama, H.B., Chenari Bouket, A., Pourhassan, Z., Alenezi, F.N., Silini, A., Cherif-Silini, H., Oszako, T., Luptakova, L., Golińska, P., Belbahri, L., 2021a. Diversity of Synthetic Dyes from Textile Industries, Discharge Impacts and Treatment Methods. Appl. Sci. **11**, 6255.

Slama, H.B., Chenari Bouket, A., Pourhassan, Z., Alenezi, F.N., Silini, A., Cherif-Silini, H., Oszako, T., Luptakova, L., Golińska, P., Belbahri, L., 2021b. Diversity of Synthetic Dyes from Textile Industries, Discharge Impacts and Treatment Methods. Appl. Sci. **11**, 6255.

Smith, B.R., Conger, M.J., McMullen, J.S., Neubert, M.J., 2019. Why believe? The promise of research on the role of religion in entrepreneurial action. Journal of Business Venturing Insights **11**, e00119.

Smith, T.M., Reynolds, R.W., Peterson, T.C., Lawrimore, J., 2008. Improvements to NOAA's Historical Merged Land–Ocean Surface Temperature Analysis (1880–2006). Journal of Climate **21**, 2283–2296.

Soffian, M.S., Abdul Halim, F.Z., Aziz, F., A. Rahman, M., Mohamed Amin, M.A., Awang Chee, D.N., 2022. Carbon-based material derived from

biomass waste for wastewater treatment. Environmental Advances **9**, 100259.

Sudeep, P.M., Narayanan, T.N., Ganesan, A., Shaijumon, M.M., Yang, H., Ozden, S., Patra, P.K., Pasquali, M., Vajtai, R., Ganguli, S., Roy, A.K., Anantharaman, M.R., Ajayan, P.M., 2013. Covalently Interconnected Three-Dimensional Graphene Oxide Solids. ACS Nano **7**, 7034–7040.

Sui, Z.-Y., Cui, Y., Zhu, J.-H., Han, B.-H., 2013. Preparation of Three-Dimensional Graphene Oxide–Polyethylenimine Porous Materials as Dye and Gas Adsorbents. ACS Appl. Mater. Interfaces **5**, 9172–9179.

Sui, Z.-Y., Han, B.-H., 2015. Effect of surface chemistry and textural properties on carbon dioxide uptake in hydrothermally reduced graphene oxide. Carbon **82**, 590–598.

Sui, Z.-Y., Meng, Y.-N., Xiao, P.-W., Zhao, Z.-Q., Wei, Z.-X., Han, B.-H., 2015. Nitrogen-Doped Graphene Aerogels as Efficient Supercapacitor Electrodes and Gas Adsorbents. ACS Appl. Mater. Interfaces **7**, 1431–1438.

Sun, Y.-N., Sui, Z.-Y., Li, X., Xiao, P.-W., Wei, Z.-X., Han, B.-H., 2018. Nitrogen-Doped Porous Carbons Derived from Polypyrrole-Based Aerogels for Gas Uptake and Supercapacitors. ACS Appl. Nano Mater. **1**, 609–616.

Sun, Z., Fang, S., Hu, Y.H., 2020. 3D Graphene Materials: From Understanding to Design and Synthesis Control. Chem. Rev. **120**, 10336–10453.

Thalgaspitiya, W.R.K., Kankanam Kapuge, T., He, J., Deljoo, B., Meguerdichian, A.G., Aindow, M., Suib, S.L., 2020. Multifunctional transition metal doped titanium dioxide reduced graphene oxide composites as highly efficient adsorbents and photocatalysts. Microporous Mesoporous Mater. **307**, 110521.

Tiwari, J.N., Mahesh, K., Le, N.H., Kemp, K.C., Timilsina, R., Tiwari, R.N., Kim, K.S., 2013. Reduced graphene oxide-based hydrogels for the efficient capture of dye pollutants from aqueous solutions. Carbon **56**, 173–182.

Tiwari, S.K., Kumar, V., Huczko, A., Oraon, R., Adhikari, A.D., Nayak, G.C., 2016. Magical Allotropes of Carbon: Prospects and Applications. Crit. Rev. Solid State Mater. Sci. **41,** 257–317.

Tiwari, S.K., Mishra, R.K., Ha, S.K., Huczko, A., 2018. Evolution of Graphene Oxide and Graphene: From Imagination to Industrialization. Chem. Nano Mat. **4**, 598-620.

Tjong, S.C., 2014. Synthesis and Structural–Mechanical Property Characteristics of Graphene–Polymer Nanocomposites, in: Nanocrystalline Materials. Elsevier, pp. 335–375.

Tran, H.N., You, S.-J., Chao, H.-P., 2016. Thermodynamic parameters of cadmium adsorption onto orange peel calculated from various methods: A comparison study. J. Environ. Chem. Eng. **4**, 2671–2682.

Van Langenhove, L., Paul, R., 2015. Insect repellent finishes for textiles, in: Functional Finishes for Textiles. Elsevier, pp. 333–360.

Velusamy, S., Roy, A., Sundaram, S., Kumar Mallick, T., 2021. A Review on Heavy Metal Ions and Containing Dyes Removal Through Graphene Oxide-Based Adsorption Strategies for Textile Wastewater Treatment. Chem. Rec. **21**, 1570–1610.

Vo, H.T., Kim, J., Kim, N.Y., Lee, J.-K., Joo, J.B., 2020. Effect of pore texture property of mesoporous alumina on adsorption performance of ammonia gas. J. Ind. Eng. Chem. **91**, 129–138.

Walker, W.S., Gorelik, S.R., Cook-Patton, S.C., Baccini, A., Farina, M.K., Solvik, K.K., Ellis, P.W., Sanderman, J., Houghton, R.A., Leavitt, S.M., Schwalm, C.R., Griscom, B.W., 2022. The global potential for increased storage of carbon on land. Proc. Natl. Acad. Sci. U.S.A. **119**, e2111312119.

Wang, D., Li, Y., Zhao, Y., Guo, Q., Yang, S., Ding, G., Mei, Y., Huang, G., 2019. Cycling-Induced Capacity Increase of Graphene Aerogel/ZnO Nanomembrane Composite Anode Fabricated by Atomic Layer Deposition. Nanoscale Res. Lett. **14**, 69.

Wang, H., Mi, X., Li, Y., Zhan, S., 2020. 3D Graphene-Based Macrostructures for Water Treatment. Adv. Mater. **32**, 1806843.

Wang, R., Jayakumar, A., Xu, C., Lee, J.-M., 2016a. $Ni(OH)_2$ Nanoflowers/Graphene Hydrogels: A New Assembly for Supercapacitors. ACS Sustainable Chem. Eng. **4**, 3736–3742.

Wang, R., Xu, C., Lee, J.-M., 2016b. High performance asymmetric supercapacitors : New NiOOH nanosheet/graphene hydrogels and pure graphene hydrogels. Nano Energy **19**, 210–221.

Wang, X., Liu, Q., Liu, J., Chen, R., Zhang, H., Li, R., Li, Z., Wang, J., 2017. 3D self-assembly polyethyleneimine modified graphene oxide hydrogel for the extraction of uranium from aqueous solution. Appl. Surf. Sci. **426**, 1063–1074.

Wang, Y., Wang, J., Ma, C., Qiao, W., Ling, L., 2019. Fabrication of hierarchical carbon nanosheet-based networks for physical and chemical adsorption of CO_2. J. Colloid Interface Sci. **534**, 72–80.

Wigley, T.M.L., 2018. The Paris warming targets: emissions requirements and sea level consequences. Climatic Change **147**, 31–45.

Wilson, C.A., Grubbs, R.K., George, S.M., 2005. Nucleation and Growth during Al_2O_3 Atomic Layer Deposition on Polymers. Chem. Mater. **17**, 5625–5634.

Wu, K., Ye, Q., Wang, L., Meng, F., Dai, H., 2022. Mesoporous alumina-supported layered double hydroxides for efficient CO_2 capture. J. CO_2 Util. **60**, 101982.

Wu, S., Chen, G., Kim, N.Y., Ni, K., Zeng, W., Zhao, Y., Tao, Z., Ji, H., Lee, Z., Zhu, Y., 2016. Creating Pores on Graphene Platelets by Low-Temperature KOH Activation for Enhanced Electrochemical Performance. Small **12**, 2376–2384.

Wu, Z.-S., Yang, S., Sun, Y., Parvez, K., Feng, X., Müllen, K., 2012. 3D Nitrogen-Doped Graphene Aerogel-Supported Fe_3O_4 Nanoparticles as Efficient Electrocatalysts for the Oxygen Reduction Reaction. J. Am. Chem. Soc. **134**, 9082–9085.

Xia, K., 2014. Hierarchical porous graphene-based carbons prepared by carbon dioxide activation and their gas adsorption properties. Int. J. Hydrog. Energy **39**, 11047-11054.

Xiao, J., Wang, Y., Zhang, T.C., Yuan, S., 2021a. rGO/N-porous carbon composites for enhanced CO_2 capture and energy storage performances. J. Alloys Compd. **857**, 157534.

Xiao, J., Wang, Y., Zhang, T.C., Yuan, S., 2021b. N,S-containing polycondensate-derived porous carbon materials for superior CO_2 adsorption and supercapacitor. Appl. Surf. Sci. **562**, 150128.

Xiao, L., Wu, D., Han, S., Huang, Y., Li, S., He, M., Zhang, F., Feng, X., 2013. Self-Assembled Fe_2O_3 / Graphene Aerogel with High Lithium Storage Performance. ACS Appl. Mater. Interfaces **5**, 3764–3769.

Xu, Y., Sheng, K., Li, C., Shi, G., 2010a. Self-Assembled Graphene Hydrogel *via* a One-Step Hydrothermal Process. ACS Nano **4**, 4324–4330.

Xu, Y., Shi, G., Duan, X., 2015. Self-Assembled Three-Dimensional Graphene Macrostructures: Synthesis and Applications in Supercapacitors. Acc. Chem. Res. **48**, 1666–1675.

Xu, Y., Wu, Q., Sun, Y., Bai, H., Shi, G., 2010b. Three-Dimensional Self-Assembly of Graphene Oxide and DNA into Multifunctional Hydrogels. ACS Nano **4**, 7358–7362.

Yan, Y., Nashath, F.Z., Chen, S., Manickam, S., Lim, S.S., Zhao, H., Lester, E., Wu, T., Pang, C.H., 2020. Synthesis of graphene: Potential carbon precursors and approaches. Nanotechnol. Rev. **9**, 1284–1314.

Yang, F., Zhu, J., Zou, X., Pang, X., Yang, R., Chen, S., Fang, Y., Shao, T., Luo, X., Zhang, L., 2018. Three-dimensional TiO_2 / SiO_2 composite aerogel films via atomic layer deposition with enhanced H_2S gas sensing performance. Ceramics International **44**, 1078–1085.

Yang, J., Liu, X., Song, K., Li, X., Wang, D., 2021. Effectively removing tetracycline from water by nanoarchitectured carbons derived from CO_2: Structure and surface chemistry influence. Environ. Res. **195**, 110883.

Yang, J., Wang, Y., Wang, J., Chan-Park, M.B., 2015. Reducing graphene oxide with a modified Birch reaction. RSC Adv. **5**, 11124–11127.

Yang, Y., Liu, R., Wu, J., Jiang, X., Cao, P., Hu, X., Pan, T., Qiu, C., Yang, J., Song, Y., Wu, D., Su, Y., 2015. Bottom-up Fabrication of Graphene on Silicon/Silica Substrate via a Facile Soft-hard Template Approach. Sci. Rep. **5**, 13480.

Yang, Y., Liu, T., Zhu, X., Zhang, F., Ye, D., Liao, Q., Li, Y., 2016. Boosting Power Density of Microbial Fuel Cells with 3D Nitrogen-Doped Graphene Aerogel Electrode. Adv. Sci. **3**, 1600097.

Ye, Y., Mart, L.V., Merch, M.D., 2022. Optimizing the Properties of Hybrids Based on Graphene Oxide for Carbon Dioxide Capture. Ind. Eng. Chem. Res. **61**, 1332-1343.

Yin, S., Niu, Z., Chen, X., 2012. Assembly of Graphene Sheets into 3D Macroscopic Structures. Small **8**, 2458–2463.

Yoro, K.O., Daramola, M.O., 2020. CO_2 emission sources, greenhouse gases, and the global warming effect, in: Advances in Carbon Capture. Elsevier, pp. 3–28.

Yousefi, N., Lu, X., Elimelech, M., Tufenkji, N., 2019. Environmental performance of graphene-based 3D macrostructures. Nature Nanotech. **14**, 107–119.

Yu, M., Wang, A., Wang, Y., Li, C., Shi, G., 2014. An alumina stabilized ZnO–graphene anode for lithium-ion batteries via atomic layer deposition. Nanoscale **6**, 11419–11424.

Yuan, Z.-Y., Su, B.-L., 2006. Insights into hierarchically meso–macroporous structured materials. J. Mater. Chem. **16**, 663–677.

Zeng, J., Ji, X., Ma, Y., Zhang, Z., Wang, S., Ren, Z., Zhi, C., Yu, J., 2018. 3D Graphene Fibers Grown by Thermal Chemical Vapor Deposition. Adv. Mater. **30**, 1705380.

Zhang, L., Zhang, F., Yang, X., Long, G., Wu, Y., Zhang, T., Leng, K., Huang, Y., Ma, Y., Yu, A., Chen, Y., 2013. Porous 3D graphene-based bulk materials with exceptional high surface area and excellent conductivity for supercapacitors. Sci Rep. **3**, 1408.

Zhang, S., Liu, G., Gao, Y., Yue, Q., Gao, B., Xu, X., Kong, W., Li, N., Jiang, W., 2019. A facile approach to ultralight and recyclable 3D self-assembled copolymer/graphene aerogels for efficient oil/water separation. Sci. Total Environ. **694**, 133671.

Zhang, X., Liu, D., Yang, L., Zhou, L., You, T., 2015. Self-assembled three-dimensional graphene-based materials for dye adsorption and catalysis. J. Mater. Chem. A **3**, 10031–10037.

Zhang, Y., Wan, Q., Yang, N., 2019. Recent Advances of Porous Graphene: Synthesis, Functionalization, and Electrochemical Applications. Small **15**, 1903780.

Zhao, J., Jiang, Y., Fan, H., Liu, M., Zhuo, O., Wang, X., Wu, Q., Yang, L., Ma, Y., Hu, Z., 2017. Porous 3D Few-Layer Graphene-like Carbon for Ultrahigh-Power Supercapacitors with Well-Defined Structure-Performance Relationship. Adv. Mater. **29**, 1604569.

Zhou, C., Xi, Z., Stacchiola, D.J., Liu, M., 2022. Application of ultrathin TiO_2 layers in solar energy conversion devices. Energy Sci. Eng. **10**, 1614–1629.

Zhou, K., Wu, J., Liu, H., 2021. Spatio-temporal estimation of the anthropogenic environmental stress intensity in the Three-River-Source National Park region, China. J. Clean. Prod. **318**, 128476.

Zhou, L., Yang, Z., Yang, J., Wu, Y., Wei, D., 2017. Facile syntheses of 3-dimension graphene aerogel and nanowalls with high specific surface areas. Chem. Phys. Lett. **677**, 7–12.

Zhou, Y., Bao, Q., Tang, L.A.L., Zhong, Y., Loh, K.P., 2009. Hydrothermal Dehydration for the "Green" Reduction of Exfoliated Graphene Oxide to Graphene and Demonstration of Tunable Optical Limiting Properties. Chem. Mater. **21**, 2950–2956.

Zhu, Y., Li, L., Zhang, C., Casillas, G., Sun, Z., Yan, Z., Ruan, G., Peng, Z., Raji, A.-R.O., Kittrell, C., Hauge, R.H., Tour, J.M., 2012. A seamless three-dimensional carbon nanotube graphene hybrid material. Nat. Commun. **3**, 1225.

Zourou, A., Ntziouni, A., Adamopoulos, N., Roman, T., Zhang, F., Terrones, M., Kordatos, K., 2022. Graphene oxide-$CuFe_2O_4$ nanohybrid material as an adsorbent of Congo red dye. Carbon Trends **7**, 100147.

Zubbri, N.A., Mohamed, A.R., Lahijani, P., Mohammadi, M., 2021. Low temperature CO_2 capture on biomass-derived KOH-activated hydrochar established through hydrothermal carbonization with water-soaking pre-treatment. J. Environ. Chem. Eng. **9**, 105074.

APPENDICES

Appendix A

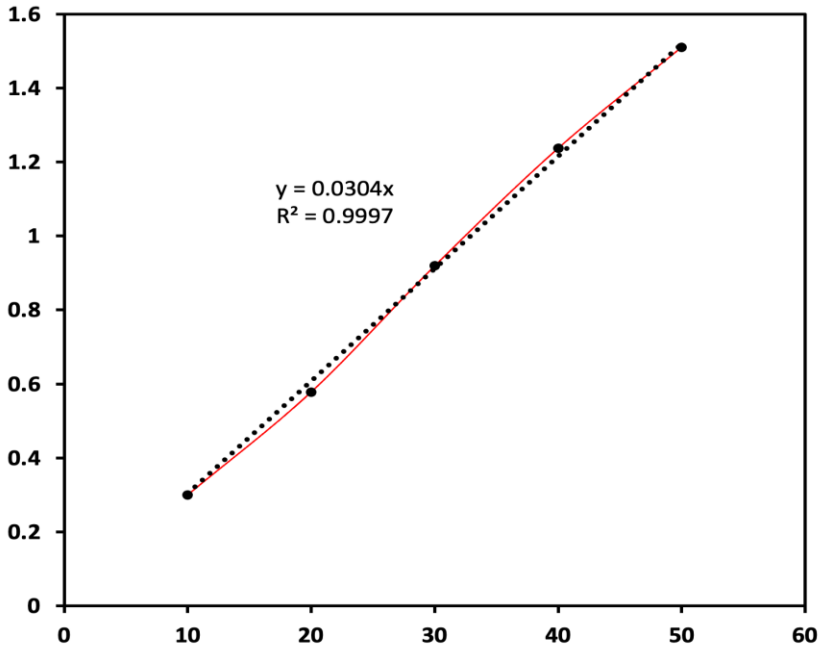

LIST OF PUBLICATION

1. Mohd Firdaus, R., Berrada, N., Desforges, A., Mohamed, A. R., & Vigolo, B. (2020). From 2D graphene nanosheets to 3D graphene-based macrostructures. Chemistry–An Asian Journal, 15(19), 2902-2924. (Published).
2. Firdaus, R. M., Desforges, A., Emo, M., Mohamed, A. R., & Vigolo, B. (2021). Physical and chemical activation of graphene-derived porous nanomaterials for post-combustion carbon dioxide capture. Nanomaterials, 11(9), 2419. (Published).
3. Firdaus, R. M., Desforges, A., Mohamed, A. R., & Vigolo, B. (2021). Progress in adsorption capacity of nanomaterials for carbon dioxide capture: A comparative study. Journal of Cleaner Production, 328, 129553. (Publish).
4. Firdaus, R. M., Melo, C.D., Migot, S., Emo, M., Pierson. J.F., Mohamed. A.R., Vigolo, B. 3D porous alumina/graphene hybrids prepared by atomic layer deposition and their performance for water treatment. Advanced Composites and Hybrid Materials, (Submitted).

Abstract. Ideal or pristine graphene is a single atom-thick layer of sp^2 hybridized carbon atoms. Besides, graphene can also be seen in other forms as graphene derivatives, including graphene oxide (GO) and reduced graphene oxide (rGO). Our study demonstrated that GO is suitable to be used as starting material and can also be chemically and physically activated to be used as an adsorbent for CO_2 capture. In addition, three-dimensional (3D) graphene materials have recently gained a great deal of interest due to their ability to preserve the intrinsic properties of 2D graphene sheets while providing advanced functions that improve performance in a wide range of applications, especially, environmental remediation. Thus, the next section of this study describes the process of developing 3D graphene based monoliths (GBMs) and chemically modified the prepared porous 3D GBMs by using atomic layer deposition (ALD) of alumina (Al_2O_3), which offers advantages such as precursor diffusion, no contamination, phase control, and the ability to deposit nanoparticles or nanofilms. Further, to better understand the characteristics of the developed materials, some standard and advanced characterization techniques (e.g.; TEM/STEM/EELS on thin lamellas prepared by FIB) have been selected to study the surface chemistry and structural properties of the chemically modified 3D GBM hybrids. Lastly, the 3D Al_2O_3 / GBM hybrid developed by ALD was tested for Congo red dye adsorption, and it showed increased adsorption capacity than pristine 3D GBMs, owing to the favourable interactions between the alumina surface and Congo red.

Résumé. Le graphène idéal est une couche d'épaisseur atomique composé exclusivement d'atomes de carbone hybridés sp^2. En outre, le graphène peut également être vu sous d'autres formes dites dérivés du graphène, y compris l'oxyde de graphène (GO) et l'oxyde de graphène réduit (rGO). Notre étude a démontré que le GO peut être utilisé comme matériau de départ et être activé chimiquement et physiquement pour être utilisé comme adsorbant pour la capture du CO_2. De plus, des matériaux à base de graphène tridimensionnels (3D) ont récemment suscité beaucoup d'intérêt en raison de leur capacité à préserver les propriétés intrinsèques des feuilles de graphène 2D tout en offrant des fonctions avancées qui améliorent les performances dans un large champ d'applications, en particulier la dépollution. Ainsi, la section suivante de cette étude décrit le processus de développement de monolithes à base de graphène 3D (GBM) et la modification chimique des GBM 3D poreux préparés en utilisant un dépôt par Atomic Layer Deposition (ALD) d'alumine (Al_2O_3). L'ALD offre des avantages tels que la bonne diffusion des précurseurs au sein des porosités, l'absence de contamination, le contrôle de phase déposée et la possibilité de déposer des nanoparticules ou des nanofilms selon l'interaction des précurseurs avec la surface à couvrir. De plus, pour mieux comprendre les caractéristiques des matériaux développés, des techniques de caractérisation standards couplées avec des approches technologiques avancées (par exemple ; TEM/STEM/EELS sur des lamelles minces préparées par FIB) ont été mises en œuvre pour étudier la chimie de surface et les propriétés structurelles des GBM 3D chimiquement modifiés. Enfin, l'hybride 3D Al_2O_3 / GBM développé par ALD a été testé pour l'adsorption du colorant rouge Congo, et il a montré une capacité d'adsorption accrue par rapport aux GBM 3D vierges, en raison des interactions favorables entre la surface d'alumine et le rouge Congo.